8-3-2023 11:00 AM

The role of DLC1β in attenuating cardiac ischemia-reperfusion injury during heart transplantation

Samantha L. Collings, *The University of Western Ontario*

Supervisor: Min, Weiping, *The University of Western Ontario*
Co-Supervisor: Zheng, Xiufen, *The University of Western Ontario*
A thesis submitted in partial fulfillment of the requirements for the Master of Science degree in Pathology and Laboratory Medicine

Abstract

Cardiac ischemia-reperfusion injury (IRI) occurs intra-operatively during heart transplantation (HTx), underpinning graft survival. Past research implicated the PI3K/Akt1 & RhoA/ROCK pathways in IRI. Rho-GTPase activity/Akt regulates Deleted-in-liver-cancer 1 protein's beta-isoform (DLC1β). Therefore, we hypothesized that DLC1β overexpression (OE) had anti-apoptotic effects. In vitro, HL-1 cells (mouse cardiomyocytes) received chamber hypoxia-oxygenation reperfusion (H/R) for 24H4R with/without DLC1β plasmid, before collection for protein/mRNA analyses. DLC1β-OE resulted in downregulated pro-apoptotic mRNA expression (Bax/Cycs/Casp3), upregulated protective mRNA targets (BCl2/Akt1) and less late/early apoptosis via flow cytometry. Results were confirmed via H9C2 (rat cardiomyocyte) cell lines. In vivo, C57/BL6 mice received heterotopic HTx with/without DLC1β-OE plasmid tail-vein injections. Grafts were analyzed POD1/7 via mRNA/protein/histopathology. Treatment with DLC1β-OE reduced IRI as evidenced by decreased cumulative injury via histopathology. In summary, future translational applications are of interest as DLC1β-OE demonstrated novel anti-apoptotic effects conferred via RT-qPCR in vitro; moreover, in vivo grafts demonstrated reduced neutrophilic infiltrate/fibrosis/overall injury.

Keywords

DLC1β, IRI, Apoptosis, fibrosis, cardiovascular research, heart transplantation, histopathology, ischemia, reperfusion, translational medicine, pathology

Summary for Lay Audience

The conducted study focuses on how we can reduce injury to the heart during heart transplantation. Cardiac ischemia-reperfusion injury (IRI) occurs when transplanting a heart from donor to recipient. The “ischemia” phase of cardiac IRI occurs when the donor heart is being collected and blood/oxygen is not going to the heart. The surgery connects the recipients blood supply back to the heart, however, the rush of blood back to the heart can result in further damage. This is known as the “reperfusion” phase in cardiac IRI. In transplantation, the heart that is removed from the donor is not being pumped with blood anymore which is why many consider IRI to be inevitable. However, if we can understand how this damage happens, we may be able to develop strategies to avoid this injury in future. Furthermore, as cardiac IRI results in poor outcomes for the patient, we may be able to use research in this field to help future recipients. Recently, a few studies have shown that a protein known as deleted in liver cancer 1 beta (DLC1β) could have protective effects on transplanted hearts against IRI. Therefore, we aimed to study whether the increase of this protein could have protective effects against IRI. This study focuses specifically on a unique form of DLC1 known as DLC1β, which has been found in heart tissue. To date, research available on this topic is currently limited. However, we wanted to conduct this study in hopes of finding targets that could be used for further research. By doing this, we hoped that this study would allow for clinical applications (human studies/drug trials) in the future. The big question that this study aimed to answer was, does manipulating DLC1β reduce I/R injury? And which pathways does DLC1β interact with? By analyzing these questions, this research might be useful in humans to potentially reduce the rate of injury during heart transplantation. To study IRI, we had to perform mouse heart transplants. We conducted the transplants on mice after they received an injection of DLC1β (or not); and then their hearts were stored in a fridge for 24hrs. This temporarily decreases the amount of oxygen the heart receives and simulates a clinical transplant-like model. Then we transplanted the hearts into new recipients and sacrificed the mice after 24hrs or 7 days to see how the heart reacted. To conclude, it is believed that this study could have potential extensions into human populations if we discover that DLC1β is protective to the heart.

Co-Authorship Statement

Assistance in the form of experimental replicates for flow cytometry was performed by our PhD student, Qi Liu for the H9C2 aspect of this project. The gating and downstream analyses of this data was done independently. Additional add in qRT-PCR replicates for H9C2 cells was contributed by our undergraduate student, Sohyun Won. However, all the qRT-PCR data for the in vitro/H9C2 aspect was done independently. Finally, all quantitative pathology analyses using QuPATH software was performed by myself, Samantha Collings.

"Research is formalized curiosity. It is poking and prying with a purpose."

- Zora Neale Hurston

Dedications

I dedicate this thesis to my late father, Roy Collings. Unfortunately, you could not be here to experience this with me and our family; however, I know you would have been so proud. You were always my biggest supporter in all aspects of my life. Your courage and tenacity made me a better person, and your lessons of pursuing curiosity has driven my passion for the field. I love and miss you every day dad. Thank you.

Acknowledgements

To my two supervisors, Dr. Weiping Min and Dr. Xiufen Zheng. I am incredibly lucky to have had your expertise and guidance throughout my project. Your advice aided me to become a better scientist and academic. I appreciate all the time, energy and resources that were spent to make sure I was always supported. I would also like to extend thanks to the members of my advisory committee, Dr. Alp Sener and Dr. Vivian McAlister. Your feedback allowed me to hone this project into something I am very proud of.

To Dr. Aaron Haig, your expertise and kindness showing me how to score tissues was a skill I surely won't forget! To Winnie and Caroline for cutting all my tissues, thank you! To Dr. Li, thank you so much for kindly providing the plasmid used for this project! And special thanks to our incredible microsurgeon, Dr. Jifu Jiang. It was a privilege to have worked alongside you all.

To my laboratory mates and Matthew Mailing Centre colleagues: Qi Liu, Hong Diao, Danielle Taray-Matheson, Adam Greasley, Sohyun Won, Helen Boles and Patrick McLeod… The help that you have provided me every day in the laboratory and personally is something I will never forget. I genuinely don't have words to express my gratitude for you guys, other than my experience in lab would not be the same without you all. Thank you for helping me with data interpretation, providing alternative strategies based on your collective experiences, and sometimes just listening when experiments have failed. Thank you for all your help and support *every single day* of my master's program!

To my mother, Susan, who has called and supported me in every way, *every day* of my thesis. Mom, you are the strongest woman I know. Your unwavering strength and love has been my scaffolding in all my endeavors. I carry your life lessons and advice with me in everything I do. I love you forever and thank you for providing me with the means to have the opportunities I have.

To my sister, Hailey. There are no words. Speaking to you and Poppy are the highlights of my day when I leave the lab. Whether it is just for a brief check-in or a 3hr call, you are always there for me to listen and provide your advice. I love and appreciate you beyond words. You have been my rock, protector, #1 cheerleader and (at times) therapist. I love you buddy, thank you for always being my built-in best friend.

I do not have enough pages to express my gratitude to my entire family, but specifically to my aunts, Ellen & Cindy, my bobe, Esther, all my cousins, and my boyfriends' family… You all have provided me with such integral support, love, and kindness throughout this incredibly taxing process of my education; thank you all! Thank you for always cheering me on from whatever distance and listening to me drawl about all and everything to do with mouse hearts xo.

To my best friends Hailey, Morgan, Emily, and Ryley; I adore you all and thank you for all your love and support always. I seriously cannot think of all the words to explain the impact you all have had on my life. You have been cheering me on since high school, always pushing me to be my authentic self and aim big. To my late best friend Charlie, I love and miss you Chooch. I know you would have done incredible things in this field if given the opportunity. There are no words; you all make me a better person.

And finally, to my amazing and supportive partner Cory. I am so unbelievably thankful for the love and kindness you have shown me through this experience. Starting grad school and moving in together have been two incredible life events to have co-existed. You have kept me sane, listened to my rambles about mouse hearts, and often were by my side through my triumphs (and more so my failures). You are my person, and I love you endlessly, always xoxo.

Land Acknowledgement

With this statement, I acknowledge that the University of Western Ontario is located on the traditional lands of the Anishinaabek, Haudenosaunee, Lūnaapéewak and the Chonnonton Nations. In addition, these lands are connected with the London Township/Sombra Treaties of 1796/ and the Dish with One Spoon Covenant Wampum.

It is with this; I extend my thanks and respect for the relationships that Indigenous Nations have to this land as the original caretakers. I furthermore acknowledge the historical injustices perpetrated against Indigenous Peoples and highlight the responsibility that academic institutions have for restoration of respectful relationships. Indigenous Peoples serve as the contemporary stewards of Canada and vital contributors to our society. And it is on their land in which my education has been possible, for this, I extend my thanks.

Table of Contents

List of Tables

List of Figures

List of Appendices

List of Abbreviations

Akt/ “PKB”	protein kinase B
Bax	bcl-2-like protein 4 or bcl-2 Associated X-protein
BCl2	B-cell leukemia/lymphoma 2 protein
Casp3	caspase 3
CVD	cardiovascular disease
Cycs	cytochrome c (somatic)
DAB	3,3′-diaminobenzidine
DLC1	deleted in liver cancer 1
DNA	deoxyribonucleic acid
FBS	fetal bovine serum
GAPDH	glyceraldehyde 3-phosphate dehydrogenase
HEPES	N-2-hydroxyethylpiperazine-N-2-ethane sulfonic acid
H&E Stain	hematoxylin and eosin stain
H/OR	hypoxia oxygenation reperfusion
HF	heart failure
HTx	heart transplantation
IP	intraperitoneal
I/R	ischemia-reperfusion
IRI	ischemia-reperfusion injury

IV	intravenous
L-glu	L-glutamine
LVEF	left ventricular ejection fraction
MHT	mouse heart transplantation
mRNA	messenger ribonucleic acid
NF-κB	nuclear factor kappa-light-chain-enhancer of activated B cells
NPP	norepinephrine
P/S	penicillin
PI	propidium iodide
PI3K	phosphatidylinositol 3-kinase
PTEN	phosphatase and tensin homolog deleted on chromosome ten
qPCR	quantitative polymerase chain reaction
RhoA	Ras homolog family member A
RNA	ribonucleic acid
ROCK	Rho-associated protein kinase
ROS	reactive oxygen species
SAC'D	sacrificed
TUNEL	terminal deoxynucleotidyl transferase dUTP nick end labelling
UW	University of Wisconsin
WB	Western Blotting

Chapter 1

1. Background

1.0 Introduction to the project

The purpose of the research conducted was to investigate the role of DLC1β in relation to cardiac ischemia-reperfusion injury. Cardiac ischemia-reperfusion injury (IRI) typically occurs during the process of transplantation, or during myocardial injury (Akande et al., 2020). Myocardial ischemia-reperfusion injury is often associated with myocardial infarction ("heart attack"). Most frequently, myocardial IRI occurs due to a narrowing of the arteries supplying the heart with blood due to severe atherosclerosis (Frank et al., 2012). However, the focus of this study is on *transplantation-associated cardiac IRI*. Intraoperative cardiac IRI occurs when the donor graft has a decrease in blood flow before it is transplanted into the recipient and actively re-perfused. It is thought that this research may have translatable potential, which could contribute to enhanced transplant efficacy in future (Akande et al., 2020; Silvis et al., 2020). To do this, a particular target DLC1β was the focus of the conducted study. Research in the field provides evidence that DLC1β is integral in mouse fetal cardiac development (Linnerz & Bertrand, 2021). Additional papers have conferred that DLC1β regulates targets such as Akt1 and RhoA, that have been associated with cardiac IRI disease pathways (Linnerz & Bertrand, 2021; Lin et al., 2014; Durkin et al, 2005; Liu et al., 2018). Therefore, the project was proposed to analyze the impact of overexpressing DLC1β in both in vitro models (cells), as well as in vivo models (mice). This is largely to discern if DLC1β has an influence on a cellular/small mammal level, that may confer potential anti-apoptotic effects. Additionally, it was of interest to elucidate what pathways these potential effects are occurring by, to analyze potential targets that may participate in the molecular mechanism of cardiac IRI. As the pathogenesis of cardiac IRI is currently elusive, this is a popular focus in transplantation medicine.

1.1 Introductory Heart Anatomy and Physiology

Firstly, before delving into cardiac ischemia-reperfusion injury, it is imperative to review the anatomy and physiology of the heart and cardiovascular system. Understanding the normal physiology of these systems aid in conceptualizing the pathophysiological processes (the injurious processes resulting in a diseased state).

1.1.1 Basic Heart Anatomy

The cardiovascular system includes the heart, as well as the blood vessels (or "vasculature"). The heart is an integral organ that fundamentally works to ensure blood (and oxygen) is constantly being provided to the tissues of the body. The heart is essentially a large pump that is comprised of three fundamental layers: the epicardium, myocardium, and endocardium. The outermost layer of the heart wall is the epicardium (Quijada et al., 2020; Streef & Smits, 2021; McCance & Huether, 2018). During fetal cardiac development, progenitor cells act as a reservoir for the formation of the epicardium (Quijada et al., 2020). The epicardium in adulthood is retained and is thought to be dormant until the progenitor cells are re-stimulated into a reparative state, as a response to injurious stimuli (Quijada et al., 2020; Streef & Smits, 2021). The middle layer of the heart is termed the myocardium, which functions as a muscular pump ("*myo*", meaning muscle in latin). Electrical impulses that stimulate the myocardium of the heart are imperative for governing the cardiac cycle (Grant, 2009). The cardiac cycle is the rhythmic contraction and relaxation of the heart due to electrical impulses, that allows for unidirectional blood flow (Tran et al., 2022). Additionally, the myocardium acts as a scaffold for the functional chambers of the heart (Tran et al., 2022). Finally, the innermost layer of the heart is termed the endocardium. Endocardium is derived from endothelial cells during embryogenesis (fetal development) (Dye & Lincoln, 2020). The endothelial cells that comprise the endocardium also aid in the formation of the valves of the heart during fetal development, in addition to their role in cardiac cell differentiation (Dye & Lincoln, 2020).

The heart is in the thoracic cavity, posterior to the body of the sternum (Anderson & Loukas, 2009). The location is referred to as the "mediastinum", where the heart is medial in respect to the lungs (Anderson & Loukas, 2009; McCance & Huether, 2018). The structures of the heart can be subdivided into five distinct, functional areas. These include the left atria, left ventricle, right atria, right ventricle, and interventricular septum (Figure 1a). The valves of the heart are grouped based on their respective locations; for valves that occur between the atria and ventricles, they are denoted as atrioventricular valves (Hinton & Yutzey, 2011; McCance & Huether, 2018). The atrioventricular valves will remain open when the heart is relaxed and will shut during the contraction of the heart to maintain unilateral blood flow (O'Donnell & Yutzey, 2020; McCance & Huether, 2018). The semi-lunar valves are classified based on their location; including the aortic semi-lunar valves as well as the pulmonic semi-lunar valve (located in the pulmonary artery) (McCance & Huether, 2018). And finally, coronary circulation refers to vasculature that supplies blood to the heart itself; coronary circulation is comprised of a vast network of coronary arteries, collateral arteries, and coronary capillaries (Figure 1b) (Ogobuiro et al., 2022; McCance & Huether, 2018).

A. **B.**

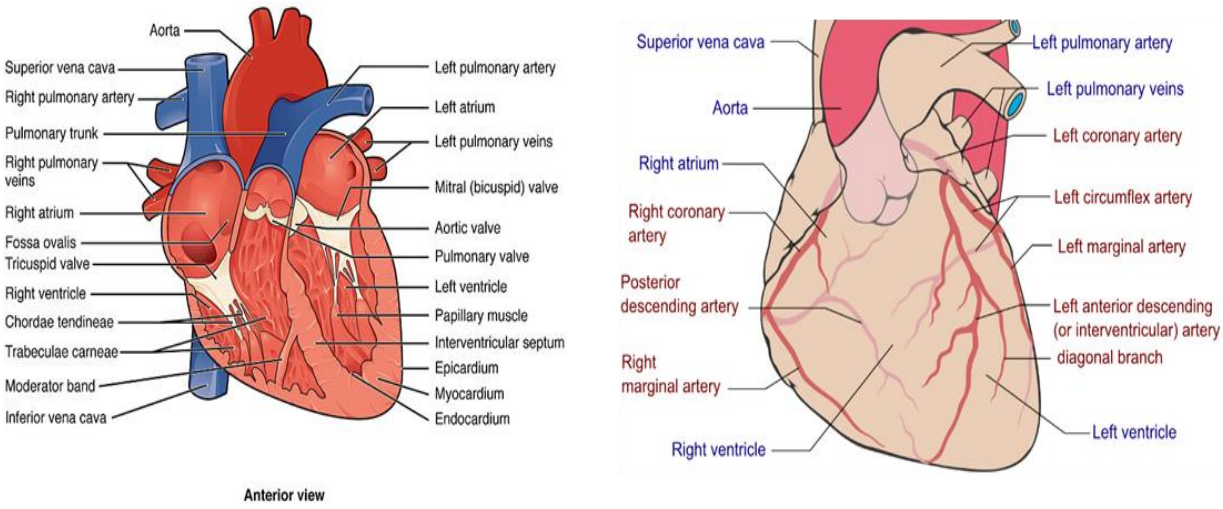

Figure 1- Basic Anterior/Gross Heart Anatomy:

In Figure 1A, one can see the primary areas of the heart with internal structures/valves labelled. The image created by OpenStax College was accessed through Wikimedia. This

file is licensed under the Creative Commons Attribution 3.0 license. In Figure 1B, the heart anatomy with associated coronary arteries/veins is depicted. The image was created by Patrick J. Lynch/Mikael Häggström and accessed via Wikimedia. The file is licensed under the Creative Commons Attribution-Share Alike 3.0 license.

1.1.2 Physiology: Circulation & Conduction

Blood that is deoxygenated, enters the heart through the inferior and superior vena cava (NCI, n.d.). After entry, blood flows through the right atria into the right ventricle by passing through the atrioventricular/ "tricuspid valve" (Figure 2a). From here, blood will exit via the pulmonary arteries during contraction of the heart to be oxygenated. Oxygenated blood will then return to the heart via the pulmonary veins and enter the left atria. Blood will then pass through the mitral valve to the muscular left ventricle, which will contract and eject blood out past the aortic valve to the aorta for systemic circulation. Systemic circulation includes perfusing the trunk of the body, the limbs, and all the major organs/tissues (McCance & Huether, 2018).

The blood that flows through the heart is also aided/ controlled by electrical impulses that govern the heart's action. This system is known as the cardiac conduction system (McCance & Huether, 2018). The electrical stimuli that travel through the myocardium of the heart are denoted as cardiac action potentials (APs). These APs are generated by cardiomyocytes (the cells of the heart) (McCance & Huether, 2018). Therefore, the conduction system of the heart involves the cardiomyocytes, specific nodes in the myocardium itself, as well as a series of bundles/fibers (Figure 2b). The conduction system of the heart works by carefully coordinating the periods of contraction and subsequent relaxation (McCance & Huether, 2018). The electrical impulses that flow through the heart start in the sinoatrial node (sometimes termed the "pacemaker") and move through the interatrial bundles to the right and left atrium (McCance & Huether, 2018). In addition, the sinoatrial node (SA) stimulates the atrioventricular (AV) node through various internodal bundles. The AV bundles carry the electrical impulses to

subendothelial Purkinje fibers, that potentiate these signals to each respective ventricle of the heart (left and right) (McCance & Huether, 2018; Park & Fishman, 2017).

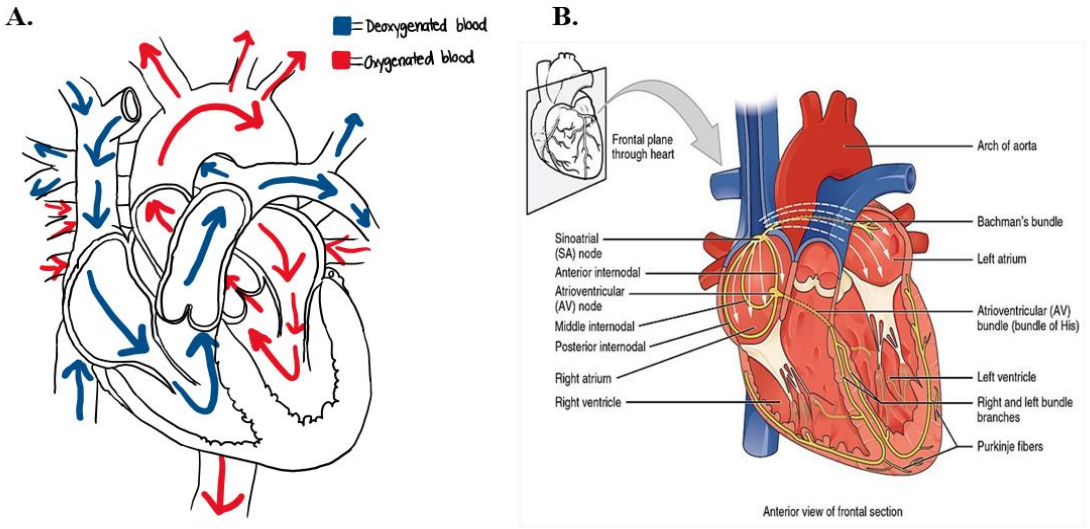

Figure 2- Blood Circulation and Conduction Pathways

In figure 2A), there is a simple depiction of blood flow through the heart. Deoxygenated blood moves through the right side of the heart to the pulmonary circuit to get oxygenated via gas exchange. The left side of the heart receives oxygenated blood and ejects this oxygen-rich blood for systemic circulation. The figure was drawn by myself, Samantha Collings. In 2B), the figure depicts the electrical conduction of the heart as detailed by OpenStax College. The image was available via WikiMedia. This file is licensed under the Creative Commons Attribution 3.0 license.

1.1.3 Brief cardiac histology

The heart itself is formed by a specialized muscle known as cardiac muscle tissue/ "*myocardium*". The cardiac muscle is unique from other muscle tissues, due to its self-contractility; the myocardium is involuntarily contracting without input from the central nervous system (the brain/spinal cord). The heart tissue appears histologically (under the microscope) as single nucleated, striated cells with the presence of intercalated discs. The sheath that surrounds cardiomyocytes within the cardiac muscle is termed, the sarcolemma (Ripa et al., 2022; McCance & Huether, 2018). Intercalated discs appear

within the sarcolemma itself and are small gaps (gap junctions) between the cardiac muscles (Sun et al., 2020; McCance & Huether, 2018). The intercalated discs aid in holding the cardiac muscle fibres together so that contraction is unified (Sun et al., 2020; McCance & Huether, 2018).

1.2 Cardiovascular/Transplantation Research Methods

Similar to many other branches of science, there are a variety of ways transplantation scientists can attempt to recapitulate natural scientific phenomena. Scientific research is broadly classed into observational and experimental research (Concato, 2004). The conducted study would fall into the experimental category. More specifically, the project implored two main research methods: an in vitro (cell-based) study, as well as an in vivo study (animal-based). Both in vitro and in vivo methods are valuable in the research setting; however, both have associated pros/cons. Before delving into the specific methodology utilized in the research project (see Chapter 2 for more details), it is important to briefly mention some of the historical significance of these models.

1.2.1 In vitro cell culture models (H9C2/HL-1 cells)

In vitro methods represent laboratory techniques carried out in cell-based models (Westreich et al., 2010). Cell cultures allow for researchers to recapitulate akin injurious processes in a laboratory setting (Saeidnia et al., 2015). These models, first utilized in the early 1900's, have remained a key pillar in scientific inquiry due to their simplistic use and high reproducibility (Jedrzejczak-Silicka, 2016; Hirsch & Schildknecht, 2019; Saeidnia et al., 2015). In addition to their reproducibility and "user friendly" nature, cells are often inexpensive to culture compared to costly, animal-based studies (Akhtar, 2015). And finally, animal-based research is extremely regulated to comply with stringent ethical guidelines (Rands, 2011; Schuppli & Fraser, 2005). It is the duty of researchers to comply with the basic principles of animal-research ethics; termed the 3R's (*reduce, replace, and refinement*) (Schuppli & Fraser, 2005). Therefore, in order to *reduce* the number of animals used, provide a valid *replacement* to extensive animal use, and also

provide a “proof of principle” to be potentially translated to animal models, cell cultures are very useful (Schuppli & Fraser, 2005).

In vitro cardiovascular research often utilizes tumor-derived immortalized cell lines to allow for serially passable cardiomyocytes (Jimenez-Tellez & Greenway, 2019). These are different to primary cells collected from the heart, as they have mutations in order to maintain active proliferation (Jimenez-Tellez & Greenway, 2019). For the purpose of the conducted study, two different pre-established immortalized cell lines were utilized for the in vitro models. The first being H9C2 cells, which are a rat-derived cardiomyocyte cell line. H9C2 cells are useful within an experimental setting as they are serially passable without losing their specific phenotype, in addition to their moderate doubling time of ~48-50hrs (Alyane et al., 2015). The second cell line utilized for the in vitro study were HL-1 cells, which are mouse-derived cardiomyocytes (Claycomb et al., 1998). HL-1 cells are also serially passable but require specific medium (food for the cells) and have a much shorter doubling time compared to H9C2 cells (~22-24hrs) (Claycomb et al., 1998). This makes them slightly more difficult to culture, but both cell lines can ultimately aid in providing key information about potential injurious processes/signalling pathways, and targets of interest (White et al., 2004). These two cell lines were utilized in this project, as they are inexpensive to culture and a commonly used model for in vitro cardiac ischemia reperfusion studies.

1.2.2 In vivo models (C57/BL6 mice models)

In vivo models, as previously mentioned, are experimental models that utilize animals. In vivo studies allow for researchers to recapture a specific disease/disease-state/injury in a living model (Graudejus et al., 2019). In vivo models are largely considered to be more reliable and translatable when compared to in vitro studies (Graudejus et al., 2019). The internal environment within an organism is not static, so being able to replicate this in cell-based research is quite difficult outside of costly 3-D models. In terms of disease-based research, it is anthropogenically useful to use small mammal models (like mice) to further our understanding of pervasive diseases through in vivo studies (Graudejus et al., 2019). Laboratory rats and mice have long served as model organisms for cardiovascular

research, due to their genomic-similarities, readiness to breed, and cardiovascular similarities (Bryda, 2013). There are still arguments about the translatable potential of mouse-based research to humans, but undeniably, animal models are an integral part of transplantation research to date (Le Bras, 2021; von Samson-Himmelstjerna et al., 2022).

For the purpose of the conducted study, C57/BL6 mice were utilized. These are commonly referred to as "black 6" mice, and are a strain derived from the Jackson Laboratory (supplied via Charles River Valley). The in vivo study utilized C57/BL6 mice as both donors and recipients for a mouse heart transplantation model ("*syngeneic transplantation*"). Overall, mice are highly regarded as the ideal small mammal for cardiovascular research, due to their short gestation times, inexpensive housing costs, and phylogenetic similarity to humans (Cesarovic et al., 2020; Zaragoza et al., 2011; Leong et al., 2015; Jia et al., 2020; Baldwin et al., 2014; Wenzel et al., 2021; Gallegos et al., 2005; Liu & Kang, 2007; Westhofen et al., 2019). For the purpose of the conducted study, both in vitro and in vivo aspects were integral to the design (and outcomes) of the conducted research.

1.3 Cardiovascular Disease (CVD) & Transplantation

Cardiovascular disease (CVD) is an umbrella term for a multitude of different diseases affecting the heart and large/small vessels of the circulatory system. Due to advances in the field, there are many different frontiers in disease-management that may slow the progression of CVD. However, many diseases under the term CVD have genetic predispositions, which entails a propensity for disease regardless of environmental/psychosocial factors. Therefore, understanding the disease processes under the CVD umbrella is of interest to potentially inform disease-management/disease-modifying treatments in the future. Specifically for the purpose of the project, *ischemic*

heart diseases (IHD) such as myocardial infarction, unstable angina, stroke, and *cardiac ischemia reperfusion injury* will be the focus.

1.3.1 CVD/IHD Epidemiology

Cardiovascular disease is a major cause of mortality in developed Western society, that is unfortunately common and accounts for a massive global burden (Virani et al., 2021). These include diseases such as peripheral vascular disease (PVD), coronary artery disease (CAD), ischemic heart diseases (IHD), heart failure and many more (Lopez, 2022; Reaven et al., 2005; Pignatelli et al., 2018). Unfortunately, based on global trends using epidemiology, it is believed that these high mortality-associated diseases will continue to increase in prevalence in years to come (Virani et al., 2021). This is mainly due to levels of cardiovascular disease also increasing in prevalence in developing countries, the obesity epidemic, and other sociopolitical factors such as food inequality/instability (Timmis et al., 2022; Savarese et al., 2022; Javed et al., 2022; Powell-Wiley et al., 2022). Therefore, it is of importance to continue to highlight deficits in treatment, care, surgeries, technologies, drugs, and research to better treat these individuals living with CVD/IHD.

1.3.2 Clinical presentation of IHD and heart failure

The heart tissue itself is comprised of cardiomyocytes, which are largely considered "permanent cells" (Atala et al., 2010; McCance & Huether, 2018). As the name suggests, cardiomyocytes are cells that are non-regenerative, as they have left the cell cycle (in a permanent quiescence) (Garbern & Lee, 2021). Due to this, when the heart tissue is damaged, the heart is unable to regenerate and must heal through scar formation (McCance & Huether, 2018). Scar deposition in the heart has adverse effects on the heart function/ ability to pump blood as effectively; sometimes referred to as "hemodynamic impairment" (McCance & Huether, 2018; Richardson et al., 2015).

Ischemic heart disease (IHD) is a subsection of cardiovascular diseases that result from the lack of blood flow to the heart/organs (dubbed, the "ischemic stimulus"). Prolonged ischemia results in cardiac cell necrosis, and the replacement of these foci of infarction

with scar tissue. Common diseases under the IHD umbrella include myocardial infarction, unstable angina, stroke, and *cardiac ischemia reperfusion injury*. Briefly, myocardial infarction is colloquially termed "heart attack", and results from a reduction of blood flow to the heart due to the presence of a coronary occlusion. When the ischemia is prolonged and the blockage is in a major coronary artery, there is considerable necrosis (or cell death) of the cardiomyocytes of the heart (Institute of Medicine, 2010). Unstable angina is another ischemic heart condition characterized by crushing chest pain due to minimal occlusion(s) of the coronary arteries with no associated cardiac cell necrosis (Institute of Medicine, 2010; McCance & Huether, 2018). Strokes are the result of occluding the lumen of a blood vessel that supplies the brain with blood/oxygen. Finally, cardiac ischemia reperfusion injury (See 1.4.3 for further details) is a period of ischemia (reduced blood flow to the heart), followed by revascularization re-establishing blood flow (reperfusion). All of the previously stated ischemic-heart conditions may result in *heart failure*.

Heart failure (HF) is a condition where the heart is unable to provide adequate blood flow to the tissues/organs of the body. Whether HF is classed as right sided or left sided is relevant clinically, as often there are different manifestations/interventional strategies (Ahmed, 2007). The clinical manifestations of a patient with left-sided HF include pulmonary congestion, difficulty breathing (tachypnea), a blue-ish hue due to poor oxygenation (cyanosis), tachycardia, and restlessness (Guazzi & Arena, 2010; Gehlbach & Geppert, 2004). Whereas right sided HF (sometimes termed, "Cor pulmonale") typically presents as enlarged liver/spleen (hepatosplenomegaly), fluid build-up in the abdomen (ascites), jugular vein distension, weight gain and peripheral edema (Weitzenblum, 2003). In sum, the clinical manifestations of HF often vary depending on the type of heart failure a patient is experiencing (Ahmed, 2007). However, both left-sided HF and right-sided HF have characteristic reductions in left ventricular ejection fraction with poor disease-associated morbidity and mortality.

1.3.3 Pathogenesis, treatments, and clinical outcomes of heart failure

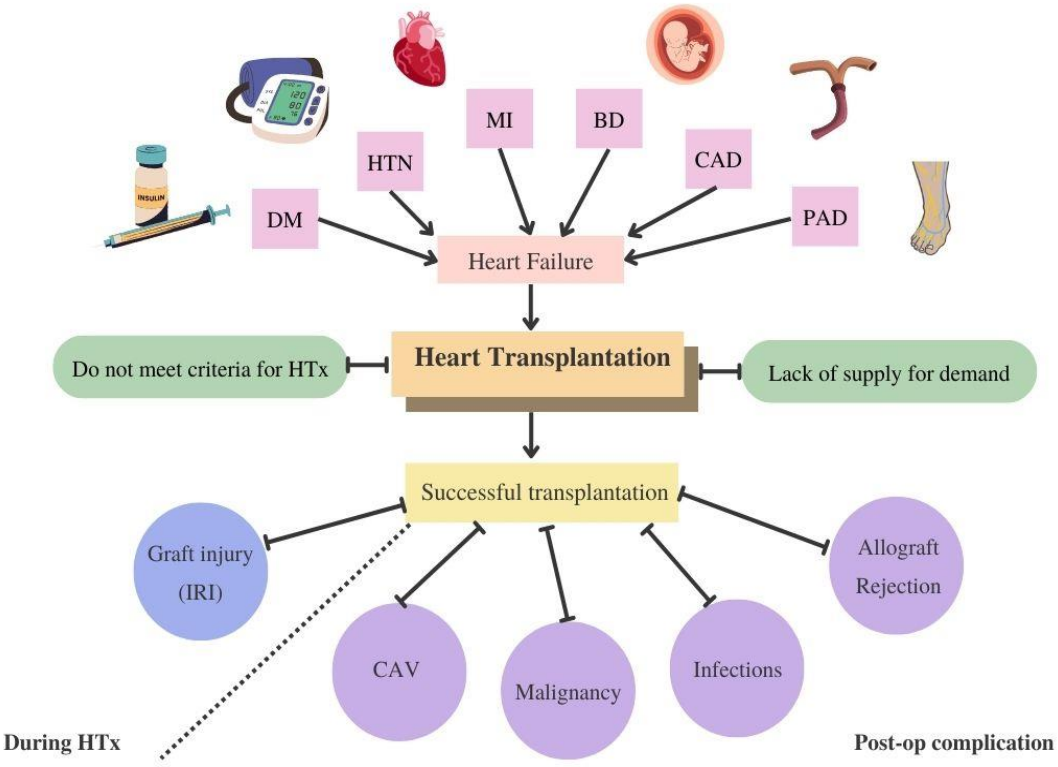

Figure 3- Heart Failure Schematic

Heart failure is a disease *consequence* that can result from a multitude of different diseases. Some of these aetiologies include diabetes mellitus (DM), hypertension (HTN), myocardial infarction (MI), birth defects (BD), coronary artery disease (CAD) as well as peripheral artery disease (PAD). The only curative means for heart failure is to ultimately transplant the heart, however, transplantation is not an option for some individuals due to stringent criteria and a vast supply/demand imbalance. Ultimately, successful transplantation is also limited by post-operative complications, as well as cardiac IRI that occurs during transplantation.

1.3.4 Transplantation criteria in Canada and comorbidities

In Canada, the criteria for heart transplantation are comprised of “absolutes” (conditions in which an individual is not eligible for transplantation) and contraindications, that may

impact transplantation efficacy (Trillium Gift of Life Network, 2018, Chih et al., 2020). Specific, “absolute” comorbidities/ contraindications outlined by the Trillium Gift of Life Network include 1) liver disease, 2) pulmonary hypertension, 3) active cancer(s), 4) pulmonary disease(s), 5) systemic, multi-organ diseases, 6) active infections, and other 7) psychosocial factors (Trillium Gift of Life Network, 2018). Based on advancements in transplantation and survivability data, the age recommendations for heart transplantation have been recently increased to individuals <70 years old/ 70+ on a case-by-case basis (Chih et al., 2020). And finally, it is now recommended that all potential recipients are also subject to a frailty index, to ensure the best post-transplant survivability (Chih et al., 2020).

1.4 Heart transplantation: Procedure/complications

1.4.1 Pre-operative complications

When heart transplantation is necessary, the majority of procured donor grafts are derived from brain stem death recipients (See Hoe et al., 2020). This is largely due to the extracorporeal perfusion maintaining graft viability and reducing exposure to cardiac ischemia reperfusion injury (IRI) (Ishii et al., 2021; Verma et al., 2002). Donation after circulatory death (DCD) is thought to be the solution to the organ supply/demand crises, however, DCD often results in pervasive cardiac IRI (See Hoe et al., 2020; Méndez-Carmona et al., 2019; Akande et al., 2020; Alomari et al, 2022). Thereby, cardiac IRI also reduces the viability of donatable organs, further highlighting the necessity for adaptive treatments (Méndez-Carmona et al., 2019).

The average, current wait time for receiving a heart transplant in Canada is 9 months to 1+ year(s) (Canadian Institute for Health Information, n.d.). These wait times vary greatly based on the supply/demand crisis for organs (as mentioned), as well as the recipient’s health at the time of transplantation (Canadian Institute for Health Information, n.d.; Chih et al., 2020). Unfortunately, individuals frequently die on the transplant list due to complications from heart failure (Mangini et al., 2015; Navas-Blanco & Modak, 2021; Ahmed & Jain, 2022). A proportion of these deaths can also be contributed to adverse

effects to the pre-operative immunosuppressants necessary to reduce rejection risk (Navas-Blanco & Modak, 2021). The waiting time between circulatory death of a donor and implantation of the organ in a suitable recipient is a factor that can impact the quality of the graft(s). Strategies that focus on reducing the time between explant to implant and ischemia/reperfusion severity are highly desired methods to prolong graft viability.

1.4.2 Basic transplantation procedure

The fundamental procedure of an orthotopic (recipient heart removed) heart transplantation begins with donor heart preparations (Ahmed & Jain, 2022; Mangini et al., 2015). These include placing the donor on cardiopulmonary bypass (CPB) after the vessels and surrounding anatomy are removed (Ahmed & Jain, 2022). The time between explant of the donor heart and implant into the recipient is thought to be critical at reducing ischemic injury (Ahmed & Jain, 2022). The majority of the recipient's previous heart is grossed/excised, with the exception of the upper left/right atria cuffs (Ahmed & Jain, 2022). Then, anastomoses ("surgical connections") between the donor right atrial cuff and recipient right atrium will be completed. This is then repeated on the left atrium and large arteries (pulmonary/aorta). After the sutures are placed, a bicaval technique is employed, which creates anastomoses between the recipient's vena cava (venous supply) and the donor's right atrium (Ahmed & Jain, 2022). After the surgical connections are placed, reperfusion (unclamping of large vessels) will occur. Finally, the patient will slowly be weaned off of the CPB before closure (Ahmed & Jain, 2022).

1.4.3 Intra-operative complications: Cardiac ischemia-reperfusion injury

Cardiac ischemia reperfusion injury (IRI) is an intra-operative complication during heart transplantation, decreasing transplantation efficacy (Liu et al., 2018; Akande et al., 2020; Mauerhofer et al., 2021; Fyfe et al., 1996). ***Ischemia*** is an injurious process resultant of reduced blood flow (and subsequently oxygen) to a tissue (Liu et al., 2018; Akande et al., 2020; Mauerhofer et al., 2021; Fyfe et al., 1996). Initially, when a donor heart is explanted from the patient, there is a period of time before it is implanted into a recipient in which the heart is not being perfused with blood (Liu et al., 2018). This time (denoted

"ischemia time") between explant to implant is typically kept to 4-6 hrs in order to maintain graft function (Liu et al., 2018). Although there are interventions to prevent donor graft ischemic damage, there is evidence that suggests that increased ischemia time is causally associated with poor, post-HTx outcomes and patient survival (Silvis et al., 2020; Jernryd et al., 2020; Binder et al., 2015; Bell & Yellon, 2011; Guariento et al., 2021). To complicate matters, after grafts are subject to ischemia, the subsequent ***reperfusion*** period supplying blood to revascularized myocardium is also injurious (Binder et al., 2015; Bell & Yellon, 2011; Guariento et al., 2021).

Currently, the typical standard practice is to transport the donor organ in cold storage, using a cardioplegic solution (such as UW solution) (Alomari et al., 2022). There are also new techniques like extracorporeal perfusion systems (colloquially known as "heart in a box"), that can transport donor grafts while actively pumping the organ with blood and maintaining stringent temperature ranges (Alomari et al., 2022). Advancements in technologies to increase graft survival are a new frontier in clinical practice; potentially addressing disparities in supply/demand by allowing for donation after circulatory death (DCD) (Alomari et al., 2022; Jacob et al., 2022). But the optimization of these systems is ongoing (Alomari et al., 2022; Jacob et al., 2022). Despite their novelty, extracorporeal systems are heavily contested due to associated costs, and a lack of consensus on optimal cardioplegic solutions/reperfusion storage temperatures (Alomari et al., 2022; Jacob et al., 2022).

1.5 Cardiac ischemia-reperfusion injury

1.5.1 Introduction to ischemia reperfusion injury

Ischemia reperfusion injury is an aberrant process that results from the reestablishment of blood supply to an organ after a prolonged period of oxygen/blood deprivation (Naito et al., 2020; Cowled & Fitridge, 2011). In the body, this can occur when the lumen of a blood vessel is occluded by an atherosclerotic plaque/thrombus/ foreign object, which reduces the blood supply to an organ (Cowled & Fitridge, 2011). Organ/tissue injury occurs when ischemia is prolonged and the subsequent perfusion/concomitant

reoxygenation further damages the tissue (Naito et al., 2020). This process of blood/oxygen deprivation and subsequent revascularization occurs during organ transplantation as well, often termed "*transplantation associated IRI*". Briefly, ischemia begins in transplant associated IRI when the donor organ is no longer being perfused (the donor is deceased, awaiting surgical explant). Then, the donor graft is stored in a cardioplegic solution in a normoxia, hypothermic/normothermic environment (Vela et al., 2018; Bona et al., 2021). The graft is then transplanted into the recipient, where it is subsequently revascularized. Transplantation associated IRI is often deemed inevitable, as the reduction of perfusion in the donor organ due to donor death is unavoidable (Cowled & Fitridge, 2011; Fernández et al., 2020; Mauerhofer et al., 2021; Marin et al., 2021; Liu & Man, 2023). However, transplant associated IRI is different then general IRI, as it is occurring across patients, intra-operatively. As IRI is bi-phasic, it is important to further characterize each distinct injurious process further to understand how it is studied in preclinical settings.

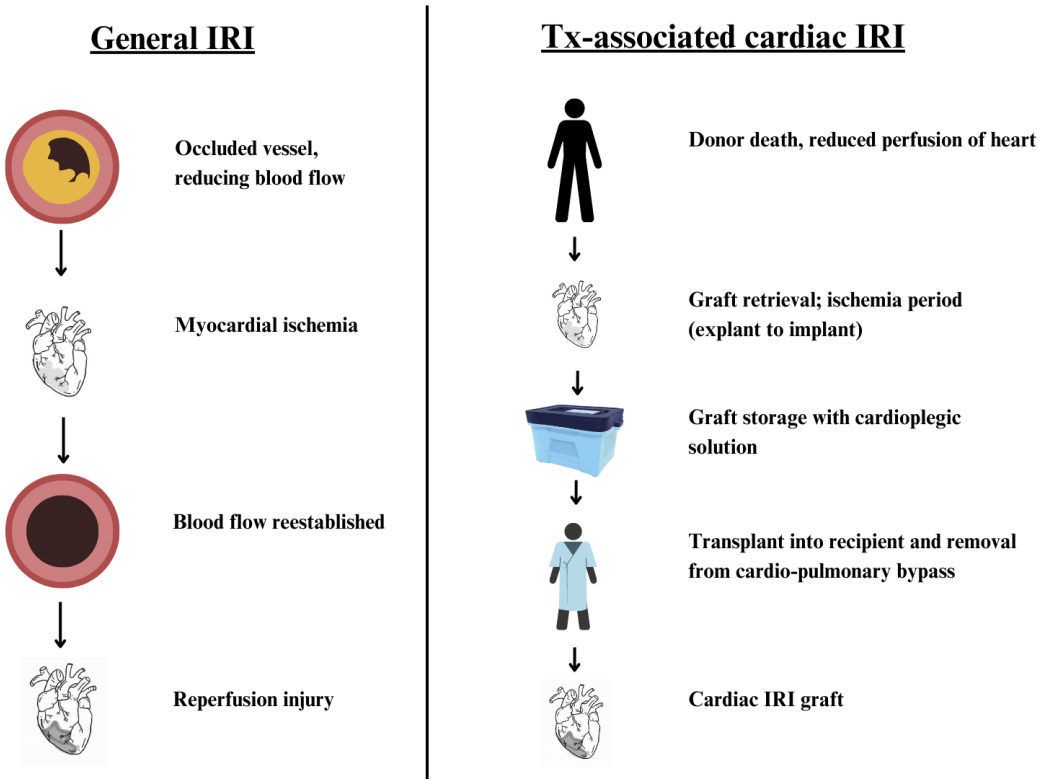

Figure 4- General myocardial ischemia-reperfusion versus transplantation-associated:

The figure depicts general myocardial ischemia-reperfusion injury, where an occlusion (most commonly) reduces the lumen of the coronary arteries supplying the heart with blood. This results in decreased myocardial perfusion, when prolonged, results in myocardial ischemia. When blood flow is subsequently re-established (via pharmacological/surgical interventions), the subsequent revascularization leads to reperfusion injury. In transplantation-associated (Tx-associated) cardiac IRI, the graft is ischemic from the point of donor death until the point of transplant into the recipient. The removal of the patient from cardio-pulmonary bypass results in reperfusion injury.

1.5.2 Ischemia

As mentioned, ischemia is a reduction of blood flow to the tissue/organ. This results in a lack of oxygen supply, triggering a multitude of different stress signals/pathways in response to this form of injury (Sánchez-Hernández et al., 2020). The heart is particularly sensitive to ischemia injury, as cardiomyocytes require vast and consistent influxes of cellular energy via adenosine triphosphate (ATP), or mitochondrial oxidation of free fatty acids (Rabinovitch et al., 2017). During the exposure to an ischemic stimulus, the cardiomyocytes are unable to adequately meet their nutritional and energetic requirements (Rabinovitch et al., 2017). This ultimately results in the cardiomyocytes rapidly consuming their stores of intracellular ATP and leads to the accumulation of adenosine-monophosphate (AMP) and reactive oxygen species (ROS) in the intracellular spaces (Rabinovitch et al., 2017; Frank et al., 2012). Additionally, during ischemic exposure there is a change in intracellular pH resulting in more sodium ions (Na+) entering the cell (Frank et al., 2012; Park et al., 1999). The influx of intracellular Na+ drives the activation of Na+/Ca2+ exchangers (Frank et al., 2012; Shattock et al., 2015; Daiber et al., 2021). Sensing the imbalance, Ca2+ is actively pumped back into the intracellular space, leading to calcium overloads (sometimes termed the “redox paradox”) (Frank et al., 2012). Increased intracellular calcium opens mitochondrial permeability transition pores (mPTPs), generating reactive oxygen species (Frank et al., 2012). ROS generation triggers downstream damage-associated molecular patterns (DAMPs), chemokines and cytokines by activating pro-inflammatory signals (Frank et al., 2012). All of which trigger neutrophils (a myeloid-lineage form of white blood cell) to extravasate to the location of the ischemic-stimulus (Perez-de-Puig et al., 2015; Frank et al., 2012).

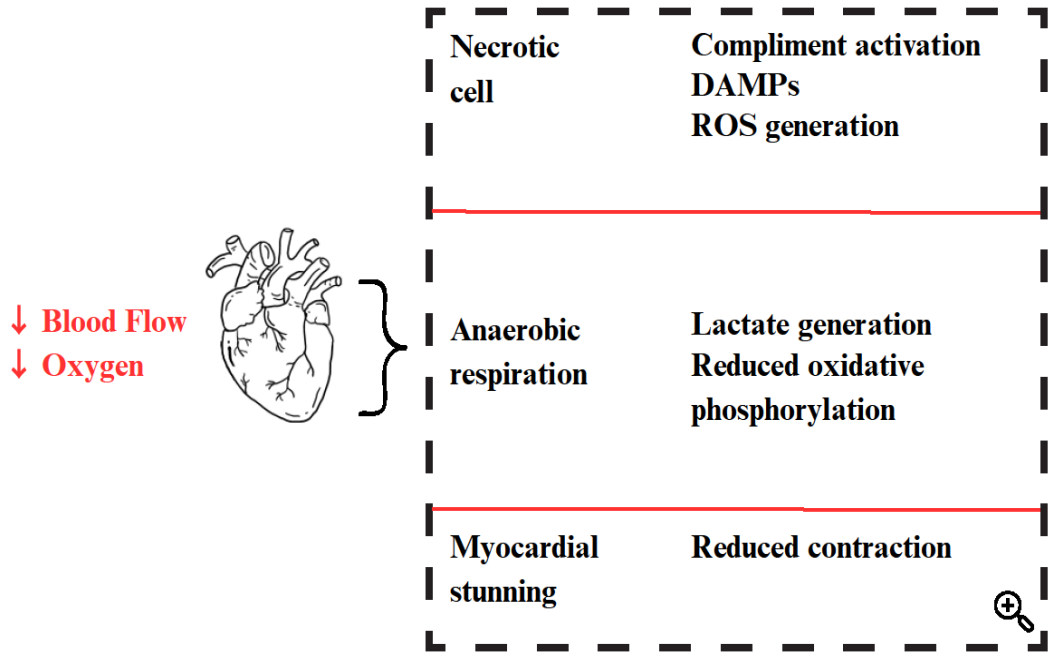

Figure 5- Response to cardiac ischemia schematic

When the blood flow to the heart is decreased, there is a decrease in oxygen provided to the cells that comprise the heart (the cardiomyocytes). This causes cell death ("necrosis"), which signals the immune system (compliment activation), and generates damage associated molecular patterns (DAMPs) in addition to reactive oxygen species. When starved of oxygen, the cells must perform anaerobic respiration, which results in the buildup of lactate and a reduced capability for oxidative phosphorylation. A phenomenon known as myocardial stunning is also noted where the cells of the heart have a reduced contractability in the acute period post-ischemia.

1.5.3 Reperfusion

The reperfusion stage of cardiac ischemia reperfusion injury begins when the previously oxygen-deprived graft is revascularized (Binder et al., 2015; Bell & Yellon, 2011; Guariento et al., 2021). This changes the environment of the cardiomyocytes from oxygen-poor to oxygen-rich; drastically increasing the production of intracellular reactive oxygen species (Sánchez-Hernández et al., 2020; Zhou et al., 2018; Nieuwenhuijs-Moeke et al., 2020). During the reestablishment of normoxia (normal oxygen levels), there is a concurrent pH normalization that further drives the overload of intracellular calcium and lactic acid (Xia et al., 2016; McKeown, 2014; Sánchez-Hernández et al., 2020; Zimmerman, 2000; Zhu et al., 2018; Nieuwenhuijs-Moeke et al., 2020). Important to mention, the revascularization of the myocardium also re-establishes previously depleted ATP (Chi et al., 2017). The aforementioned state changes result in protease activation as well as the mitochondrial permeability transition pore (mPTP) opening (Stansfield et al., 2014; Nieuwenhuijs-Moeke et al., 2020). Both of which trigger the activation of many different injurious pathways due to lipid peroxidation/carbonylation (Stansfield et al., 2014). From here, cell death pathways can be activated via direct damage from cell swelling, or through secondary “death signals”/ubiquitination (Kalogeris et al., 2012). The most common forms of death modalities associated with cardiac ischemia reperfusion injury include 1) necrosis, 2) apoptosis, 3) necroptosis and 4) autophagy (Zhao et al., 2000; Kalogeris et al., 2012; Nieuwenhuijs-Moeke et al., 2020; Chi et al., 2017).

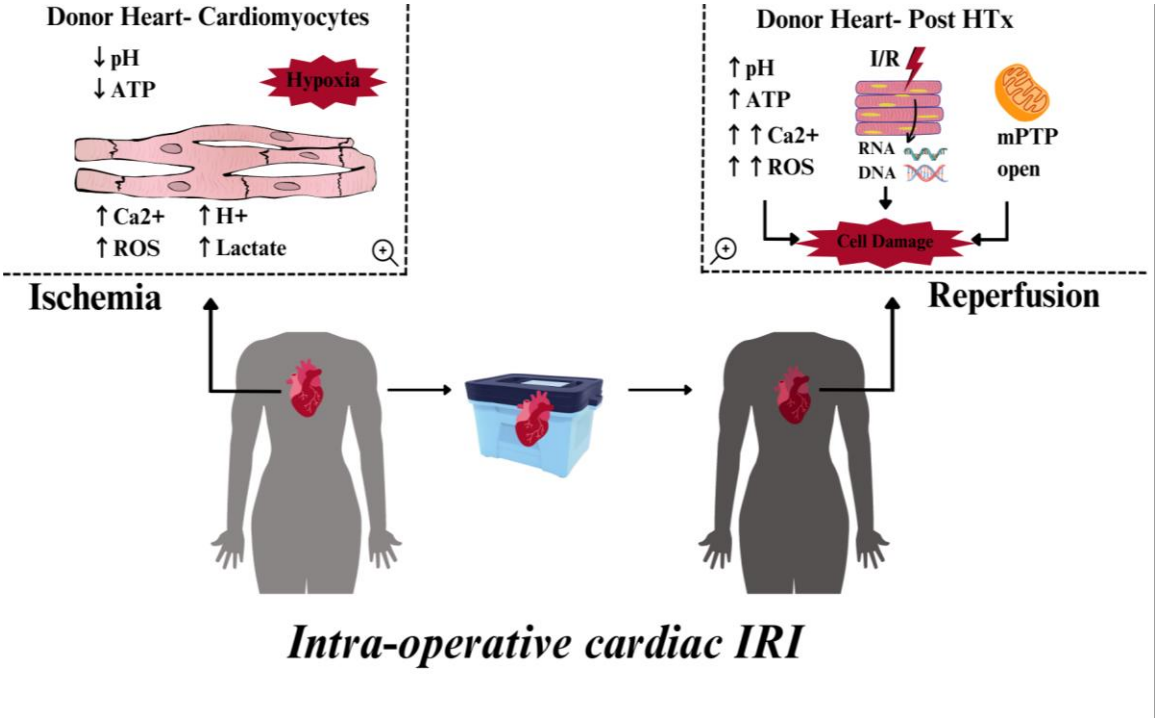

Figure 6- Ischemia Reperfusion Schematic

The schematic represents key events during the process of ischemia-reperfusion injury that result in cell death. Initially, the donor graft is subject to ischemia which deprives the heart of oxygen and increases anaerobic respiration. Subsequently, a decrease in intracellular pH, mPTP opening and the buildup of intracellular Ca2+ in the cytoplasm of the cardiomyocytes occurs. When the previously ischemic graft is transplanted into a recipient and revascularized, another injurious cascade is triggered. This results in even greater calcium redox, inhibited oxidative phosphorylation, increased ROS generation, greater mPTP opening, pro-inflammatory cytokine production /DAMP release, and the signaling to cell death pathways.

1.5.4 Current preventative approaches of cardiac IRI

The current approaches in the field to prevent/reduce cardiac IRI severity include pharmacological agents (vasodilators, antioxidant therapies, & ROS inhibitors), surgical interventions (angioplasty/PCI, reducing ischemic period, manipulating graft storage conditions), and pre/post-conditioning (Daiber et al., 2021; Sárközy et al., 2021; Tong et al., 2002; Ma et al., 2021).

Briefly, pharmacological agents and ischemic preconditioning are interventions that could be administered to the donor to prepare the heart for the onslaught of ischemia (Sárközy et al., 2021; Tong et al., 2002; Ma et al., 2021). Pharmacological agents aim to reduce IRI exposure by dilating the blood vessel to provide more blood to the tissue/organ (vasodilators), improve reactive oxygen species exchange/ reduce ROS amount (antioxidants/ROS inhibitors), or reduce mitochondrial stress (PARP inhibitors/H_2S donors) (Daiber et al., 2021; Patel et al., 2021). Preconditioning entails exposing the heart to an ischemic stimulus briefly, to trigger intrinsic homeostatic mechanisms that produce better outcomes when facing subsequent ischemia (Daiber et al., 2021; Patel et al., 2021).

Interventions during surgery to reduce cardiac IRI include (at times) re-routing blood supply in general/myocardial IRI to re-establish blood flow due to occlusion. These interventions commonly include percutaneous coronary intervention (PCI)/angioplasties after anti-thrombolytics are administered, and typically occur in acute settings (Daiber et al., 2021). Surgical interventions for transplantation associated cardiac IRI include reducing the time between explant/implant to improve patient outcomes, the use of cardioplegic storage solutions, as well as controlling graft storage temperature (Vela et al., 2018; Bona et al., 2021).

1.5.5 Models of cardiac IRI in vitro and in vivo

When attempting to recapitulate the complexities of cardiac IRI, there are many ways this is simulated in vitro and in vivo. Even with multiple models (of varying complexity) however, the relevance/ability to recapitulate human conditions is heavily contested (Chen & Vunjak-Novakovic, 2018; Hidalgo et al., 2018; Ming et al., 2021; Portal et al., 2013). These models can be loosely grouped into anaerobic respirator models and hypoxia-oxygenation-reperfusion (H/OR) chambers in vitro, and clamping/heterotopic transplantation in vivo. In vitro, anaerobic respirator bags (such as the GENbags used for the H9C2 study performed) are the most cost-effective means to create an anaerobic "hypoxic" environment for cell cultures (Zheng et al., 2021; Menéndez-Menéndez et al., 2017). These bags are advantageous due to their ease of use, minimal bench space, and

ability to control temperature by placing in a fridge. However, it is imperative to work quickly and avoid excess oxygen exposure, as the ascorbic acid can result in a slight exothermic reaction. This can be easily negated by monitoring the internal environment in the GENbag using a thermometer/pH strips and hypoxia-litmus indicators provided with the kits. However, anaerobic respiration is only a temporary state in the injurious pathogenesis of cardiac IRI, and these models do not recapture metabolic stressors. Hypoxia-oxygenation reperfusion chambers are widely considered the ideal method of recapturing "ischemia-reperfusion" in vitro (Koeppen et al., 2018; Chen & Vunjak-Novakovic, 2018; Rahman et al., 2023; Hillman et al., 2022). As ischemia refers to the lack of blood flow to a tissue/organ, it by extension insinuates a period of hypoxia. However, hypoxia (a reduction of oxygen) does not encompass the changes in environment that ischemia would result in. Thereby, for the purpose of in vitro models, these are akin to a portion of the injuries process of IRI, but not exhaustive.

In vivo, syngeneic mouse heart transplantation models are typically used to model cardiac IRI (Silvas et al., 2022; Mori et al., 2014; Westhofen et al., 2019). Syngeneic transplantation is when the donor and recipient mouse are of the same genetic background (e.g. C57/BL6 donor & C57/BL6 recipient). The benefit of using syngeneic models in transplantation research is to wean out confounding effects of the recipient's immune system on the graft (Niimi, 2001). This allows for transplantation without the risk of graft rejection and other downstream complications of allogeneic transplantation (Niimi, 2001). The specific procedure of inducing cardiac IRI either occurs through cuffing or true transplantation (Rahman et al., 2023). The cuffing technique is often performed via suturing the left anterior descending coronary artery (LAD) for 5+ minutes ("ischemia time"), before the suture is released, and the area is allowed to revascularize (a "reperfusion" equivalent) (Rahman et al., 2023). However, these clamping models are better at simulating myocardial ischemia reperfusion injury patterns that model STEMI myocardial infarctions, rather than global ischemia associated with transplantation injury (Rahman et al., 2023). Therefore, heterotopic transplantation (transplantation of an additional heart) into the abdomen or cervical region is largely the method of choice (Fang et al., 2013; Liu & Kang, 2007; Westhofen et al., 2019).

1.6 Cell signalling pathways in cardiac IRI pathogenesis

Cardiac IRI results in “hallmark” injuries, including apoptosis, aberrant angiogenesis, cell death (in the heart, foci of infarction), and hypertrophy (Martin & Blaxall, 2012). The involvement of many pathways in cardiac IRI cell signaling has been largely displayed in the research space, however the entire molecular mechanism/coordination of these pathways is still poorly understood. The focus of the conducted study was on apoptosis-related pathways and Rho-GTPase signaling pathways. A brief summary of the key pathways that have been empirically validated in association with cardiac IRI can be seen below (Figure 8/Section 1.6.1). But fundamentally, cell signalling pathways function by having regulatory proteins that use chemical signals to incite communication to other cells (Alberts et al., 2015).

Necrosis and apoptosis are two of the many key cell death modalities associated with cardiac IRI (Eefting et al., 2004). Necrosis is a rapid form of cell death where the intracellular contents are released post-cell swelling (Eefting et al., 2004). Necrotic cell signaling incites an inflammatory response, whereas apoptosis (another death modality), does not (Eefting et al., 2004). Apoptosis is a programmed cell death process resulting in DNA/cellular fragmentation that is immune-independent (Eefting et al., 2004). When ischemia, oxidative stress and intracellular stress is sensed, the *PI3K/Akt pathway* is activated to regulate/execute cell apoptosis (Yu et al., 2021; Walkowski et al., 2022; Scheiermann et al., 2011).

1.6.1 Apoptosis Pathways: PI3K/Akt pathway signaling in cardiac IRI

Phosphoinositide 3-kinases (PI3K) are a form of intracellular kinases that become activated by receptor tyrosine kinases/G-PCRs. PI3Ks are key regulators of cell fate pathways that impact growth, survival, proliferation, migration, differentiation, apoptosis, interleukin signaling, etcetera (Vanhaesebroeck et al., 2010; Alberts et al., 2015). PI3Ks are broadly classed based on their catalytic functions/regulatory functions (Vanhaesebroeck et al., 2010). Class 1 PI3Ks (p110-α) are the focus in the context of

cardiac IRI due to the downstream activation of protein kinase B (Akt). Akt regulates pro-/anti-apoptotic targets to control apoptosis induction in a context-dependent fashion.

During IRI, PI3K/Akt pathway signaling is initiated by death signals and associated oxidative stress (Yu et al., 2021; Walkowski et al., 2022). Activated PI3K will then drive the conversion of PIP2 (phosphatidylinositol (4,5)-bisphosphate) into PIP3 (phosphatidylinositol (3,4,5)-trisphosphate) (Walkowski et al., 2022). PIP3 will induce the activation of PDK1 (3-phosphoinositide-dependent protein kinase-1), that selectively phosphorylates Thr(308) on Akt (Dangelmaier et al., 2014; Bozulic & Hemmings, 2009). Actively inhibiting this conversion from PIP2 to PIP3 is PTEN (Phosphatase and tensin homolog) (Salmena et al., 2008). Once activated, Akt will reduce the pro-apoptotic initiator, Bim (Adams et al., 2019; Putcha et al., 2003). While Akt is actively antagonizing Bim, Akt will also negatively regulate the pro-apoptotic effector, Bax (Adams et al., 2019; Putcha et al., 2003). This, in conjunction with BCl-2 (an anti-apoptotic protein), leads to the abrogation of apoptosis (Yu et al., 2021). This pathway is thought to become inhibited during cardiac ischemia reperfusion injury, resulting in significant injury via aberrant cell apoptosis (Yu et al., 2021; Nagoshi et al., 2005; O'Neill & Abel, 2005; Walkowski et al., 2022; Vassalli et al., 2012; Arumugam et al., 2009).

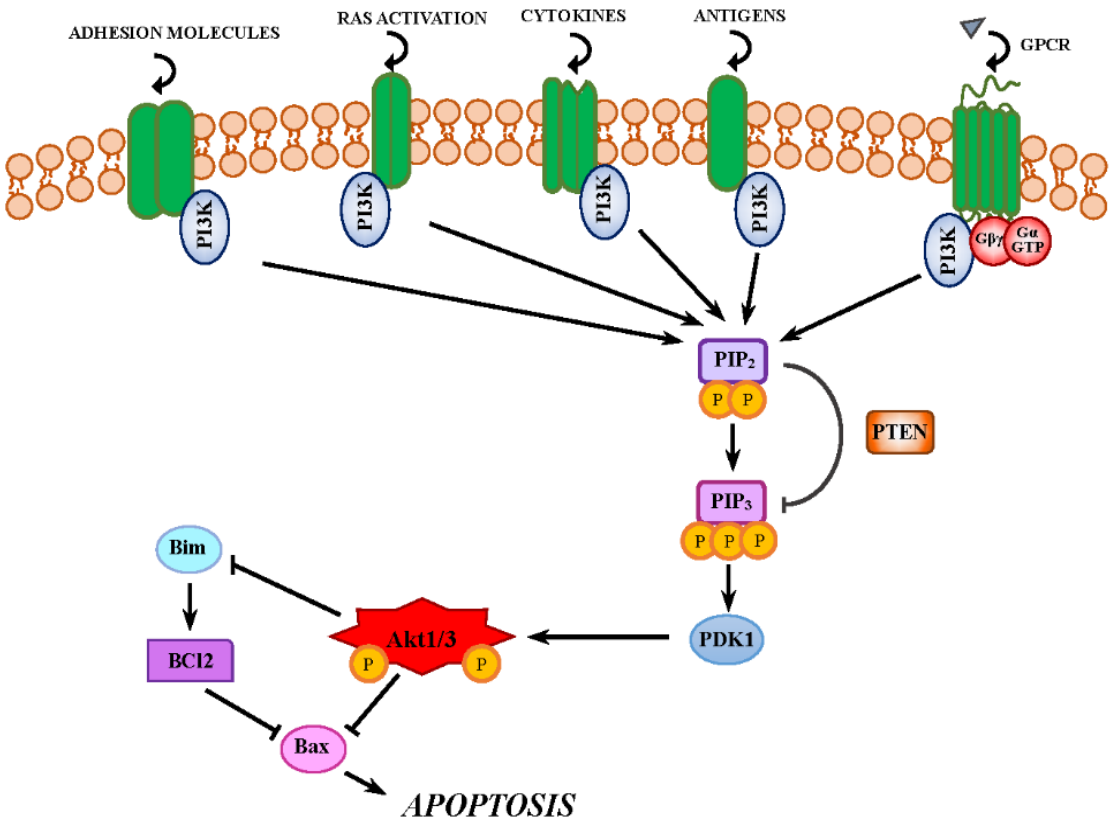

Figure 7- Simplified PI3K/Akt Pathway:

This figure displays a simplified version of the PI3K/Akt pathway, and how it specifically governs cell survival by abrogating apoptosis. The specific downstream targets of the Akt isoforms (1-3) can incite the caspase cascade that systematically control apoptosis activation/execution. Notably, Akt has many interactions and governs multiple downstream pathways that were omitted here for ease of view.

1.6.2 Apoptosis Pathways: Caspase cascade in cardiac IRI

After Akt activates associated BCl2 family apoptotic proteins, the initiation of apoptotic machinery/signals in the cell are carried out by downstream caspases (Riedl & Shi, 2004). Caspases are thought to be imperative for the activation and initiation of the apoptotic processes (Riedl & Shi, 2004). During cardiac IRI, Bax (the pro-apoptotic effector) is translocated to the mitochondria (Riedl & Shi, 2004). In response to Bax

translocation, cytochrome c-mediated caspase activation occurs (Del Re et al., 2019). Cytochrome c is a mitochondrial apoptotic protein that is necessary for the function of the mitochondrial electron transfer chain (Spiess et al., 1999; Jiang & Wang, 2004). Activator caspases (caspase 9) activate effector caspases (caspases 3 & caspase 7), resulting in the execution of mitochondrial-induced apoptosis and cell death receptor apoptosis (Jiang & Wang, 2004; Del Re et al., 2019).

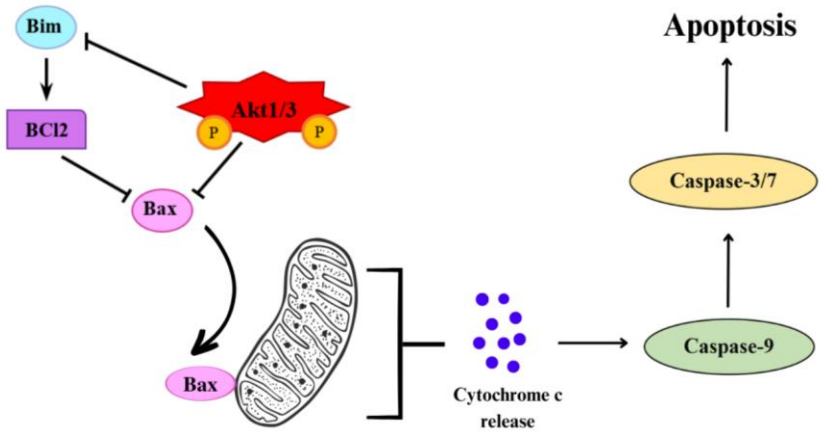

Figure 8- Simplified caspase cascade:
The figure displays the result of inducting activator and effector caspases after Bax is translocated to the mitochondria. This process is abrogated by Akt and is one of the methods in which Akt has anti-apoptotic effects. After Bax translocation, it signals for the release of cytochrome c (a pro-apoptotic mitochondrial protein), which activates caspase 9. Caspase 9 initiates the response of caspases 3/7, which can carry out apoptosis.

1.6.3 Rho-GTPases in cardiac IRI

Another pathway garnering interest in cardiac IRI is signalling by Rho-GTPases. Rho-GTPases are enzymes that convert nucleotide guanosine triphosphate (GTP) to guanosine diphosphate (GDP) (Hodge & Ridley, 2016; Salazar-Gonzalez et al., 2022). Rho-GTPases act as molecular switches in order to regulate cellular processes such as cell motility, cell growth, cell differentiation, etcetera (Shang et al., 2012; Hodge & Ridley,

2016; Buul et al., 2014). However, the most common role of Rho-GTPases is to regulate the actin cytoskeleton (Steichen et al., 2022). The speed of the conversion from GTP to GDP is enhanced by GTPase activating proteins (GAPs) (Buul et al., 2014). Further regulating the active/inactive GTP/GDP-bound conformations are guanine nucleotide exchange factors (or "GEFs") (Buul et al., 2014; Shang et al., 2012). There are many different small Rho molecules, however RhoA, and Rho-associated kinase (ROCK) are largely the focus in cardiac IRI research due to their involvement in angiogenesis, inflammation, and cell adhesion (Shang et al., 2012; Buul et al., 2014; Strassheim et al., 2019; Kilian et al., 2021). Active PI3K can also regulate RhoA/ROCK-induction, which can then have downstream effects on cell survival (Strassheim et al., 2019). RhoA in particular has been reported to have both cardioprotective and injurious effects in a context-dependent fashion (Auer et al., 2012; Strassheim et al., 2019; Kilian et al., 2021). Additionally, ROCK inhibition was demonstrated to have cardioprotective effects at abrogating IRI severity (Bao et al., 2004; Shang et al., 2012; Liu et al., 2017). Therefore, further understanding of the interplay of these small Rho's may be integral for IRI research.

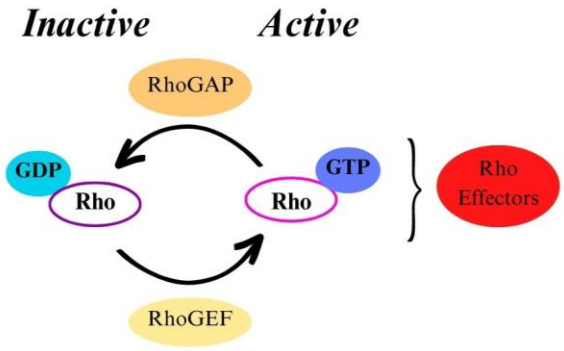

Figure 9- Rho GTP signaling:

The figure depicts small Rho molecule activation, which entails converting GDP-bound Rho to its active form (GTP-bound). This is aided by RhoGEFs and abrogated by RhoGAPs. When Rho is activated/GTP-bound, it can signal to downstream Rho effectors (such as ROCK).

1.7 Deleted-in-liver-cancer 1 (DLC1)

1.7.1 Human DLC's

Human DLC1 RhoGTPase activating protein (DLC1), is a protein coding gene located on chromosome 8 at 8p22 (NC_000008.11) (NCBI, n.d.; Gene Symbol Report, n.d.). Currently, DLC1 has 18 known transcript variants, of which 9 are protein-coding (GeneCards, n.d.; Ensembl, n.d.). DLC1 belongs to the "Deleted in liver cancer" or *DLC family* and has 2 closely related gene paralogs DLC2 and DLC3 (Wang et al., 2016). Each DLC gene paralog has distinct isoforms, but DLC1 (the interest of this project) has many including: DLC1α, DLC1β, DLC1γ, etc. The DLC1 gene is also orthologous (retained across species), which allows for preclinical research in small animal models. Recently, a plethora of different DLC1 isoforms have been further expanded upon to better understand their function/localization (Sabbir et al., 2010). DLC1α is the most common isoform of DLC1, which has a large overlap of unspecific exons shared with the DLC1β isoform (Fat Ko et al., 2010). Human DLC1β (also termed DLC1 isoform 1) is the longest associated isoform of DLC1 (Lin et al., 2014; Sabbir et al., 2010). The equivalent ortholog of DLC1β in mice is DLC1 transcript variant 1 (see table 1 for accession numbers). The focus of the study was on DLC1β; this was due to its high expression in the heart, necessity for fetal cardiac development, and the ability to control small Rho molecule expression.

Table 1- Information about human and mouse Deleted in Liver Cancer 1 β-isoform

Name:	Species:	NCBI Information:	Homology
DLC1 Rho GTPase activating protein (DLC1), transcript variant 1	Homo sapiens	7412 bp mRNA (NM_182643) & 1522 aa's (NP_872584.2)	*Needleman-Wunsch global alignment on NCBI:*
Deleted in liver cancer 1 (DLC1), transcript variant 1	Mus musculus	7636 bp mRNA (NM_001194940.2) & 1543 aa's (NP_001181869.1)	76% global alignment (Human & Mouse)

1.7.2 DLC1: Cancer and Rho-GTPase activity

DLC1 confers multiple isoforms of Rho-GTPase activating proteins, that have a specific affinity for the small Rho molecules (Ren & Li, 2021; Joshi et al., 2020; Braun & Olayioye, 2015). It has been characterized in the literature that DLC1 has preferential affinity for RhoA, but also interacts with RhoB, RhoC and CDC42 (Heering et al., 2009). DLC1 exhibits its Rho-GTPase activity by terminating the activation of Rho molecules to their activated, GTP-bound form (Kim et al., 2009). This in turn, terminates their downstream signaling and makes DLC1 an interesting target for disease-based applications, as many Rho molecules are implicated in aberrant physiological processes (Heering et al., 2009; Kilian et al., 2021).

As the name suggests, DLC1 has a connotation with liver cancer, as it is a tumour suppressor that is commonly lost in hepatocellular carcinomas (Wong et al., 2008). DLC1 functions as a tumour suppressor largely through its RhoGAP domain (Joshi et al., 2020; Ren & Li, 2021). Literature as dubbed DLC1 as crucial in normal and oncogenic states, due to its ability to control actin cytoskeletal remodeling, focal adhesions, cell migration and proliferation (Heering et al., 2009; Kawai et al., 2009). In oncogenic states, cancerous cells have increased metastatic abilities to extravasate and travel to form secondary/tertiary sites (Kim et al., 2009). Commonly, tumour suppressors are downregulated in cancers as an evolutionary adaptation of the cancer, to increases it's metastatic/proliferative abilities (Frey et al., 2022). DLC1 has been found to be downregulated via both genetic/non-genetic mechanisms in many cancers to date, including various colorectal, breast, prostate, and lung cancers (Sanchez-Solana et al., 2021; Frey et al., 2022; Ren & Li, 2021; Kim et al., 2009).

1.7.3 Cardiovascular indications of DLC1β

Interestingly, aside from DLC1's canonical role in cancers, an emerging role of DLC1 in the heart was later characterized. The DLC1β isoform specifically was found to be differentially expressed in the heart compared to other isoforms DLC1α and DLC1γ (Lin et al., 2014; Linnerz & Bertrand, 2021; Sabbir et al., 2010). Later, research interest in

DLC1β for its cardiovascular implications was spurred when studies were able to demonstrate that DLC1β loss/mutations was tied to cohorts of Chinese sporadic congenital heart disease (Lin et al., 2014). Since then, multiple studies have demonstrated that DLC1β is imperative for normal fetal cardiac development in zebrafish models (Durkin et al., 2005). This was further corroborated in mice, when researchers attempted to create DLC1β knockout mice for cancer-based research (Lin et al., 2014; Durkin et al., 2007; Sotillos et al., 2018). Ultimately, these mouse pups had poor viability due to an incomplete formation of the heart (Lin et al., 2014; Durkin et al., 2007; Sotillos et al., 2018). This provides evidence that DLC1β may be necessary for normal fetal cardiac development. Furthermore, it has been displayed that DLC1 is necessary for the normal vasculogenesis of the placenta (Linnerz & Bertrand, 2021).

Due to all of the stated cardiovascular implications, it was believed that DLC1β may be an important target in cardiovascular pathologies. However, the role of DLC1β in transplant associated cardiac IRI is currently uncharacterized. As mentioned, DLC1β's Rho-GTPase activity allows for the inactivation of RhoA, keeping it in its GDP-bound state (Tripathi et al., 2017). If this process could be targeted, it would be of interest in cardiac IRI research as RhoA inhibition is thought to be directly cardioprotective (Kilian et al., 2021; Tripathi et al., 2017; Tuuminen et al., 2011; Lauriol et al., 2014). DLC1-based RhoA regulation was demonstrated to be a result of Akt-phosphorylation in cancer-based studies (Tripathi et al., 2017). Further analyses of these interactions using proteomic approaches further substantiated that Akt was able to phosphorylate/modify DLC1 (Mertins et al., 2016). Studies have also demonstrated the ability of Akt/DLC1 to bind to one another and characterized a potential axis between PI3K/Akt/DLC1/RhoA (Hers et al., 2006). Although studies highlighting the interplay of PIK3CA (PI3K p110α subunit) and DLC1 in the context of cardiac IRI are limited, an interaction on an epigenetic level was noted in cancer-based/Paget's disease models (Kang et al., 2012). Therefore, it is of interest to further elucidate DLC1β's role in cardiac IRI, due to its cardiovascular implications and interactions with IRI-associated pathway targets. This would be the first preclinical study to characterize the role of DLC1β in transplant associated cardiac IRI and H/R models that is known.

1.8 Hypothesis and objectives

1.8.1 Hypothesis

It is hypothesized that DLC1β overexpression (OE) attenuates cardiac IRI by abrogating apoptotic injury via the PI3K/Akt & RhoA/ROCK pathways.

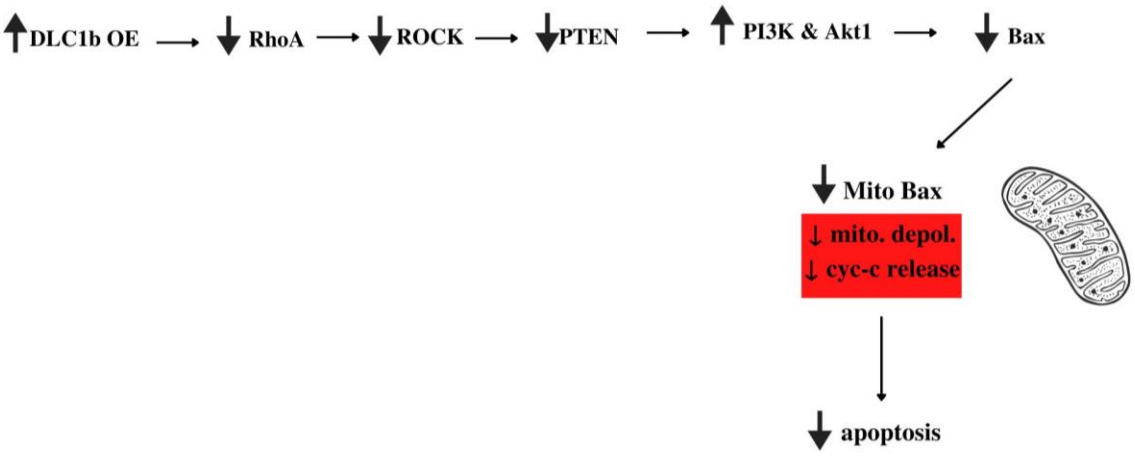

Figure 10- Schematic of working hypothesis of the study.

1.8.2 Specific Aims

The specific aims of the study include 1) To investigate DLC1β's role in cardiac IRI, 2) to analyze if DLC1β is a novel cardioprotective target, and 3) to explore pathways involved in DLC1β's protective effect against IRI.

1.8.3 Rationale

DLC1β's role specifically as a Rho-GTPase activating protein was a contributing factor to the formulation of the hypotheses. Rho-GTPase activating proteins or "GAPs" inactivate Rho-GTPases by GTP hydrolysis (as discussed in 1.6.3). This keeps the Rho-GTPase bound to GDP, and thereby reduces GTPase-specific signalling. DLC1β is a Rho-GTPase activating protein that impacts many small Rho molecules antagonistically but has a particular affinity for RhoA (Qian et al., 2007). It has been extensively studied

in literature that small Rho molecules have a pervasive role as “molecular switches” for disease-interacting pathways (Lauriol et al., 2014). Many studies have demonstrated the impact of modulating RhoA specifically on the development, extensiveness, and propensity to develop cardiovascular diseases (Lauriol et al., 2014). RhoA also has demonstrated an interplay with targets such as Akt1 and PI3K (Mertins et al., 2016; Tripathi et al., 2017; Hers et al., 2006; Prakash et al., 2000; Wong et al., 2001; Krugmann et al., 2002; Santy & Casanova, 2002; Xu et al., 1999; Rodrigues et al., 2000; Jackson et al., 2004; Voigt et al., 2006; Murga et al., 2000; Mitra et al., 2011). Therefore, due to DLC1β’s ability to negatively regulate RhoA by activating Rho-GTPases with specific RhoA affinity, it was of interest to analyze if this would have cytoprotective effects in the context of cardiac IRI.

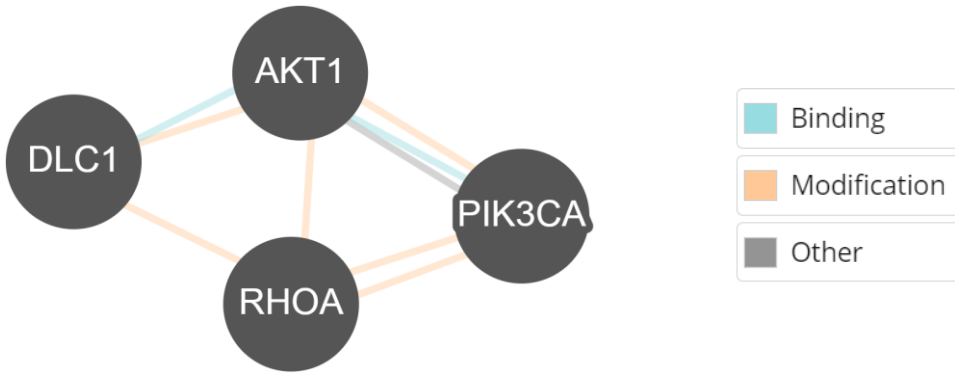

Figure 11- Pathway commons DLC1/Akt1/PI3K/RhoA interaction

The interactions between DLC1/Akt1/PI3K (PIK3CA is the gene name for the p110α subtype), and RhoA was visually demonstrated via Pathway Commons. The color lines represent binding, modification or other interactions noted in literature between the genes of interest. Image retrieved from Pathway Commons (www.pathwaycommons.org) for open access use.

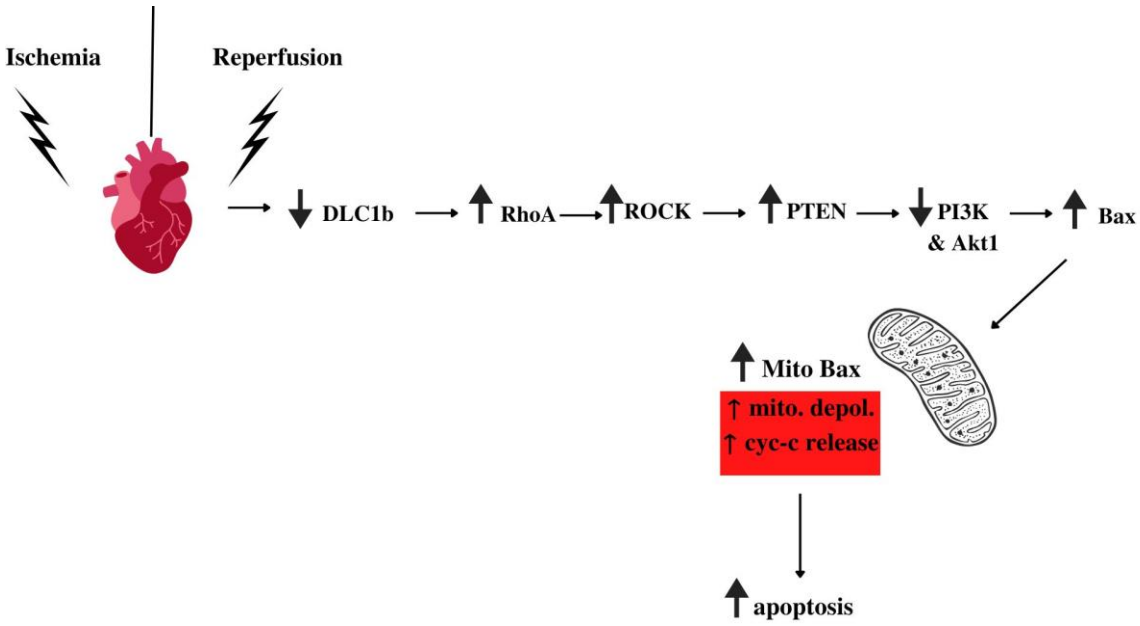

Figure 12- Proposed mechanism of cardiac IRI DLC1β downregulation

It is believed that DLC1β may be inactivated/downregulated or potentially lost during cardiac IRI. Due to this, there would be an increase in RhoA/ROCK/PTEN. An increase in PTEN would abrogate PI3K/Akt activation, increasing mitochondrial Bax translocation and subsequent apoptosis activation.

Chapter 2

2. Materials & Methods

The following are the specific protocols that were used to carry out all the experiments of the project, in addition to the materials necessary to complete them.

2.1 Animals

C57/BL6 male mice (6-8 weeks old and 23-25 grams) were purchased from Charles River Canada. Animals were transferred into the Matthew Mailing Centre Facility at least 48hrs before donor/recipient mice were utilized. All work with the animals was done by trained staff and was compliant with the approved animal use protocols (AUP#2020-033).

2.2 Cell Cultures

Two distinct established cell lines H9C2 (rat cardiomyocytes) as well as HL-1 (mouse cardiomyocytes) lines were used in the study. Cell-line specific methods will be denoted below. The specific volumes/concentrations/recipes of all solutions used for cell cultures can be summarized in Table 2 and Table 3 below.

Table 2- H9C2 Cell Culture Reagents

H9C2 Cell Culture Reagents	
Reagent:	***Recipe/Preparation:***
Culture Medium (CM)	44 mL Dulbecco′s Modified Eagle′s Medium (DMEM) + 5 mL Fetal bovine serum (FBS) + *500 µL penicillin/ streptomycin (P/S)* + 500 µL HEPES + 50 µL 2-Mercaptoethanol (2-ME)
Transfection Medium (TM)	44 mL DMEM + 5 mL FBS + 500 µL HEPES + 50 µL 2-ME

Table 3- HL-1 Cell Culture Reagents

HL-1 Cell Culture Reagents	
Reagent:	***Recipe/Preparation:***
Culture Medium (CM)	43.5 mL Claycomb Medium + 5mL FBS + *500 µL P/S* + 500 µL L-glutamine (L-glu- 100mM stock → 1mM final/ 50mL CM volume) + 500 µL Norepinephrine (NPP- 10mM stock → 0.1 mM final/ 50mL CM volume)
Transfection Medium (TM)	43.5 mL Claycomb Medium + 5mL FBS + 500 µL 100mM L-glutamine + 500 µL 10mM Norepinephrine
Precoating	Precoating was prepared by placing 0.2g of gelatin into a 1000 mL beaker. 1000 mL of sterile, distilled water was added before autoclaved (0.02% gelatin). Then, 250 µL of 1mg/mL fibronectin (Cat #F1141) was added to 49.75 mL 0.02% gelatin before filter-sterilized using a 50mL syringe + 0.2 µm Acrodisc filter (Cat #NC0784274). After filtering, the solution was placed in a 4°C fridge until use, and long-term storage aliquots were placed at -20°C. To use, 1mL precoating was added per T-25 flask, before incubated at 37 °C for at least an hour. Right before passaged cells were placed into flasks, the solution was vacuum-aspirated.
Norepinephrine	Firstly, a 30mM ascorbic acid solution was prepared: 100mL of 30mM ascorbic acid (Cat #A92902-25G) + 100mL ultra-pure RNAse/DNAse free water (Cat #10977035). Then, 80 mg norepinephrine + 25 mL 30mM ascorbic acid were added to beaker and mixed with a sterile disposable pipette. The solution was then filter-sterilized in a class- b safety cabinet using a 50mL syringe + 0.2 µm Acrodisc. 1.5 mL aliquots were placed in Eppendorf tubes and stored at -20°C until use (stock concentration of 10mM).
Soybean trypsin inhibitor	25mg of soybean trypsin inhibitor (Cat #17075029) + 100 mL Dulbecco's phosphate buffered saline were mixed in sterile beaker, and filter-sterilized (50mL syringe + 0.2 µm Acrodisc). 50mL aliquots were placed in 4°C fridge for use.

2.2.1 H9C2 Cells

H9C2 cells (rat cardiomyocytes) were cultured in T-75 flasks (Cat #83.3911.002) in culture medium consisting of Dulbecco′s Modified Eagle′s Medium (DMEM) (Cat #219-010-XK), fetal bovine serum (FBS) (Cat #080-150), P/S (Cat #450-201-EL), HEPES (Cat #SH30851.01) and 2-Mercaptoethanol (2-ME) (Cat #21985-023). When the cells were 80% confluent, they were dissociated with 0.05% trypsin (Cat #325-042-CL) after being washed with 3mL/ T-75 flask of Dulbecco's phosphate-buffered saline (D-PBS) (Cat #311425208). After brief washing, D-PBS was removed using a sterile tip/vacuum aspiration, before 3mL of 0.05% trypsin was added to the monolayer. The flask was then placed in an incubator at 37°C for 1-2 minutes until cells became un-adherent. Then, 6mL of pre-warmed culture medium was added to neutralize the trypsin, washing the monolayer using a serological pipette (Cat #1770). Then, the mixture of trypsin, medium and cells was placed in a 15mL conical tube (Cat #62.554.100) and centrifuged at 1500 rpm for 5 minutes. Supernatant was removed using a sterile tip and vacuum aspiration, before ~3mL of fresh medium was added to resuspend the cells. After resuspension, the cells were counted using a hemocytometer, and a portion would be used to analyze viability via trypan blue (see cell viability methods for further details). Approximately 250,000 cells/ T75 flask were re-seeded post-trypsin. Observed doubling time was ~ every 50 hrs.

2.2.2 HL-1 Cells

HL-1 cells were grown/passaged in T-25 flasks (Cat #83.3910.002) in culture medium consisting of Claycomb Medium (Cat #51800C-500ML), fetal bovine serum (FBS), penicillin/streptomycin (P/S), L-glutamine (L-glu) (Cat #609-065-EL), and norepinephrine (NPP) (Cat #A0937-5G). When the cells were approximately 80% confluent, they were dissociated using trypsin in the following manner. Firstly, a T-25 flask was precoated flask approximately 1hr before passaging (see Table 1 for precoating recipe followed). During this time, reagents were pre-warmed to room temperature in the dark for ~30 minutes before passaging (Claycomb medium is photosensitive). Cells were checked under a light microscope for typical morphology, confluence, and overall

medium color before splitting. Next, the medium was aspirated with a sterile tip and vacuum before the monolayer was briefly washed using 3 mL of pre-warmed D-PBS. D-PBS was aspirated 1mL of pre-warmed 0.05% EDTA trypsin was added. After 1 minute, the trypsin was removed using vacuum aspiration, before adding an additional 1mL of fresh 0.05% trypsin. Cells were allowed to incubate at room temperature for 2 minutes, before 1 mL (or equivalent trypsin volume) soybean trypsin inhibitor was added. Then, 2mL of culture medium was added and a serological pipette was used to wash the flask and transfer to a 15mL conical tube. The cells were centrifuged at 500g for 5 minutes, before the supernatant was aspirated and pellet was resuspended with at least 3mL of culture medium (depending on pellet size). Cell numbers were determined using a hemocytometer, and then cells were added into 5mL of fresh CM in a pre-coated flask. Typically, 70,000-150,000 cells/T-25 flask per passage was ideal to passage cells every 2 days. Observed doubling time was ~ every 22hrs.

2.2.3 Cryopreservation

Firstly, cryoliquid was prepared in a 15mL conical tube for re-suspension of desired aliquots. To prepare the cryoliquid, 9.0 mL of FBS was added to the 15mL tube using a 10mL serological pipette and pipette-aid (Cat #13-681-19). 1 mL of Dimethyl sulfoxide (DMSO) (Cat #3176) was then added to the FBS before mixing with a 1000 μL micropipette. Once cells were suspended with the prepared cryoliquid, they were placed in cryovials (Cat #377234) and placed in a -80°C freezer. For H9C2 cells, cryopreserved aliquots were typically at a concentration of 500,000 cells/1mL cryoliquid. For HL-1 cells, cryopreserved aliquots were typically at a concentration of 200,000 cells/1mL cryoliquid for best quality retrieval.

To retrieve cells post-cryopreservation (H9C2): A 37°C water bath was prepared, and cryovial with cells was removed from the -80°C fridge. The vial was placed in the water bath until fully melted, before being sprayed down with 70% ethanol and placed in the cell culture biological safety cabinet. Cells were then placed dropwise into a 15mL conical tube containing ~6mL of pre-warmed H9C2 culture medium. Then, cells were centrifuged at 1500 rpm for 5 minutes. The pellet was gently resuspended in 15mL of

culture medium, which was placed in a T-75 flask for incubation at 37°C (5% CO2) after brief observation under the microscope. The next day, cells were analyzed under the microscope to ensure adherence.

To retrieve cells post-cryopreservation (HL-1): Firstly, a T-25 flask was pre-coated with a 1mL of 0.02% gelatin/fibronectin solution (filter-sterilized using 0.2 µm Acrodisc). The flask was then placed in an incubator (37°C; 5% CO2) for 1hr. A 37°C water bath was prepared, and the cryovial was placed in the bath until melted (approximately after 2-3 minutes). The vial was not agitated at this time as it was noted this was injurious. Then, the cryovial was sterilized with 70% ethanol before transferred dropwise into a 15mL conical tube containing ~6mL of pre-warmed HL-1 culture medium. The cells were then centrifuged for 5 minutes at 500 g, before the supernatant was removed via vacuum aspiration, and the pellet was resuspended in 5mL of culture medium (pre-warmed). The T-25 flask containing pre-coating was then removed from the incubator, and precoating was removed before the cells/medium was added. Cells were briefly examined with a light microscope before being placed back in the incubator for 24hrs. 24hrs post-thawing, cells were checked to ensure monolayer adherence, and supplemental prewarmed medium was added (~2-3mL).

2.3 DLC1β plasmid overexpression model

2.3.1 In vitro DLC1β transfection

EndoFectin Max transfection reagent (Cat #EF013) was utilized to transfect H9C2 and HL-1 cells with either control pcDNA3.1 “empty” vectors, or DLC1β overexpressing plasmid. The DLC1β overexpression plasmid was received from Dr. Shawn Li, which was comprised of a human DLC1β insert with a pcDNA3.1 backbone. This was used due to its high homology to mouse and rat (see Table 1). The cells were seeded into 6-well plates 24hrs before transfection so that they were ~80-90% confluent. 1hr before transfecting, all of the necessary reagents were brought to room temperature in the dark, to ensure optimal conditions (as per company recommendations). Then, the plasmid DNA of interest (control or DLC1β) was diluted in Opti-MEM (Cat #31985-070). Next,

the EndoFectin reagent was gently mixed before being added to Opti-MEM to incubate at room temperature for 5 minutes. After incubation at room temperature, the EndoFectin + Opti-MEM mixture was then added to the Opti-MEM + DNA mixture. This was allowed to sit at room temperature for approximately 15 minutes, before being added to transfection medium (no antibiotic). This was then added to 6-well plates of cells (previous medium was vacuum-aspirated) and allowed to sit in a 37°C incubator for 24hrs. After 24hrs, downstream uses with transfected cells were carried out. The volumes of all reagents used per well of a 6-well plate can be found in the figure below.

Table 4- EndoFectin Max reagent volume/well (6-well plate):

Transfection	Cell #	TM (mL)	Opti-MEM (µL)	Endofectin (µL)	Plasmid DNA (µg)
Plasmid overexpression	100,000 cells/well (6-well plate)	1.8	195	2.5	2.5

The figure displays the amount of transfection medium, DNA (µg), transfection reagent and Opti-MEM medium required per well of a 6 well plate. This can then be scaled to fit the experiment of interest by multiplying by the number of wells needed per sample.

2.3.2 In vivo (Tail Vein Injection)

24hrs pre-donor heart retrieval, donor mice were given tail vein injections with solution containing in vivo-jetRNA Polyplus transfection reagent and pc3.1 empty vector control plasmid DNA/DLC1β overexpression plasmid DNA. The transfection reagent used followed standard operative procedures detailed by the company. A “blank” group of mice (un-transfected) were also given a tail-vein injection of just saline 24hrs pre-donor heart retrieval. Firstly, the plasmid was prepared ~20 minutes before injection. 40µg of plasmid DNA was added to labelled, Eppendorf tubes containing 100 µL of 5% glucose

solution. In a separate Eppendorf tube, the transfection reagent was prepared by adding 4.8 µL of vivo-jetPEI transfection reagent into a tube containing 100 µL 5% glucose solution. These were then briefly vortexed and mixed with a 1000µL pipette before adding plasmid DNA solution to the in vivo-JET solution. This solution was incubated at room temperature for 15minutes, before drawn into a 1mL syringe (27-gauge needle). For the tail vein injections, the tail of the donor mouse was placed in warm water. After which the mice were placed into a restraint device. Then, the tail vein injection was performed with the in vivo-jetPEI transfection reagent (summarized in figure 8). The mouse was then removed from the restraint and placed into its respective cage for observation. 24hrs post-IV, the donor mouse was sacrificed for experimental endpoint. The total preparation time of the plasmid was approximately 20 minutes, and the procedure time for the mouse was 2-3 minutes maximum. All tail vein injections were performed by our laboratory technician.

2.4 Ischemia-Reperfusion Models

2.4.1 GENbag Anaerobic Respirators (H9C2)

GENbag anaerobic respirators (Cat #97067-038) were utilized to simulate hypoxia for H9C2 cells. To do this, H9C2 cells were grown to ~80% confluence before the medium was removed and the cells were briefly rinsed with D-PBS (room temperature). Then, the cells were dissociated with 0.05% trypsin, before pelleted at 1500 rpm for 5 minutes. Following this, they were resuspended with prepared (pre-warmed) culture medium. Cells were counted via hemocytometer, to determine optimal concentrations. 2mL of culture medium was added per well of a 6-well plate, before ~200,000 cells/well were added. The cells were then placed in a 37°C incubator overnight to become adherent. The cells were then checked after 24hrs to ensure they became adherent, and then transfected (according to transfection protocols) when they had reached ~80% confluence. 24hrs post-transfection, the cells with transfection medium were removed from the incubator and medium was aspirated using a vacuum and sterile tip. Cells were briefly washed with 1mL D-PBS per well, carefully rotating the plate to ensure coverage before vacuum-removing again is then performed. And then, cardioplegic solution was added to each

respective well (1mL of UW solution/well of a 6-well plate). The plates were labelled and placed into the GENbag with the CO2 generator inside. A thermometer, as well as an anaerobic indicator strip were both added to the bag before sealing to ensure any exothermic reactions are documented/ the reaction was occurring. Then, excess air was removed from the bag, and the bag with plates/indicators inside were clip sealed. Sealed GENbags were then placed in the 4°C fridge overnight, for 24hr "hypoxia". After 24hrs, the plates were removed from the fridge, and the UW solution was carefully vacuumed aspirated. After which pre-warmed culture medium was added to the cells (2 mL/well of a 6-well plate) to simulate "oxygenation reperfusion" for 4 hrs.

2.4.2 Hypoxia/Oxygenation Reperfusion Chambers (HL-1)

Hypoxia-oxygenation reperfusion (H/R) experiments were carried out in a Whitley H85 hypoxystation (H/OR). Firstly, the gas tanks required for the experiment were checked to ensure was no leaking/enough gas to perform the experiment (~50 bar for overnight was average). 24hrs before the experiment was conducted, the refrigeration unit on Whitley H/OR chamber was turned on, and the temperature was set to 10°C. In addition, an external A/C unit was added in the room to ensure the desired temperature was reached. The next day, the chambers oxygen calibration was done approximately 2hrs before the experiment was started. When this calibration was done, the oxygen set point was re-entered, to ensure the set point (0.5% O2) was reached before adding plates into the chamber. 48hrs pre-H/R experiments, HL-1 cells were dissociated with trypsin, and seeded into 6-well plates (~70,000 cells/well). 24hrs pre-H/R, plates were transfected using Endofectin transfection reagent (see 2.3.1 for more details) before placed the incubator for an additional 24hrs in transfection medium (no P/S). After the chamber was calibrated, plates were removed from the incubator and transfection medium was vacuum aspirated. Acrodisc (0.2µm) filter-sterilized University of Wisconsin (UW) solution was added to plates- 1mL/well for a 6-well diameter. Then, the plates were placed in the chamber for 24hrs of hypoxia at 0.5% O2, 95% CO2 & 4.5% N. After 24hrs, the plates were removed from the machine, after the side chamber and main chamber was calibrated. Very quickly, the removed plates were checked under the microscope before UW solution was removed via vacuum aspiration and pre-warmed TM (2mL/6-well) was

re-added. The plates were then placed back in a 37°C incubator for 4hrs, and this time of adding fresh TM was considered the oxygenation-reperfusion period. For the project, 24hrs of ischemia and 4hrs of oxygenation-reperfusion was the selected timepoint.

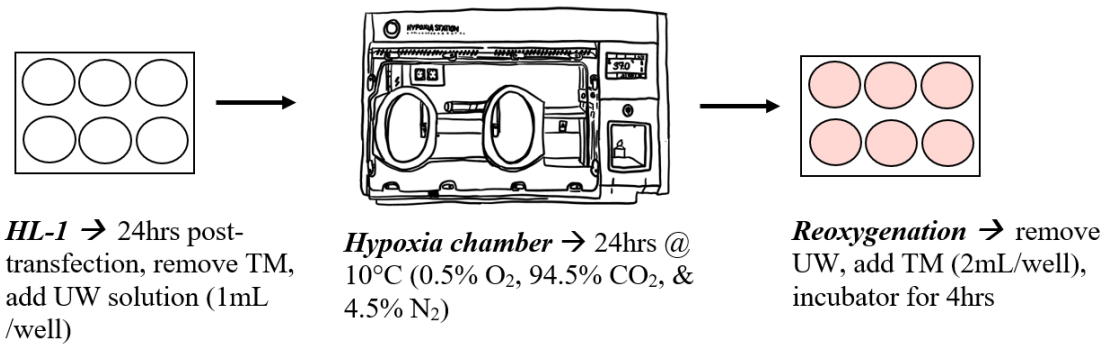

Figure 13- H/OR in HL-1 cells 24H/4R

The schematic above displays a summary of the workflow of H/OR experiments in HL-1 cells. First, cells are seeded and transfected the next day (24hrs pre-experiment). 24hrs post-transfection, the TM in the plates is changed out for UW solution, and placed in the chamber for 24hrs of hypoxia @ 10°C. After 24hrs, the plates are removed, and UW is carefully aspirated. Then, TM is added, and the plates are placed back at 37°C for 4hrs of reperfusion.

2.4.3 Ischemia-Reperfusion models: Syngeneic C57/BL6 Mouse Heterotopic Heart Transplantation (In vivo)

Organ retrieval and cold ischemia induction

In vivo, the ischemia time was considered the time between donor heart explant, until heterotopically transplanted into the syngeneic recipient mouse. Ischemia time for the study was 24hrs, and grafts were stored in UW solution at 4°C on ice until transplantation.

Mouse heart transplantation (MHT)

Then, donor mice grafts were obtained by the microsurgeon via median sternotomy. The excised graft is kept in UW solution for 24hrs post-explant at 4°C. 24hrs later, recipient mice are anesthetized with ketamine/xylazine (2% isoflurane maintenance during operation), before a midline laparotomy is performed to revascularize the donor heart via an "end-to-side" abdominal aorta anastomosis. Grafts were briefly rinsed with DLC1β/ pcDNA3.1 control vector and UW solution before transplantation. The wound was then sutured, and then mice were given buprenorphine.

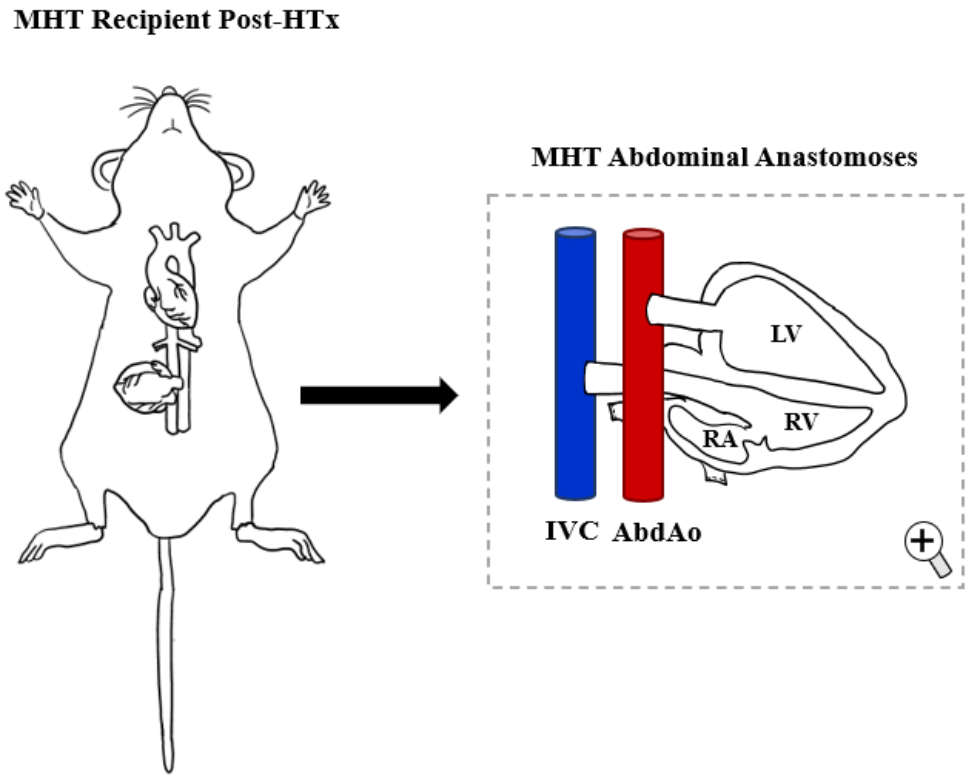

Figure 14- Mouse Heart Transplant Recipient Anastomoses schematic:
The figure depicts a schematic of the recipient mouse anatomy post-MHT. The abdominal donor heart graft is inferiorly located and palpable for heartbeat assessments. Post-operative care includes inspecting the wound to ensure the surgical site remains closed and clean. Drawn via Canva/Microsoft Draw function, inspired by Westhofen et al., 2019 PLoS one image(s) of mouse heterotopic transplantation.

End-point assays

The mice were sacrificed, and transplant hearts were collected at post-op day 1 (POD1), as well as post-op Day 7 (POD7) to examine the effect of overexpression of DLC1β on IRI via histopathological changes, apoptosis, cell infiltration, and fibrosis, by H&E staining, TUNEL, and Trichome staining.

Oct frozen sections for Immunohistochemistry

Tissues for frozen sections were placed in a cryomold. Then, the tissues were covered with ~2 drops of OCT compound (Cat #23-730-571), ensuring that no bubbles were present. Then, the labelled cryomold was covered with plastic wrap and placed in a -80°C fridge until use. When indicated for immunohistochemistry, frozen blocks of tissue were given to the histopathologist cryotome sectioning/subsequent staining.

Formalin-stored tissues for histopathology

Grossed tissue that was stored in formalin, was placed in pencil-labelled cassettes after being thoroughly washed with PBS to remove any blood. Cassettes with tissues were placed in labelled, specimen collection tubes and covered with 10% formalin. These tissues were allowed to sit for at least 24hrs before given to the histopathologist for paraffin-embedding for downstream storage/stains.

2.5 Cell Death/Viability Methods

2.5.1 Incucyte Sytox Green Assay

SYTOX Green dead cell stain (Cat #S34860) was utilized as a nucleic acid stain to perform cell death assays using an IncuCyte machine. Cells were passaged and seeded into Corning, 96-well plates 48hrs before analysis. 24hrs before analysis, cells were transfected with EndoFectin reagent and the plasmid of interest (see 2.2.1 for greater details). 24hrs after transfection, when cells are at an approximate density of 10,000 cells/well, 20 nM SYTOX Green was added/well in addition to 100μL of fresh transfection medium. The plates were then placed into the IncuCyte for 24-48hrs. Images

were taken of the plate every hour, and confluence/Green object count (cell death) were processed in the software and plotted.

2.5.2 Propidium Iodide (PI) microscopy

To visualize dead cells using propidium iodine, a 1mg/mL stock solution was created and 1μL/ well of a 6-well plate was added. After ~5 minutes, the plates were imaged under brightfield/red-fluorescence channel using an Upright, Nikon Eclipse microscope. Exported TIFFs were then used in QuPATH analyses to quantify the number of cells using a basic cell count feature/individual annotation for dead/fluorescent cells within the 4x field of view (40x magnification).

2.5.3 Trypan Blue Cell Viability

To determine viability with trypan blue, 0.4% trypan blue solution was prepared from stock (Cat #15250-061). Then, the cell suspension was pelleted at 500g for 5 minutes. The supernatant was then discarded, and cells were resuspended in 1mL of 1x PBS. After resuspension, 10 μL of PBS/cells + 10 μL of cell suspension was mixed together in an Eppendorf tube. This was incubated for 2 minutes at room temperature, before blue cells were counted via hemocytometer. The cells that were blue were considered to be non-viable/dead cells, and the un-stained cells were viable. Then, the percentage of viability was determined by the number of viable cells, divided the total number of cells (multiplied by 100).

2.6 Apoptosis Assay Flow Cytometry

2.6.1 Annexin V Apoptosis Assay

Firstly, 10x Annexin V binding buffer was diluted to 1x using ddH_2O. When cells had completed the desired H/OR timepoint, an ice-cold PBS scrape was used to collect the cells post-IRI. These samples were then pelleted via centrifugation at 500g for 5 minutes (~ 4 X 10^5 cells/sample). Then, the pellets were resuspended in ~100 μL of 1x Annexin V

binding buffer, before 1 µL of Annexin V- FITC and 5 µL of propidium iodide (PI) was added (100 µg/mL). This was then incubated in the dark for 10-15 minutes and run on a Cytoflex-S flow cytometer. The FITC signal detector/ phycoerythrin emission signal detectors (FITC/PE channels) were utilized for the visualization. Forward scatter (FS) versus side scatter (SS) area was used to highlight double negative cells. Then, non-debris populations are used for quadrant gating on Annexin V/PI plots. The acquisition settings (gain) utilized to acquire the apoptosis assay data was: FSC (150), SSC (150), FITC (10), YFP (10), APC (200), PE (5), PC7 (200).

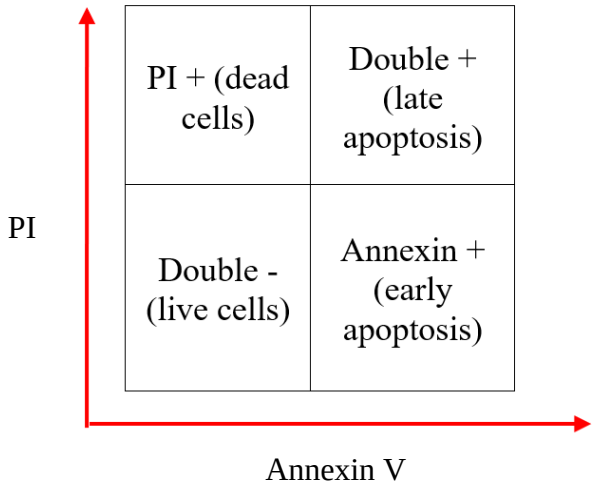

Figure 15- Quadrant gating for Annexin V/PI apoptosis assay via flow cytometry
The figure displays what the respective quadrants correspond to in apoptosis assay gating.

2.7 Cell Cycle Flow Cytometry

2.7.1 PI Cell Cycle Assay

Firstly, reagents needed were prepared including (sterile ice-cold PBS, ice-cold 70% ethanol, RNase A solution, and a Propidium Iodide (PI) solution (see Table 4). Next, 400,000 cells/well were seeded and transfected as per standard protocols. Post-trypsin dissociation, culture medium containing ~1,000,000 cells/tube were centrifuged at 500g/5

minutes. Then, supernatant was vacuum aspirated, and the pellet was resuspended with 3mL of ice-cold PBS. The cells/PBS were spun down again at 300g for 5 minutes. Then after pelleting, the PBS was vacuum aspirated, and cells were fixed using 3mL of ice-cold 70% ethanol added dropwise while vortexing. Then, the cells were kept on ice to fix for 30 minutes. After fixing, cells were pelleted at 300g for 5 min, and ethanol was vacuum aspirated with 10 µL tip to avoid loss. Then, the pellet was resuspended in 500 µL of PBS with an additional 50 µL of RNAse A solution. The solution was incubated at room temperature, protected from light for 30 minutes, before 5 µL PI was added per tube. After PI addition, the samples were incubated another 30 minutes in the dark.

Flow cytometry analysis

A Cytoflex S flow cytometer was used for all flow cytometry applications. After quality control analyses were done, graphs necessary for doublet discrimination/gating strategies were set up (SSC-A/FSC-A, PE-area vs PE-height, & a PE-A histogram). PE-height/PE-width to exclude doublets after debris/discrimination were both used. Then, samples were run slow at 40,000 events until complete, and gates were used to label the different phases of the cell cycle. Typically, the large peak is equivalent of the G0/G1 phase, the middle population is the S phase, and the final peak is the G2/M phase.

Table 5- Reagents for Cell Cycle Flow Cytometry

Reagent:	**Preparations necessary:**
Sterile-filtered, ice-cold PBS	Place 15-50mL (depending on the number of samples) in the -20 freezer or on ice.
70% ethanol	Prepare 15mL aliquot by adding 10.5mL 100% ethanol to a conical tube with 4.5mL ddH20 (or RNase free/culture grade).
RNAse A solution:	Dissolve 5mg RNAse A (100mg/mL stock) in 5mL of PBS (1mg/mL final). Add 0.1% of volume in Tween-20. Place in water bath at 95°C (30 min), followed by on ice (1hr) After the 1hr, use 0.2 µm Acrodisc to filter-sterilize. Aliquot and store in -20°C.
Propidium Iodide (PI) solution:	Dissolve PI in RNase-free water/ddH20 at 1mg/mL concentration. Store in -20°C for 2 years/4°C protected from light for ~2 months.

2.8 mRNA qPCR Analyses

2.8.1 Trizol RNA isolation (In vitro)

For the in vitro study, TRIzol (Cat #15596026) was used for RNA isolation. As adherent cells that were in a monolayer were used, medium was first removed and 1mL of TRIzol/ well of a 6-well plate were used (approx. 1.2 X 10^6 cells/1mL TRIzol). TRIzol was allowed to sit on the monolayer for 5 minutes (37°C) before cells were scraped and incubated with TRIzol for an additional 5 minutes (37°C). The lysate was pipetted up and down to wash the well and homogenize the cells, before being transferred into labelled Eppendorf tubes. At this time, the samples were either stored at -80°C until use, or RNA was isolated immediately. Cell samples in TRIzol were left for 5 minutes to allow for dissociation, before 0.2 mL of chloroform was added per 1mL tube. These were inverted 3-4 times, and then incubated at room temperature for 3 minutes. The samples were centrifuged at 12,000 g for 15 minutes (4°C). Next, the aqueous layer (clear) was transferred into fresh, labelled Eppendorf tubes. Then, 500 µL of isopropanol was added to the samples before 10-minute incubation at room temperature. The samples were centrifuged again at 12,000 g for 10 minutes (4°C), before the supernatant was discarded. 1 mL of 75% ethanol was used to wash the pellet after isopropanol supernatant was removed with a micropipette. The samples then were vortexed and centrifuged at 7500 g for 5 minutes (4°C). Additional 75% ethanol was decanted, and the samples were briefly centrifuged (~2 minutes) to remove additional ethanol. After, RNAse free water was used to resuspend the pellet, before samples were placed on a heat block for 10 minutes at 55°C. Following this, samples were left on ice for ~10 minutes, and centrifuged again to measure RNA concentration and 260/280 ratios via a Nanodrop machine.

2.8.2 cDNA conversion

All cDNA converted from mRNA for the project was done using a Moloney Murine Leukemia Virus (M-MuLV) Reverse Transcriptase kit from New England BioLabs (Cat #M0253L). In 200µL sterile tubes, 1 µg of template RNA was added to 2 µL M-MuLV buffer, 2 µL (50 µM) d(T)23VN/ “oligo DT’s”, 1 µL MuLV Reverse transcriptase (RT),

1 µL (10 mM) dNTP, and RNase-free water (added until 20 µL total volume/sample). The reaction was then placed in a Thermocycler at 42°C for 1hr; 65°C for 20 minutes. After this time, cDNA was removed, and diluted to appropriate volume with RNAse free water. Then, tubes were labelled with a symbol to denote dilution and placed in a -20°C freezer until use. Final diluted cDNA concentration of cDNA 10 ng/ µL (used 2 µL/20 µL reaction volume).

2.8.3 Quantitative Polymerase Chain Reaction (qPCR)

For qPCR analyses, a Low-ROX QuantStudio 3 Real Time PCR system was used to run samples. The samples were prepared on ice, using qPCR-specific pipettes, and sterile reagents to avoid no-template control (NTC) contamination from environmental contaminates. The master mix was prepared in 200 µL tubes by adding 10 µL Blastaq SYBR (Cat #G891), 7 uL RNase free water (Cat #10977015), and 1 µL of 10µM solution with forward primer/reverse primer (See Table 6 for sequences). The master mix was mixed with a micropipette before it was transferred into PCR tube strips. After which, 2 µL of cDNA was added well, the samples were briefly centrifuged in a Stratagene picofuge (Cat #31370). Then, the tube strips were placed in a machine-specific tube-strip retainer and lidded (Cat #4316567). The 20 µL reactions were subject to Comparative CT experiments with an initial 95°C 3-minute hold, followed by 40 cycles of 95°C (15 secs)/ 60°C (1 min), and a melt curve stage of 95°C (15 sec)/ 60°C (1 min)/ 95°C (5 sec). The annealing temperature of 60°C was used for all primers, except for the mouse DLC1β endogenous primer (61°C annealing temperature). Amplification and melt curves were analyzed in the Design & Analysis Software 2.6.0, and relative expression was calculated via the 2^-ΔΔCt method using GAPDH as a loading control (significance $p = < 0.05$).

Table 6- qRT-PCR primer sequences

Species	Target	NCBI Accession	Forward Seq (5'-3')	Reverse Seq (3'-5')
Mouse	Akt1	NM_001382431.1	TTCTGCAGCTATGCGCAATGTG	TGGCCAGCATACCATAGTGAGGTT
Mouse	Akt2	NM_001243027.3	CAAGGATGAAGTCGCTCACACA	GAACGGGTGCCTGGTGTTC
Mouse	Akt3	NM_181690.2	GTCGAGAGAGCGGGTGTTCT	TGTAGATAGTCCAAGGCAGAGACAA
Mouse	Bax	NM_017059	ATGGAGCTGCAGAGGATGATT	TGAAGTTGCCATCAGCAAACA
Mouse	BCl2	U34964	TGGGATGCCTTTGTGGAACT	TCTTCAGAGACTGCCAGGAGAAA
Mouse	Casp1	NM_012762.3	ACTCGTACACGTCTTGCCCT	AACATCAGCTCCGACTCTCCG
Mouse	Casp3	U49930	AATTCAAGGGACGGGTCATG	GCTTGTGCGCGTACAGTTTC
Mouse	Cttnb1	NM_001165902.1	GGCGGCCGCGAGGTA	TTAGTGGGATGAGCAGCGTC
Mouse	Cycs	NM_012839.2	CTGTGGAAAAAGGAGGCAAGC	TCCATCAGGGTATCCTCTCCC
Mouse	DLC1α	NM_001194940.2	AAAGCCATGGCTGCTCCGTG	ATCAATAGGGAACAGTAGATCTTC
Mouse	DLC1β	NM_001194941	GCTGGATGCTATCTGGAAAAAC	ATCAATAGGGAACAGTAGATCTTC
Mouse	GAPDH	NM_001289726	GGGGTGAGGCCGGTGCTGAGTAT	CATTGGGGTAGGAACACGGAAAGG
Mouse	MLC1	XM_036162915.1	GCCCTAGGACGAGTGAA	CCAAACATCGTGAGGAAC
Mouse	PI3K	NM_001256045.2	GGTTGTCTGTCAATCGGTGACTGT	GAACTGCAGTGCACCTTTCAAGC
Mouse	PTEN	NM_000314.8	GGTTGCCACAAAGTGCCTCGTTTA	CAGGTAGAAGGCAACTCTGCCAAA
Rat	Bax	NM_007527.4	TGGTTGCCCTCTTCTACTTTG	GTCACTGTCTGCCATGTGGG
Rat	Casp3	NM_012922.2	GAGCTTGGAACGCGAAGAAA	CTCTGAGGTTAGCTGCATCG
Rat	Cycs	NM_012839.2	CTGTGGAAAAAGGAGGCAAGC	TCCATCAGGGTATCCTCTCCC
Rat	DLC1β	NM_001370997.1	TGTCGTGGGTCAGAGACAAG	AAGGTGCAGATCGGAGTCAG
Rat	GAPDH	NM_017008.4	GGCACGTCAAGGCTGAGAATG	ATGGTGGGTGAAGACGCCAGTA
Rat/Mouse	DLC1-pl	N/A	TGACCCAGCCTTTAAACTTCTCTT	GATTGGGTGTCTTTGGTTTCA

2.9 Western Blotting

2.9.1 SDS-PAGE Gel Preparation

First, glass plates and spacers for the gel casting unit were washed/rinsed with 100% ethanol and left to dry. After dried, the gel casting unit was assembled, and the percentage gel of interest was prepared (see table below for details). Typically, 10% SDS-PAGE gels were used unless a large molecular weight target (such as PI3K/ROCK1) were the target antibody. After resolving gel of interest is prepared, a

disposable pipette is used to mix the solution before carefully pipetting into the casting unit. When it was ensured, the unit wasn't leaking, the resolving gel was pipetted until ~1.5-2mm from the top. The plates were then toped with 100% ethanol to ensure the gel did not dry out and then allowed to sit for 30 minutes at room temperature. After 30 minutes, the 4% stacking gel (recipe below) was prepared. Any additional 100% alcohol was decanted from the casting unit, before topped with 4% stacking gel and 1.5mm comb. These gels were prepared at least 30 minutes before use to ensure adequate time to set up or kept covered at 4°C until use.

Table 7- SDS-PAGE gel recipes

SDS-Gel %	Recipe
4% Stacking Gel	6.1 mL ddH_2O + 1.33 mL 30% Acrylamide/Bis Solution, 29:1 (Cat #1610156) + 2.5 mL Tris stacking gel buffer (0.5 M, pH 6.8) (Cat #1610799), + 100 µL 10% SDS + 50 µL 10% Ammonium Persulfate (APS) (Cat #1610700) + 10 µL TEMED (Cat #1610801).
8% Resolving Gel	4.7 mL ddH_2O + 2.7 mL 30% Acrylamide/Bis Solution, 29:1 + 2.5 mL Tris resolving gel buffer (1.5 M, pH 8.8) (Cat #1610798) + 100 µL 10% SDS + 50 µL 10% APS + 10 µL TEMED.
10% Resolving Gel	4.1 mL ddH_2O + 3.3 mL 30% Acrylamide/Bis Solution, 29:1 + 2.5 mL Tris resolving gel buffer (1.5 M, pH 8.8) (Cat #1610798) + 100 µL 10% SDS + 50 µL 10% APS + 10 µL TEMED.

2.9.2 Protein Isolation

24hrs post-transfection, as well as post-IRI samples were collected for Western Blotting by ice-cold PBS scraping. Initially, cell medium was vacuum aspirated, before 1mL of cold PBS/well of a 6-well plate was added. A cell scraper/1000 µL sterile pipette tip were used to scrape the cells and transfer into labelled Eppendorf tubes. The samples were then centrifuged at 500g for 5 minutes, before the PBS was carefully aspirated. The pellet was

then resuspended with ice-cold 1x RIPA buffer (See table below). These samples were then stored at -80°C until use.

When samples were to be used, they were removed from the -80°C freezer and thawed. Samples were vortexed twice, before being kept on ice for 30 minutes. Then, samples were centrifuged at 13,000g for 20 minutes (4°C). Following spin down, supernatant was collected and transferred to freshly labelled tubes. Bradford 1x dye (495 µL + 5 µL supernatant) was utilized to measure protein concentrations using a Genesys 10S spectrophotometer, after a 5-minute incubation step at room temperature (dark). Additional supernatant was stored in the -80°C freezer until use. The concentrations were recorded (µg/µL) and desired concentrations for samples were calculated. After adding appropriate amounts of 1x/4x loading buffer to supernatant, samples were boiled in water for 10 minutes at 100°C.

Table 8- Western Blotting Reagents

Reagent:	Preparations necessary:
1x RIPA lysis buffer	400 µL ddH_2O + 100 µL 5x RIPA lysis buffer + 5 µL PMSF (Cat # 36978O)
1x TBST	450 mL ddH_2O + 50 mL 10x TBST + 500 µL Tween-20
10x TBST	24 g Tris (Cat #15504020) + 88 g NaCl + 900 mL ddH_2O → adjust pH 7.6 (adjust volume to 1L)
1x Running buffer	450 mL ddH_2O + 50 mL 10x Running buffer
10x Running buffer	30.0 g Tris + 144.0 g glycine (Cat #G8898) + 10.0 g SDS + 1L ddH_2O (final pH 8.3)
Stripping buffer	7.5 g glycine + 0.5 g SDS + 5 mL Tween 20 + 400 mL ddH_2O → adjust pH to 2.2 → (adjust volume to 500 mL with ddH_2O)
Transfer buffer	14.40 g Glycine + 3.03 g Tris + 800 µL ddH_2O + 200 µL methanol (67-56-1) (-20°C for 1hr before use)
4x Loading buffer	1mL Tris-HCl (pH 6.8) + 0.4 g SDS + 2.0 mL glycerol (100%) + 0.2 mL β-mercaptoethanol (Cat #21985-023) + 500 µL 0.5 M EDTA + 4 mg bromophenol Blue (Cat #B0126)
1x Loading buffer	125 µL 4x loading buffer + 375 µL ddH_2O
5% Milk- Blocking Buffer	2.5 g powdered milk + 50 mL 1x TBST

2.9.3 Gel Electrophoresis

Firstly, protein standards were prepared using 5μL precision plus protein standards (colorimetric ladder) in 25μL 1x loading buffer. Then, prepared SDS-PAGE gels were placed in an electrophoresis apparatus after wells are briefly washed with some ddH2O. Then, the electrophoresis tank was filled with prepared running buffer (See Table 6) before samples were loaded. The gel was run at 80V for ~30 minutes until the ladder began to separate and all standards were visible. Then, run at 90V until ran to desired separation (~ another 1hr).

2.9.4 Transfer/Blotting

Firstly, after gel electrophoresis, the excess stacking gel was trimmed away. Then the membrane (Cat #1620264) was briefly soaked in methanol, before the transfer sandwich was assembled. It was ensured that all items of the transfer sandwich were continually cloaked in transfer buffer to ensure nothing dried out. Then, the cassette was placed in the transfer tank with a stir bar, ice pack, and transfer buffer. The tank was then surrounded by ice and run at 90V for 1.5 hrs on a magnetic stirrer. After this time, the membrane was removed from the sandwich and inspected to ensure adequate transfer occurred. The membranes were then blocked, shaking at room temperature in 5% milk (See Table 6). Prepared and thawed primary antibody was then added to the membrane after 1hr blocking was complete, and the membrane was left to shake at 4°C for 24hrs.

2.9.5 Secondary Antibody incubation, Imaging & Stripping

After 24hrs of primary antibody incubation, membranes were removed from primary antibody and washed 3 times (10 minutes/wash) in 1x TBST (See Table 6). After washing, rabbit anti-goat secondary antibody (1:5000) was added the to membrane until entirely covered, and this was allowed to incubate at room temperature, shaking for 1 hr. After which, the membrane was washed again 3 times (@ 10 minutes/wash) in 1x TBST. Following this, Clarity ECL developing solution (Cat #1705061) was added for 2 minutes, before the membranes were covered with plastic wrap and additional developing

solution was removed. Then, the membranes were imaged using a ProteinSimple FluorChem imaging system.

After imaging, membranes were stripped using stripping buffer (see Table 6). This stripping buffer was added to the membranes in a lidded container until covered, then agitated. The membrane + stripping buffer was then placed in a 37°C incubator for 30 minutes (removed to agitate every 5 minutes). Then, the membrane/stripping buffer container was placed to shake at room temperature for 10 minutes. After this, the membrane was rinsed with ddH_2O, re-blocked in 5% milk for 1hr, before 24hrs of primary antibody incubation at 4°C with antibody of interest.

Table 9- Western blotting primary antibody information

Antibody:	**Dilution:**	**Company**	**Cat #:**	**Molecular Weight:**
Akt-pan Rabbit mAb	1:1000	Cell Signal	#4691T	60
Bax Rabbit mAb	1:1000	Cell Signal	#14796	20
BCl-2 Rabbit mAb	1:1000	Cell Signal	#3498T	26
Caspase-3 Rabbit pAb	1:1000	Santa Cruz	#sc-7148	32
DLC1 Rabbit pAb	1:2000	ProSci	#30-796	52
GAPDH mAb	1:3000	Invitrogen	#AM4300	36
PI3K p110α Rabbit mAb	1:1000	Cell Signal	#4249T	110
PTEN XP® Rabbit mAb	1:1000	Cell Signal	#9188T	54
RhoA Rabbit mAb	1:1000	Cell Signal	#2117T	21
ROCK1 Rabbit mAb	1:1000	Cell Signal	#4035T	160

2.9.6 Densitometry via AlphaView

Analyses in AlphaView were conducted by exporting file information from the ProteinSimple FluorChem system and setting number of lanes in AlphaView. Then,

bands were auto detected (adjusted where necessary), and “width” was adjusted to be 20. Then, the data was exported to excel where densitometry could be performed. This was done by determining the densities of the protein of interest and the housekeeping control (GAPDH was used). Then, using the housekeeping control with the highest density, all housekeeping control values were divided be the highest density value. This resulted in the generation of the relative negative control density, which each sample could then be divided by their respective control.

2.10 Heart tissue preparations

2.10.1 Mouse Heart Grossing for Various Applications

Recipient mice were sacrificed via exsanguination under anesthesia (ketamine/xylazine) for experimental endpoints (POD1/POD7). After death was confirmed, heart grafts were excised using needle-nose forceps and surgical scissors during dissection. Grafts were bisected down the midsagittal plane and rinsed with sterile PBS to remove excess blood. The further details of the dissection can be seen in Figure 16 below.

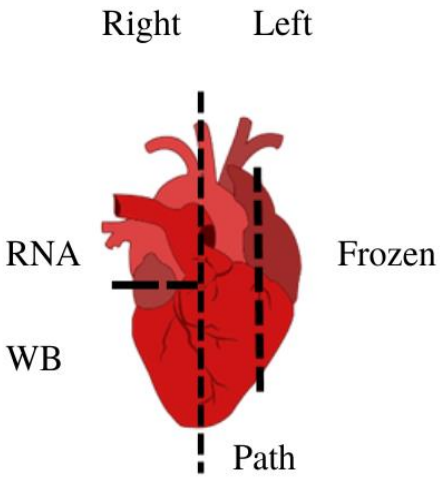

Figure 16- Mouse heart gross for applications

A peripheral section of the left side of the graft was grossed using a scalpel and forceps for frozen tissue preparations. Next, the right half of the bisected graft is grossed

horizontally for mRNA and protein applications. And finally, the residual aspect of the left-bisected graft is placed in a cassette and fixed in 10% formalin for histopathology.

2.10.2 Tissue homogenization for RNA/Protein isolation

Tissues were homogenized for RNA/Protein preparation isolation using a stick homogenizer and trizol reagent or ice-cold 1x RIPA buffer (respectively) (Cat #15596-026). *For RNA*: 1mL of Trizol was added to the tissue in flat bottom tubes. After the homogenizer is sterilized, the homogenizer was placed into the sample tube until sample is entirely ground. Then, the tip of the homogenizer was rinsed in 1X PBS every time it was used. After each rinse, the homogenizer was dried with kim-tech wipes (Cat # S-8115) to remove any additional PBS. Then, samples were stored at -80°C until use. *For protein*: 1mL of 1x RIPA buffer was added to the tissue in flat bottom tubes. After the homogenizer is sterilized, the homogenizer was placed into the sample tube until sample is entirely ground. Then, the tip of the homogenizer was rinsed in 1X PBS every time it was used. After each rinse, the homogenizer was dried with kim-tech wipes to remove any additional PBS. Then, samples were stored at -80°C until use.

2.11 Histopathology

Histopathology was performed by the histopathology core at Western University/ Robarts Research Institute.

2.11.1 Hematoxylin & Eosin (H&E)

Hematoxylin and Eosin (H&E) staining was performed using paraffin embedded heart tissues. The formalin-fixed tissues were processed and embedded in paraffin blocks for downstream stains. For H&E, the samples were initially deparaffinized, before they were dehydrated. They were then stained with hematoxylin, before differentiated and a bluing agent was applied. After which, the eosin stain was applied, the samples were dehydrated again, and cleared for cover-slipping and imaging with brightfield microscopy. Sections for H&E were 5 μm thickness. Slides were scored single-blinded by an academic pathologist (specialized in histopathology). For H&E staining, grafts were scored semi-

quantitatively from 0-4 based on injury category (0= 0%, 1= <25%, 2= 25-50%, 3= 50-75%, 4= 75+%). The categories for H&E-stained tissues included neutrophilic infiltrate (PMN's), lymphocytic infiltrate, infarction/pre-infarction, and overall injury grade.

2.11.2 Terminal deoxynucleotidyl transferase dUTP nick end labeling (TUNEL)

10 μm paraffin sections were deparaffinized, washed and permeabilized following TUNEL kit instructions (Cat #ab206386). Then, sections were washed and blocked before labelling and counterstain was applied. No hematoxylin overstain was applied. Slides were scored single-blinded by an academic pathologist (specialized in histopathology). For TUNEL slides, grafts were scored based on the pathologist's estimated percentage of DAB+ nuclei. For further quantification of DAB+ nuclei, QuPATH 0.4.3 was utilized. Briefly, in QuPATH 0.4.3, an initial directory was created. Next, whole slide images of TUNEL-stained tissues were imported into the software for TUNEL+ quantification. After importing, each sample was noted at "Hematoxylin-Other". A region of interest (ROI) for hematoxylin positive (nuclear) cells was selected, and stain vector was set to the ROI. DAB+ stain vectors were set using ROI, and then stain vectors were estimated.

2.11.3 Trichrome Staining

Connective tissue staining was completed using a trichrome kit (Cat #ab150686). Paraffin embedded tissues were used for staining and were initially deparaffinized. Samples were then stained with a series of solutions (Weigert's Hematoxylin, Biebrich Scarlet/ Acid Fuchsin/ Aniline Blue) before they were rinsed and mounted for brightfield microscopy. POD7 slides that were subject to trichrome (TRI) staining were scored single-blinded by an academic pathologist (specialized in histopathology). Grafts were scored semi-quantitatively from 0-4 based on injury category (0= 0%, 1= <25%, 2= 25-50%, 3= 50-75%, 4= 75+%). The POD7 grafts stained with TRI were scored semi-quantitatively based on the amount of fibrosis, neutrophilic infiltrate, lymphocytic infiltrate, infarction/pre-infarction, and overall injury grade. Total injury scores/category were

compiled for comparison, dubbed, “cumulative injury grade”. Histopathology images were taken post-stain where Control vector POD7 and DLC1β-OE grafts sections were imaged at 20x, 40x, 100x, and 200x magnification using a Nikon 90I microscope. Whole slide imaging was also conducted on all trichrome samples by tiling 40x magnification images via Nikon 90I brightfield microscopy.

2.11.4 Imaging/QuPATH analyses

All of the imaging for the project was conducted on a Nikon 90I microscope. Images were taken for each sample with brightfield microscopy at 20x, 40x, 100x, and 200x magnification. Whole slide imaging was completed using NIS-Elements software and the Nikon 90I microscope, by tiling 40x magnification images. Downstream applications such as TUNEL+ percentage, cell counts and annotations were conducted via QuPATH 0.4.3 software (Bankhead et al., 2017).

2.12 Statistical Analyses

2.12.1 GraphPad Prism

GraphPad Prism (version 8) was utilized to conduct statistical analyses. Student’s t-tests for two groups and or One-way ANOVAs for three groups or plus were utilized for data analyses. Data was plotted using calculated means, +/- standard deviation. At least 3 replicates were utilized for each sample, noted by n= # samples in each respective figure caption. A p-value of < 0.05 was utilized for statistical significance.

Chapter 3

3. Results

3.1 In vitro, H/R results in cell death/apoptosis

To study the effect of H/R on heart cells in vitro, mouse cardiomyocyte cell line HL-1 cells were cultured overnight, subjected to hypoxia (10°C; 0.5% O2) in a hypoxia-oxygenation reperfusion chamber with UW solution for 24hrs, followed by reoxygenation for 4hrs (37°C; 5% CO2, & 21% O2).

Trypan blue staining was used to analyze HL-1 cell viability post-H/R (Figure 17A). After 24H2R, the cell viability was reduced compared to the normoxia group, however, the change was insignificant ($p=0.2554$). When the reperfusion time was increased to 24H4R, cell viability was significantly decreased compared to normoxia groups ($p=0.0010$). Additionally, an even more significant reduction in viability was noted after 24H8R ($p= <0.0001$).

Changes in cell morphology were also noted as reperfusion time increased (Figure 17B). At 24H2R, HL-1 cells appeared more confluent, with little circularized cells (Figure 17B). Overall, at 24H4R, the morphology of the cells was similar to normoxia controls. This is conjunction with the insignificant viability was why this time point was not selected for the ideal timepoint. At 24H4R and 24H8R, the morphology of the cells displayed phenotypic changes including increased circularity, notable detached cells, and a slightly-angiogenic shape (Figure 17B). Due to the feasibility of this time points completion within the workday, as well as its high replicability, 24H4R was utilized for H/R experiments going forward.

Next, I detected the mRNA of apoptosis related genes (Akt1, Bax, Caspase 3 and Cycs) by qRT-PCR. The relative expression of Akt1 (an anti-apoptotic target) was statistically downregulated after 24H/4 R ($p=0.0405$) compared with normoxia groups. It was also observed that pro-apoptotic targets such as Bax ($p=0.0002$), Casp3 ($p=0.0118$), and Cycs ($p=0.0011$) were all statistically increased after H/R (Figure 17C).

I also investigated H/R on rat H9C2 cells to validate the findings in HL-1 cells. H9C2 cells were cultured overnight, subjected to hypoxia in GENbag anaerobic respirators with UW solution at 4°C for 24hrs. After hypoxia, the cells were subject to 4hrs of reoxygenation in a complete medium at 37°C (5% CO2, & 21% O2). After the timepoint was complete, proteins were collected and analyzed by Western blotting. The membranes were imaged and displayed in Figure 17D with normoxia controls as well as 24H4R groups. It was seen that Bax protein expression increased after H/R, however the difference was insignificant ($p=0.0904$) (Figure 17E). Additionally, after hypoxia Caspase 3 protein expression was found to be statistically increased ($p=0.0142$) (Figure 17E).

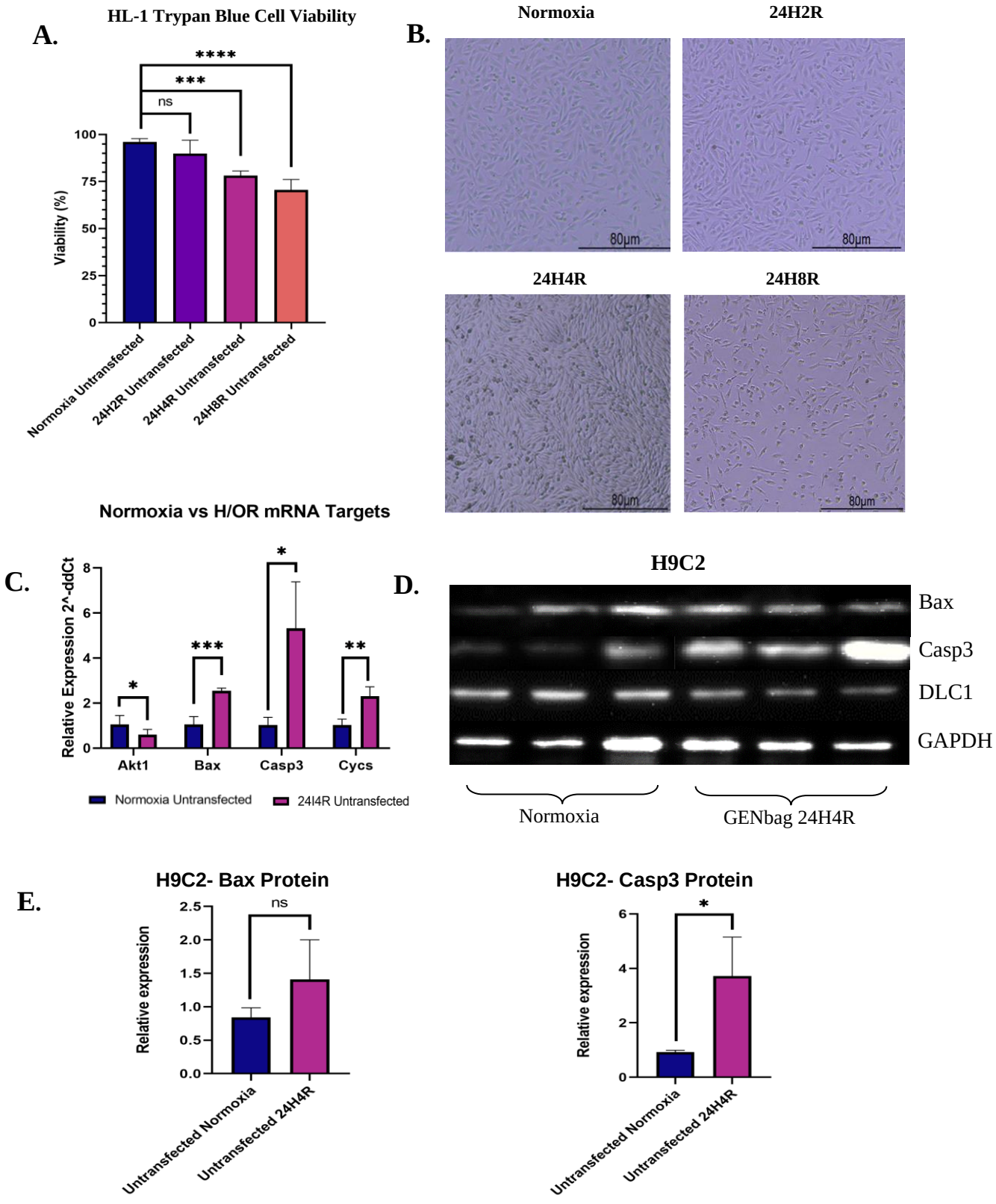

Figure 17- H/R increased cell death and apoptosis.

(A) Normoxia HL-1 cells and H/R samples with various reperfusion times were analyzed via trypan blue hemocytometer analyses for cell viability. (B) A Nikon Eclipse

microscope was used for imaging with brightfield microscopy at 40x magnification to analyze cell morphology of HL-1 samples (Normoxia/24H2R/24H4R & 24H8R). (C) mRNA relative expression of anti-apoptotic targets (Akt1) and pro-apoptotic targets (Bax, Casp3, Cycs) was performed via qRT-PCR, and displayed as relative expression (2^-ddCt). (D) Western blotting was performed on normoxia/24H4R H9C2 for mAb's Bax/Casp3/and DLC1. (E) Protein relative expression was calculated using GAPDH as a housekeeping/normalizing control. Data is shown as mean ± SD (n=3) where *=p<0.05, **=p<0.01, ***=p<0.001, ****=p<0.0001.

3.2 DLC1β is downregulated in cardiomyocytes post-H/R

To determine DLC1β expression after H/R, H9C2 cells were subject to protein/mRNA analyses via qRT-PCR and Western blotting. In rat (H9C2) cells after 24H4R of GENbag anaerobic respiration, DLC1β mRNA was statistically downregulated compared to un-transfected/normoxia cells (p= 0.0171) (Figure 18A). These findings were further substantiated in H9C2 cells on the protein level, demonstrating a statistically significant reduction of DLC1β after 24H4R (Figure 18C/E, *P*=0.0164).

HL-1 DLC1β expression after 24H4R of chamber H/R was also measured, and cells were subsequently collected for protein and mRNA analyses via qRT-PCR and Western blotting. It was demonstrated that DLC1β mRNA was statistically downregulated in HL-1 cells compared to un-transfected/normoxia cells (p= 0.0164) (Figure 18B). Furthermore, DLC1β downregulation after H/R was demonstrated in HL-1 cells on the protein level DLC1β after 24H4R (Figure 18D/F, *P*=0.0087). Therefore, both in vitro cell lines demonstrated DLC1β downregulation after H/R.

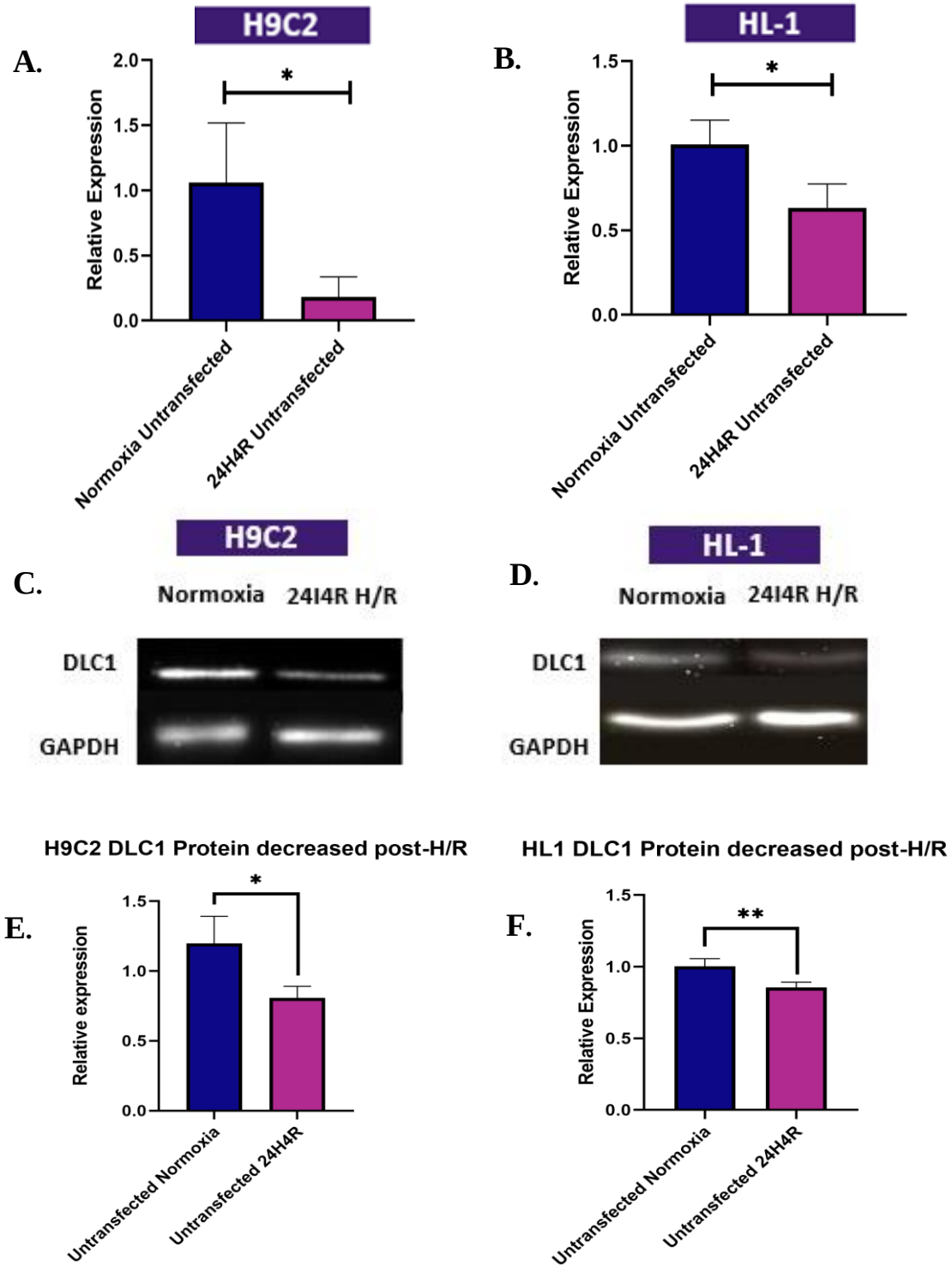

Figure 18- DLC1β is downregulated in rat/mouse "cardiac IRI" models.

H9C2 cells were cultured and subjected to normoxia/24H4R in GENbags. (A) DLC1β mRNA relative expression standardized to normoxia controls was calculated. (B) HL-1 cells subjected to normoxia/24HR (H/OR chamber) were also analyzed for DLC1β

mRNA expression. Western blotting with DLC1 antibody (1:1000) was performed on H9C2 (C) and HL-1 cells (D) respectively, and relative expression standardized to GAPDH normalizing controls were used to calculated densitometry via AlphaView software (E/F, respectively). Data is shown as mean ± SD (n=3) where *=$p<0.05$, & **=$p<0.01$.

3.3 DLC1β plasmid is capable of overexpression in transfected H9C2/HL-1 cells

A DLC1β-OE plasmid kindly provided by Dr. Shawn Li was utilized for the purpose of the study (See Appendix A for the human DLC1β insert sequence in the pcDNA3.1 backbone).

HL-1 cells were cultured and passaged at least 3 times after recovery from cryopreservation. The HL-1 cells were then collected 24hrs after Endofectin transfection with the DLC1β-OE plasmid for mRNA analyses via qRT-PCR. Under normoxia conditions, it was found endogenous expression was not affected, but a statistically significant increase in mRNA relative expression via RT-qPCR was found ($p=0.0091$) (Figure 19A).

HL-1 cells were further cultured and subjected to 24H4R via H/R chambers. After 24H4R, HL-1 samples transfected with DLC1β-OE plasmid were collected for mRNA analyses via qRT-PCR. It was displayed that transfected with DLC1β-OE plasmid resulted in a significant upregulation of DLC1β plasmid mRNA compared to control-vector transfected and un-transfected controls ($p=0.0052$) (Figure 19B). This statistically significant increase in plasmid-specific mRNA did not affect endogenous DLC1β levels during 24H4R (Figure 19B) This demonstrates the ability to overexpress DLC1β mRNA in HL-1 cells after hypoxia/reperfusion (24H4R) as well without impacting endogenous DLC1β expression.

On a protein level, statistically significant overexpression of DLC1 was noted when HL-1 cells were transfected with DLC1β-OE plasmid during both normoxia conditions ($p=0.0009$) (Figure 19C/D) and 24H4R conditions ($p=0.0253$) (Figure 19E/F).

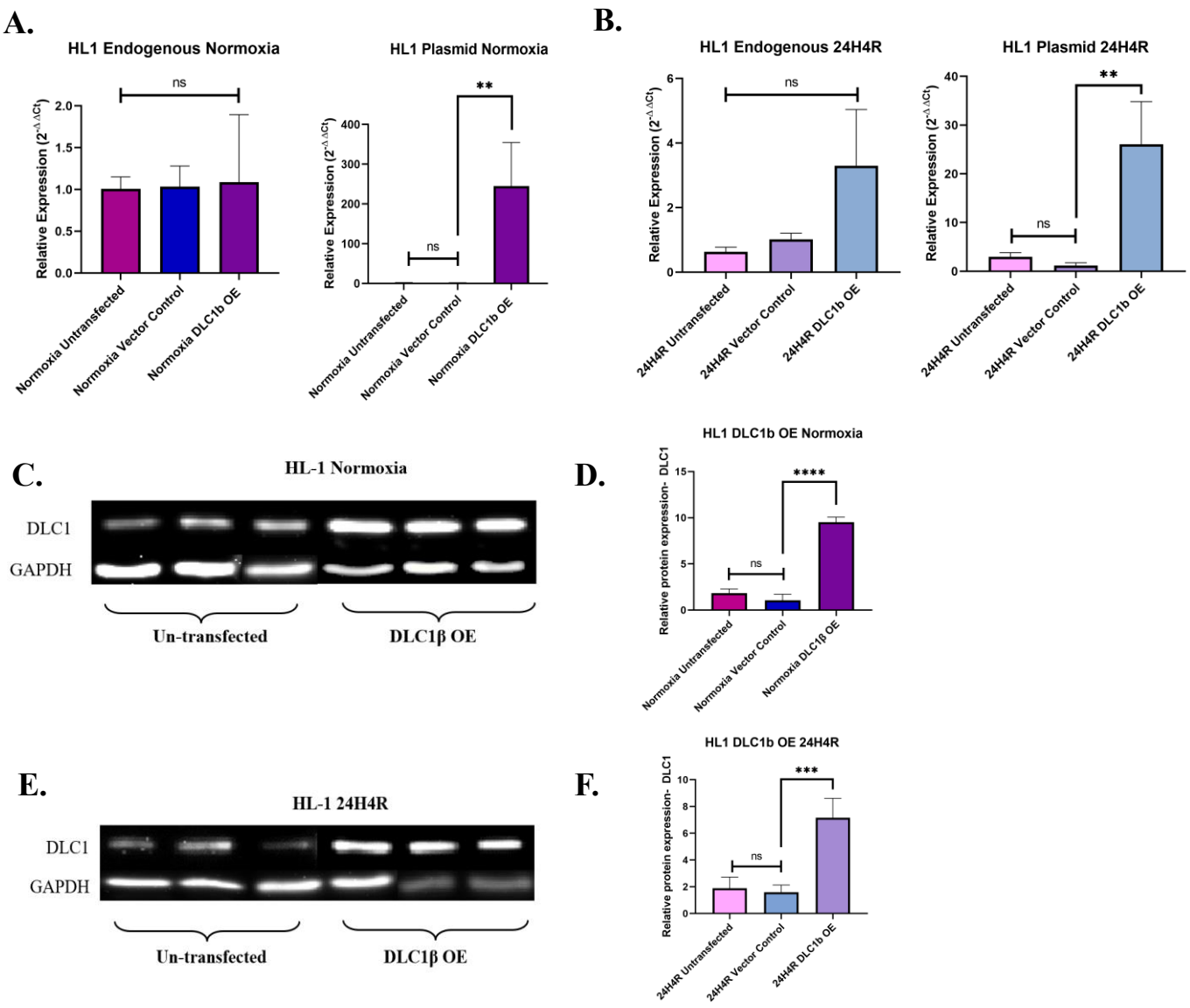

Figure 19- DLC1β is overexpressed in HL-1 cells transfected with DLC1β plasmid. HL-1 cells were serially passaged and subjected to normoxia and 24H4R H/R. Some samples were additionally transfected with DLC1β-OE plasmid to observe if overexpression was possible. (A) Under normoxia conditions, DLC1β-OE was possible without significantly impacting endogenous DLC1β expression; visible via qRT-PCR relative expression analyses. (B) HL-1 cells subjected to 24H4R also demonstrated statistically significant increases in DLC1β mRNA conferring overexpression. (C) DLC1β protein expression was further analyzed under normoxia conditions via Western blotting using GAPDH as a normalizing control. (D) Relative protein expression for normoxia conditions was expressed via AlphaView densitometry. (E) HL-1 cells post-

24H4R were also analyzed via Western Blotting, and (F) relative expression was also determined. Data is shown as mean ± SD (n=3) where *=p<0.05, **=p<0.01, & ***=p<0.001.

3.4 Overexpression of DLC1β reduced H/R induced cell apoptosis

Annexin V flow cytometry was used to quantify the number of apoptotic/alive and necrotic cells in samples subjected to H/R. The assay characterizes the cells as follows: Annexin V + cells (early apoptotic), PI + cells (necrotic) and double + (late apoptotic) cells. H9C2 cells 24hrs post-EndoFectin transfection were subjected to GENbag H/R (24H4R). After reperfusion time was completed, the cells were collected for annexin V flow cytometry. Un-transfected, control vector transfected, and DLC1β-OE cells were compared in H9C2 models after 24H4R H/R (Figure 20A/C). In H9C2 cells, DLC1β-OE samples displayed statistically less annexin V+ cells (p= 0.0110) and double positive cells (p=0.0102) compared to vector controls (Figure 20A/C). No statistically significant difference in PI+ cells was found in H9C2 cells.

Annexin V flow cytometry was also performed in HL-1 cells post-24H4R chamber H/R for cell apoptosis/death. In HL-1 cells subjected to 24H4R H/R, DLC1β-OE resulted in statistically less annexin V+ cells and double positive cells compared to un-transfected/control vector samples (Figure 20B/D) (Annexin V+ p= 0.0039 & Double + p= 0.0253). There also appeared to be a reduction in necrotic cells (PI+) in HL-1 samples, however it was not statistically significant (p= 0.1524) (Figure 20D).

Samples of control vector-transfected/DLC1β-OE-transfected HL-1 cells were also collected post-24H4R H/R for mRNA 2^-ddCt relative expression. The anti-apoptotic targets analyzed were Akt1, Akt2, BCl2, and MCL1 (see Table 6 for sequences/NCBI accession information). In DLC1β-OE samples post-H/R (24H4R), significant upregulation of Akt1 (p=0.0476) and Bcl2 (p=0.0036) was noted compared to vector controls. A slight downregulation appeared present between Akt2 and MCL1 in DLC1β-OE samples, however this was insignificant (p= 0.0998; p= 0.1183 respectively) (Figure 21A). The analyzed mRNA pro-apoptotic targets were Bax, Cycs, Casp3, and Casp1

(Figure 21B). Bax (p=0.0321), Casp3 (p= 0.0023), and Cycs (p=0.0160) were all statistically downregulated in DLC1β-OE cells compared to vector controls post-H/R. However, the pro-apoptotic target Casp1 had an insignificant difference compared to vector controls post-4H4R H/R (p=0.0760) (Figure 21B).

HL-1 cells were additionally subjected to brightfield/fluorescence microscopy using a Nikon Eclipse microscope after 24H4R, once 1μL of PI was added per well of a 6-well plate (Figure 21C). The samples were imaged at 40x magnification with brightfield microscopy, and slight differences in morphology were observed between Untransfected/transfected samples. These changes in morphology noted include increased circularity, slightly angiogenic shape, and notably more cells detached from the monolayer. The PI fluorescence microscopy was also performed at 40x magnification in a stack with the brightfield photos, for later quantification via QuPATH software (Figure 21C).

The brightfield and PI images were added into QuPATH software and subjected to initial basic cell counts. This determined the number of cells within the field of view via the brightfield images, used later for calculations. Then, the PI fluorescence images were imported into QuPATH, and used to train a pixel classifier. The software was then used to quantify the number of red objects within the field of view, which was utilized in conjunction with the total cell count (Figure 21D). PI positive percentage (PI + %) was then calculated and repeated for 3 more experimental replicates (n=3) to generate Figure 21E. However, no significant differences in cell death post-H/R (24H4R) were notable between vector control and DLC1β-OE samples via QuPATH PI quantification (p=0.2105) (Figure 21D).

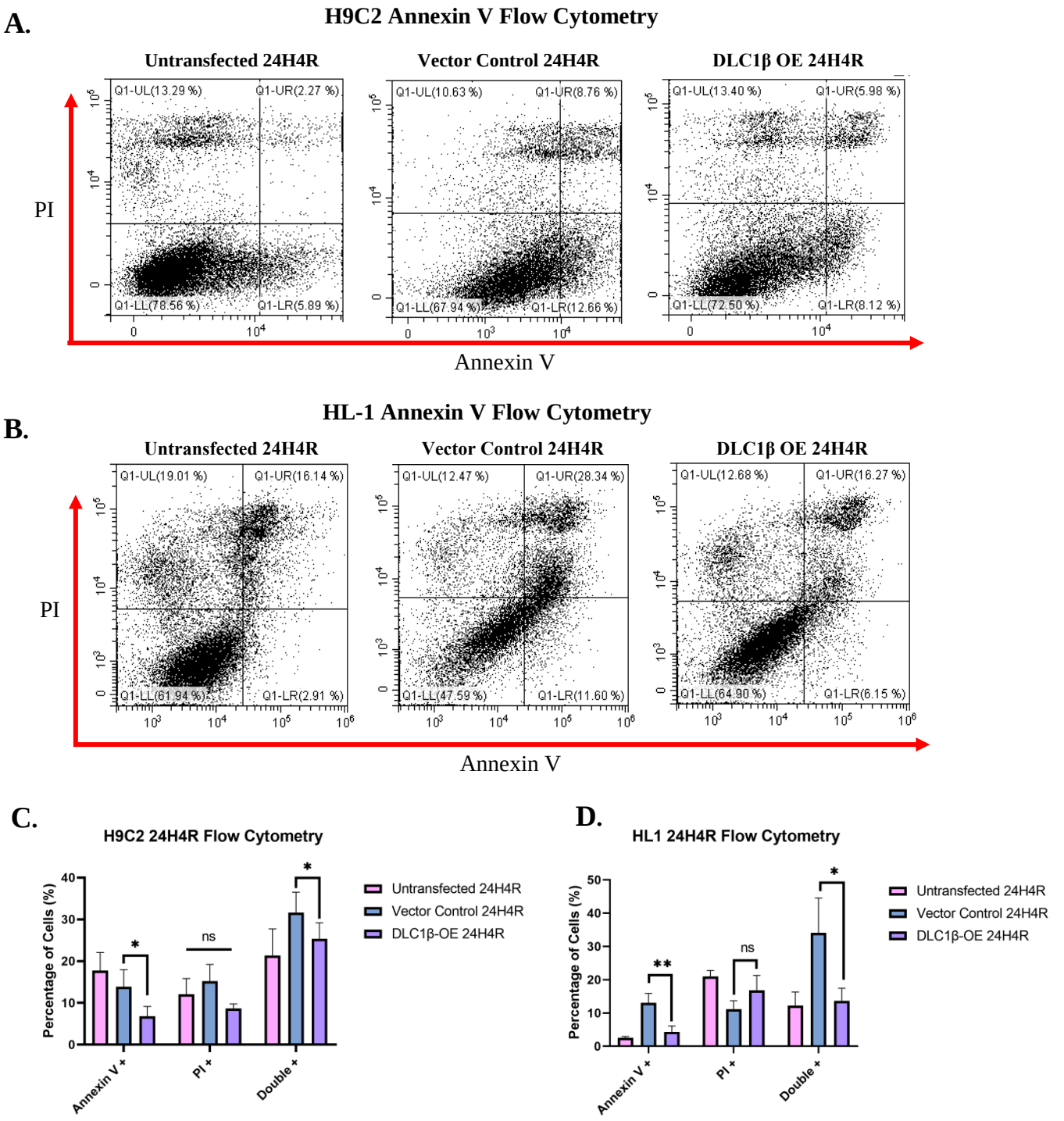

Figure 20- DLC1β overexpression reduced apoptosis induced by H/R.

(A) H9C2 24H4R un-transfected cells, control vector cells and DLC1β-OE cells output from Annexin V flow cytometry. (B) HL-1 24H4R un-transfected cells, control vector cells and DLC1β-OE cells output from Annexin V flow cytometry. (C-D) Represent H9C2/HL-1 percentage of cells from the quadrant gates where data is shown as mean ± SD (n=3) where *=$p<0.05$, & **=$p<0.01$.

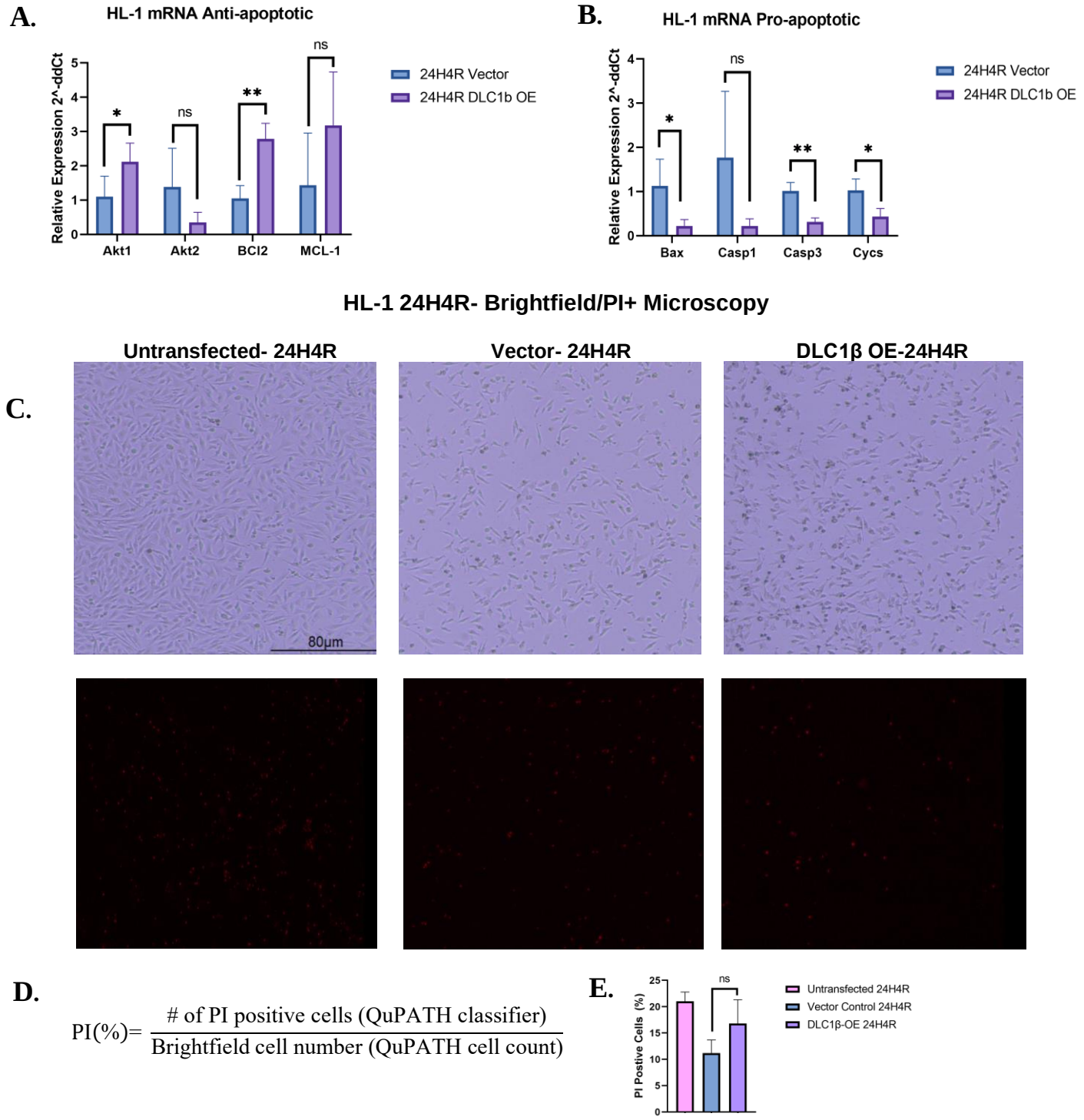

Figure 21- DLC1β-OE in HL-1 cells impacts pro/anti-apoptotic mRNA post-H/R. (A) After 24H4R, DLC1β-OE samples were collected for mRNA analyses via 2^-ddCt qRT-PCR to analyze anti-apoptotic targets (A) and pro-apoptotic targets (B). (C) After 24H4R, cells were treated with PI and imaged via Nikon Eclipse via brightfield/ fluorescence microscopy. (D) The number of PI positive cells and total cell counts were

generated via QuPATH functions. (E) Overexpression of DLC1β did not have a significant impact on necrotic cells measured via QuPATH/PI fluorescence microscopy. Data is shown as mean ± SD (n=3) where *=p<0.05, & **=p<0.01.

3.5 Overexpression of DLC1β in vivo attenuates I/R injury in a murine heart transplantation (MHT) model

To investigate the impact of DLC1β on preventing IRI in vivo, a mouse heterotopic heart transplantation model was used. C57/BL6 mice were pretreated with either the DLC1β overexpression plasmid (DLC1β-OE group), a pc-3.1 empty control vector (Control vector group), or regular saline ("normal" control group). Syngeneic murine heterotopic HTx (MHT's) were conducted. At POD1 and POD7, heart grafts were analyzed with H&E staining, and imaged via 20x, 40x, 100x, and 200x brightfield microscopy with a Nikon 90I microscope. At POD1, DLC1β-OE grafts appeared to be more similar to normal mouse heart groups, due to the grafts displaying less inflammatory cell infiltration and infarcted cardiomyocytes (Figure 22A). Eosinophilic regions of anucleate cardiomyocytes were determined to be "peri-infarct" and were noted in both control vector/DLC1β-OE grafts (Figure 22A). However, the DLC1β-OE grafts in general, displayed a more acute appearance. At POD1, control vector syngeneic recipients had statistically increased neutrophilic infiltrate in scored in their grafts on average compared to DLC1β-OE mice (p=0.0462) (Figure 22B). Mean acute injury grade was determined via single-blinded semi-quantitative scoring, including measures of inflammatory cell infiltration/infarction. Overall mean acute injury grade was statistically reduced in DLC1β-OE mice compared to control vector groups at POD1 (p= 0.0460) (Figure 22C).

To confirm mRNA and protein overexpression of DLC1β when DLC1β-OE plasmid was delivered to POD1 mice, qRT-PCR and Western blotting was performed (Figure 22D/E). It was demonstrated that DLC1β-OE did not statistically impact endogenous expression (p= 0.8822) of DLC1β mRNA, while statistically upregulating DLC1β-plasmid specific mRNA (p= <0.0001) (Figure 22D). This demonstrates the capability of overexpression in in vivo models at POD1, when delivering the plasmid via tail vein injection 24hrs prior to

transplantation. Additionally, DLC1 protein expression was statistically upregulated in POD1 MHT's that received the DLC1β-OE (Figure 22E) (p= <0.0001). Therefore, the feasibility of this model was confirmed in POD1 MHT samples.

Histopathology of DLC1β-OE POD7 grafts versus control vector grafts displayed consistently less inflammatory cell infiltration (Figure 23A). There also appeared to be better cardiomyocyte organization, with notable reductions in fibrosis (charactered greater in sub-chapter 3.7). Neutrophilic infiltrates characterized at POD7 were statistically reduced in DLC1β-OE grafts (p=0.0062) (Figure 23B). However, there were no significant differences in semi-quantitative score for lymphocytic infiltrate in POD7 control versus DLC1β-OE grafts (Figure 23C). At POD7, the amount of cumulative injury grade (a sum of each category of semi-quantitative injury scoring) was statistically reduced in DLC1β-OE grafts at POD7 compared to control vector graft (p=0.0227) (Figure 23D).

To confirm mRNA and protein overexpression of DLC1β was also possible at POD7, mRNA and protein analyses were performed. It was demonstrated that DLC1β-OE did not statistically impact endogenous expression (p= 0.0957) of DLC1β mRNA, while concurrently resulting in statistically significant upregulation of DLC1β-plasmid specific mRNA (p= <0.0001) (Figure 23E). This further demonstrates the capability of overexpression in in vivo models, even at later collection times such as POD7. Additionally, DLC1 protein expression was also statistically upregulated in POD7 MHT's that received the DLC1β-OE (Figure 23F) (p= 0.0009).

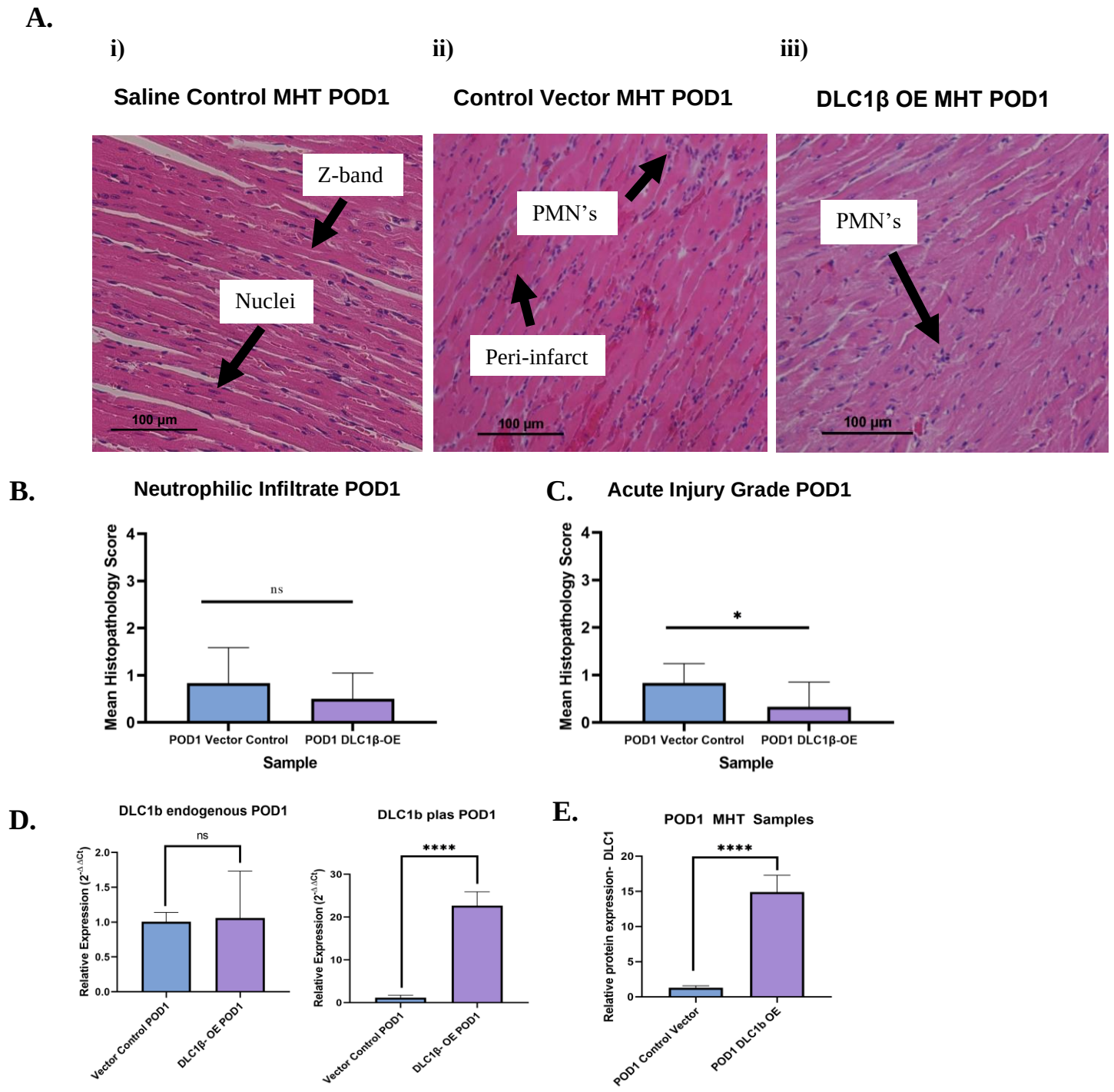

Figure 22- At POD1, DLC1β-OE grafts display less neutrophilic infiltrate.

C57/BL6 syngeneic heterotopic HTx were performed post- 24hr 4°C donor heart storage in UW solution. Mice were sacrificed at POD1, where grafts were collected and grossed for H&E staining. (A) Representative images of heart graft tissues stained with H&E. Images were taken at 200x magnification on a Nikon 90I microscope. Where i) an

additional control mouse heart with only saline at POD1; ii) control vector graft POD1 and iii) DLC1β-OE grafts POD1. The normal saline control heart displays typical organization, characteristic Z-bands and branching cardiomyocytes. DLC1β-OE POD1 hearts display (B) less neutrophilic infiltrate that has extravasated the tissue and (C) less acute injury grade compared to control vector samples. (D) qRT-PCR was performed on POD1 MHT samples and DLC1β-OE resulted in upregulated DLC1β mRNA relative expression without manipulating endogenous expression (n=4). (E) Demonstrated upregulated DLC1 protein with DLC1β-OE in POD1 MHT samples (n=4). Mean semi-quantitative score data is shown as mean $\pm$ SD (n=6) where *=$p<0.05$.

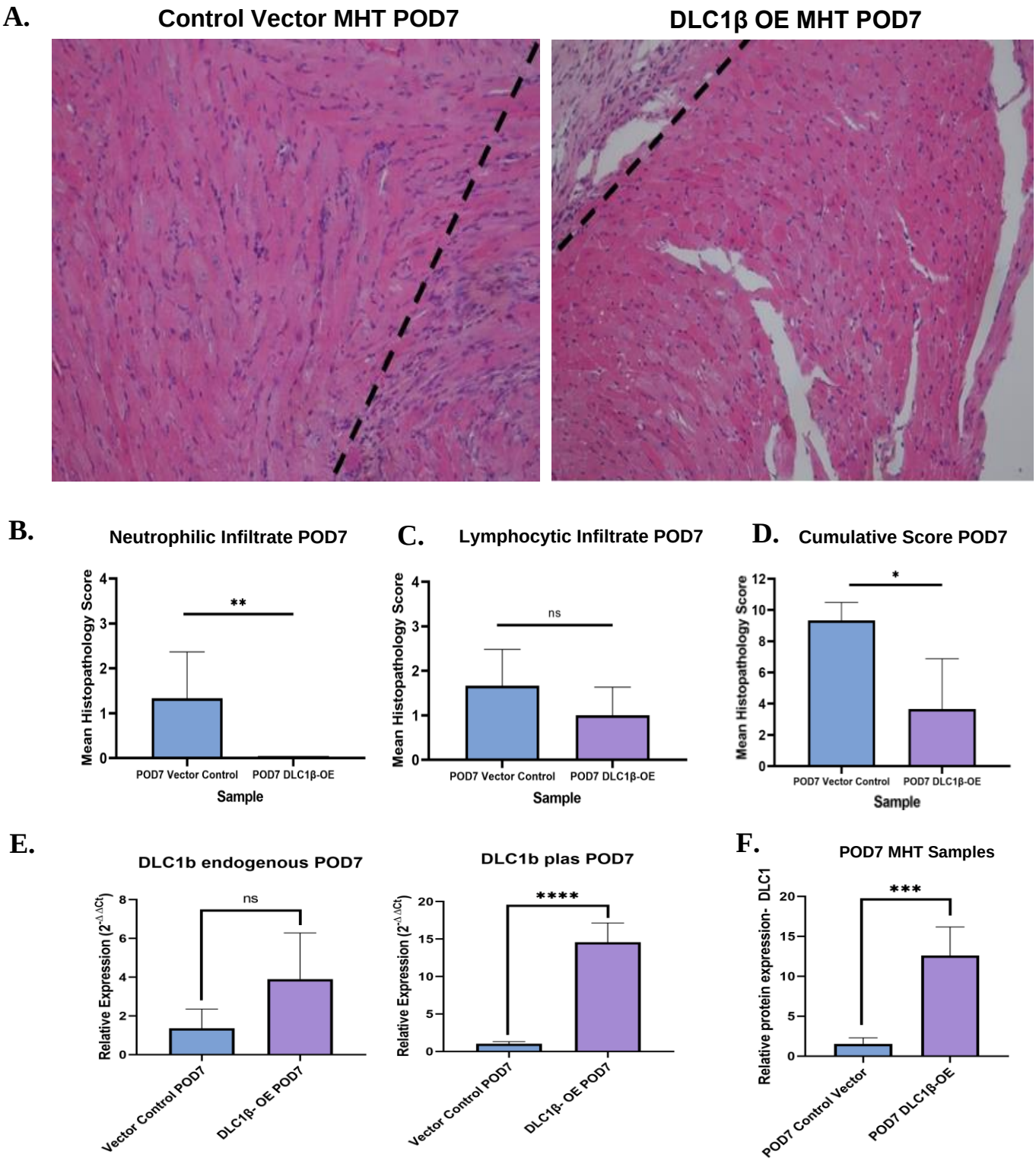

Figure 23- At POD7, DLC1β-OE grafts display less overall injury.

C57/BL6 syngeneic heterotopic HTx were performed in control vector/DLC1β-OE mice. Mice were sacrificed at POD7 for the chronic injury timepoint, where grafts were

collected and grossed for H&E staining. At POD7, less cellular infiltrate is notable in control vector MHT's (A) compared to DLC1β-OE grafts via H&E staining. Grafts were grossed and imaged via a Nikon 90I microscope at 100x magnification. Mean histopathology scores for control POD7 grafts vs DLC1β-OE grafts for neutrophilic infiltrate (B), lymphocytic infiltrate (C) and cumulative score (D) were noted. (E) qRT-PCR was performed on POD7 MHT samples and DLC1β-OE resulted in upregulated DLC1β mRNA relative expression without manipulating endogenous expression (n=4). (F) Demonstrated upregulated DLC1 protein with DLC1β-OE in POD7 MHT samples (n=4). Mean semi-quantitative score data is shown as mean $\pm$ SD (n=6) where *=$p<0.05$, & **=$p<0.01$.

3.6 Overexpression of DLC1β reduced in vivo apoptosis at POD1

In vivo, apoptosis was measured via TUNEL assay staining where normal nuclei are blue, and apoptotic cell nuclei are brown/ "DAB+". Statistically less apoptotic cell bodies were found in DLC1β-OE grafts compared to control vectors at POD1 ($p=0.0003$) (Figure 24A/C). Images for all POD1 grafts were taken with a Nikon 90I microscope at 20x, 40x, 100x, and 200x magnification, noting DAB+ nuclei where possible.

Whole slide imaging was additionally performed on TUNEL stained tissues at 40x magnification per image. After which, photos were imported into QuPATH software, where positive cell detection was run using optical density sum & Sigma factor of 1/Nucleus: DAB OB Mean (0.2/0.4/0.6 for intensity threshold parameters). The number of positive cells/total cell number was converted to a percentage and directly compared (Figure 24B). DLC1β-OE grafts displayed statistically significant reductions in DAB+ % compared to controls (Figure 24B) ($p= 0.0003$). For analyses, n=4/group for QuPATH TUNEL %.

In vivo heart tissue of POD1 MHT's was also compared via qRT-PCR for anti-apoptotic/pro-apoptotic targets (Figure 24D/E). The mRNA relative expression of pro-apoptotic targets Bax and Casp3 was statistically downregulated in DLC1β POD1 grafts compared to control vector POD1 ($p= 0.0487$; $p= 0.0103$ respectively) (Figure 24D). In

addition, anti-apoptotic targets Akt1 and BCl2 were upregulated in DLC1β-OE grafts POD1 ($p=0.0273$; $p=0.0006$ respectively) (Figure 24E).

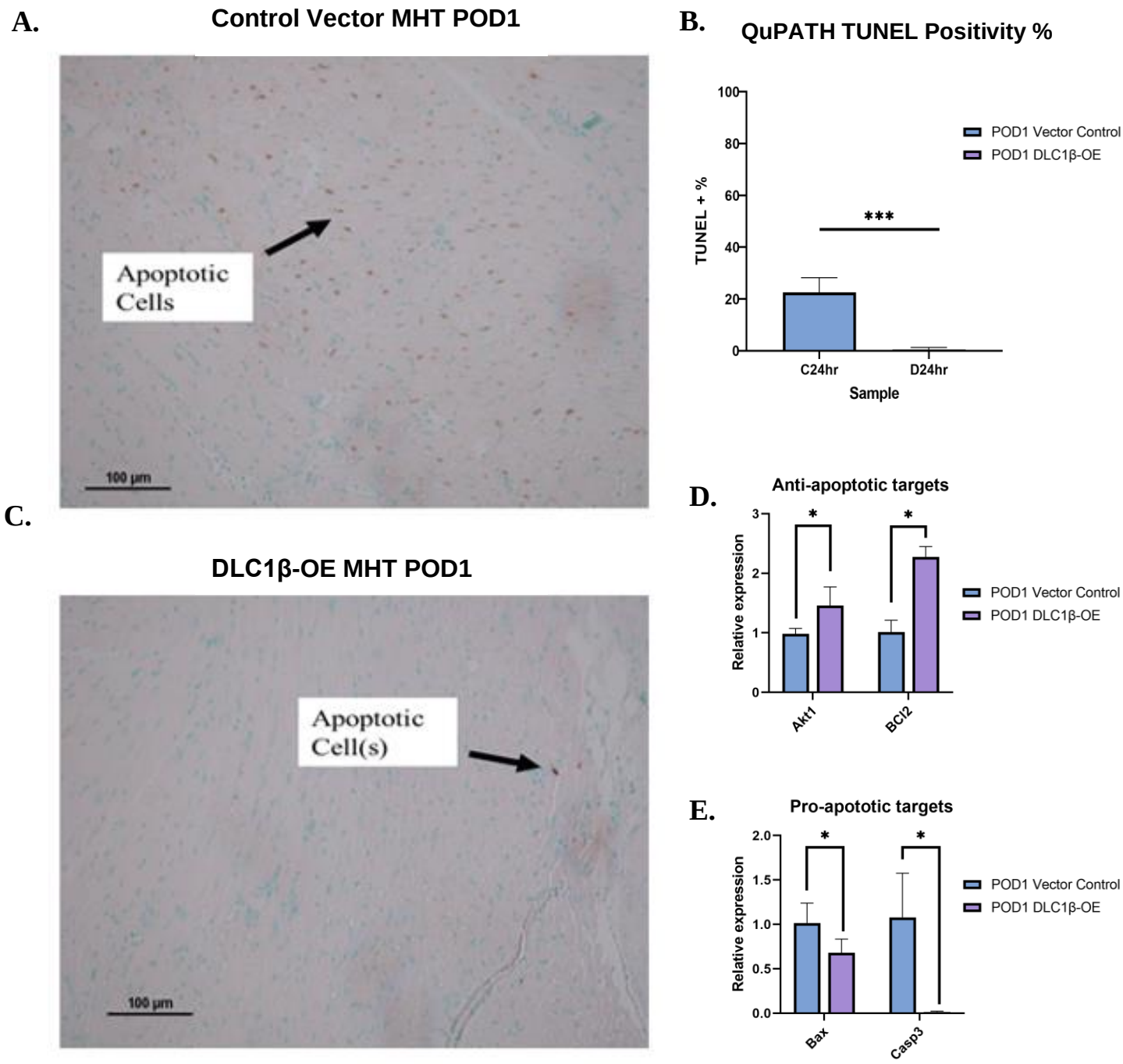

Figure 24- At POD1, DLC1β-OE grafts display less apoptosis via TUNEL staining. (A) Displays a control vector POD1 graft imaged at 100x magnification where DAB+ nuclei (brown) are notable. (B) The calculated TUNEL+ percentage via QuPATH TUNEL positive quantification is graphed. (C) Displays a DLC1β-OE graft imaged at 100x magnification where few DAB+ nuclei are notable. (D-E) Depicts mRNA

expression of anti-apoptotic and pro-apoptotic targets in in-vivo tissues. Data is shown as mean ± SD (n=3) where *=$p<0.05$, **=$p<0.01$, & ***=$p<0.001$.

3.7 Overexpression of DLC1β mitigates in vivo fibrosis at POD7

POD7 MHTs were grossed for histopathology applications where fibrosis was further quantified using connective tissue trichrome staining. The slides stained with trichrome were sent to a single-blind histopathologist for semi-quantitative scoring. It was observed that the control vector POD7 grafts displayed substantially more interstitial or "wedging" fibrosis that extravasated the cardiomyocytes (Figure 25A). This was statistically significant when compared to the slight perivascular fibrosis noted in DLC1β POD7 grafts (Figure 25C). Overall injury grade at POD7 was statistically reduced in DLC1β mice compared to control vector grafts ($p=0.0148$) (Figure 25B). The notable differences in appearance of the slides were conferred via the scoring of fibrosis at POD7 in control vector grafts was statistically increased compared to DLC1β-OE grafts ($p=0.0247$) (Figure 25D).

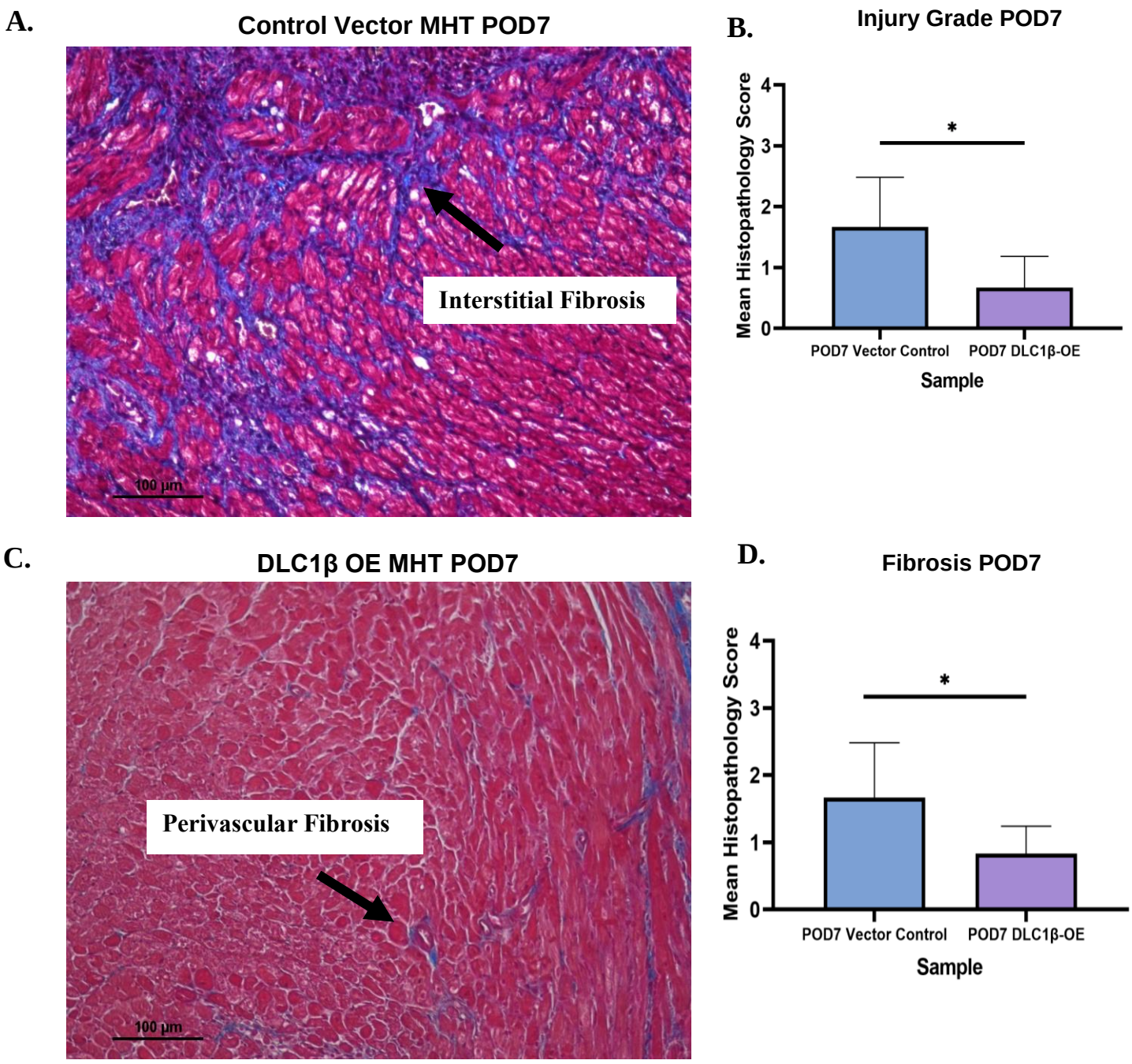

Figure 25- At POD7, DLC1β-OE grafts display less fibrosis/overall injury.

(A) Displays interstitial fibrosis in vector D7 MHT grafts imaged at 100x magnification. This is significantly reduced in (B) DLC1β-OE grafts POD7. The mean histopathology scores of overall injury (C) and fibrosis (D) were also reduced in DLC1β-OE grafts. Mean semi-quantitative score data is shown as mean $\pm$ SD (n=6) where *=$p<0.05$.

3.8 DLC1β overexpression upregulated Akt1 and downregulated RhoA

To understand the molecular signaling pathway involved in H/R models of cardiac IRI, mRNA and protein-based analyses were conducted on common pathway targets were conducted. DLC1β-OE transfected HL-1 cells were compared to control vector samples under normoxia conditions via mRNA relative expression for pathway targets of interest (Figure 26A). Under normoxia conditions, transfecting HL-1 cells with DLC1β-OE plasmid for 24hrs resulted in statistically significant increases in Akt1 ($p=0.0140$). Akt isoform (Akt2) appeared to be downregulated in DLC1β-OE groups, however the change was statistically insignificant ($p=0.0874$). BCl2 mRNA expression was statistically upregulated in DLC1β-OE HL-1 samples under normoxia conditions ($p=0.0340$). Concomitantly, Casp3 expression was statistically downregulated in normoxia DLC1β-OE samples ($p= 0.0160$). When examining PI3K and PTEN targets, there appeared to be no statistically significant change in expression under normoxia conditions under normoxia conditions in HL-1 cells ($p=0.3397$; $p=0.0655$, respectively). RhoA expression was noted to be statistically downregulated compared to control vector samples when DLC1β was overexpressed in normoxia conditions ($p=0.0379$). And finally, ROCK1 expression appeared to be downregulated in DLC1β-OE groups, but this finding was not significant ($p=0.1099$).

DLC1β-OE HL-1 samples were compared to vector control samples after H/OR (24H4R) to analyze relative expression of Akt1, Akt2, BCl2, Casp3, PI3K (Class I p110α subunit), PTEN, RhoA and ROCK1. at the mRNA level (Figure 26B). It was found that after 24H4R, Akt1 expression was significantly upregulated in DLC1β-OE samples compared to vector controls ($p= 0.0413$). Akt2 expression was was not significantly impacted by DLC1β-OE after 24H4R ($p=0.1475$). After 24H4R, BCl2 upregulation was no longer statistically significant in DLC1β-OE grafts compared to normoxia samples ($p= 0.2464$). However, there was still a notable and significant reduction in Casp3 after 24H4R compared to vector controls ($p= 0.0462$). Neither PI3K nor PTEN mRNA displayed no significant differences in expression when DLC1β was overexpressed ($p=0.3099$;

p=0.1037 respectively). RhoA and ROCK1 however, displayed a statistically significant reduction in mRNA relative expression when DLC1β was overexpressed (p= 0.0475; p=0.0369).

On a protein level, Akt-pan, BCl2, PTEN, RhoA and ROCK1 expression was measured via Western Blotting for HL-1 samples under normoxia and 24H4R conditions (Figure 27A). GAPDH served as a normalizing control for each sample for densitometry analyses. It was found that during normoxia, DLC1β-OE resulted in a significant upregulation in Akt-pan protein (p=0.02208), a statistically significant upregulation in BCl2 (p= 00015) (Figure 27B). Additionally, DLC1β-OE samples displayed statistically downregulated levels of PTEN (p= 0.048) compared to vector control samples at normoxia (Figure 27B). RhoA protein relative expression was statistically reduced in DLC1β-OE groups (p=0.0048) (Figure 27B). Whereas ROCK1 also appeared reduced, however the downregulation was insignificant in DLC1β-OE groups under normoxia conditions.

HL-1 samples after 24H4R were also subject to Western Blotting (Figure 27A). After 24H4R, DLC1β-OE samples displayed a statistically significant increase in Akt-pan expression (p=0.0472) compared to vector controls (Figure 27C). BCl2 was also upregulated after IRI compared to vector controls, similar to normoxia conditions (p= 0.0480) (Figure 27C). PTEN was statistically reduced in DLC1β-OE samples compared to vector controls (p=0.0384) (Figure 27C). Finally, RhoA was additionally statistically downregulated on a protein level when DLC1β was overexpressed, similar to normoxia conditions (p=0.0239). Whereas ROCK1 also appeared reduced compared to control vector samples, however the downregulation was insignificant in DLC1β-OE groups under 24H4R conditions.

A.

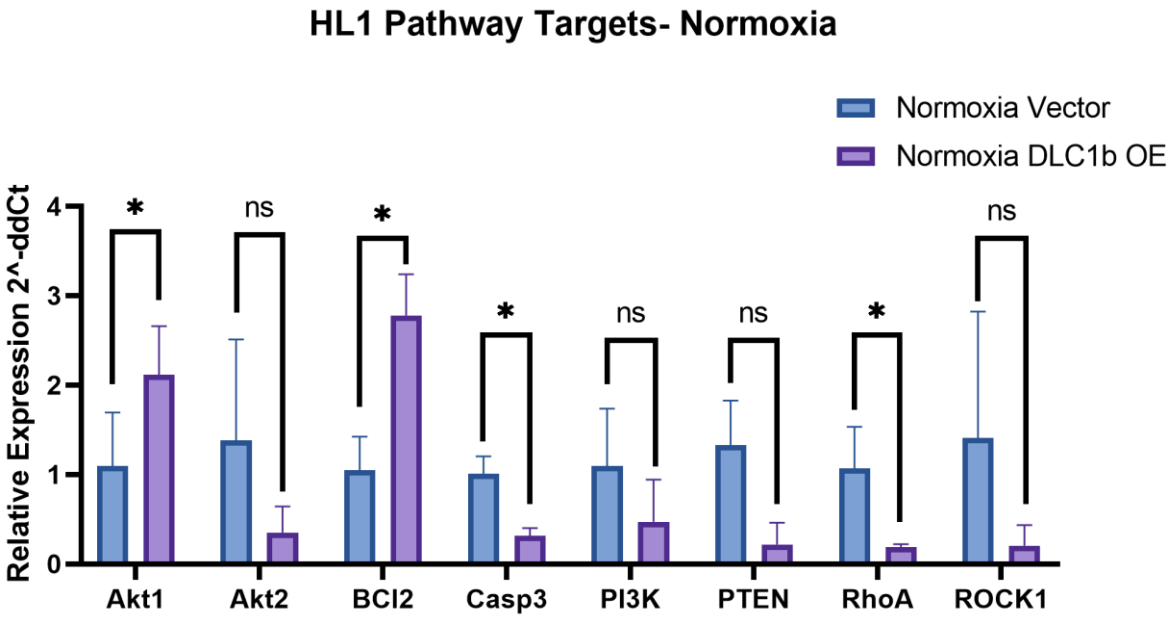

B.

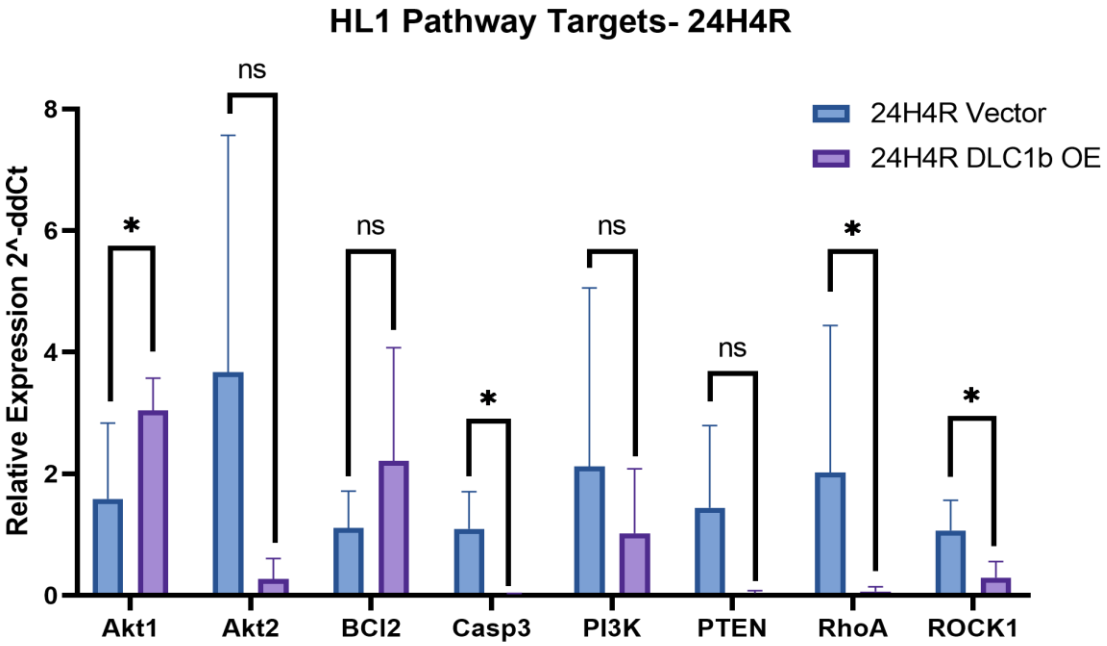

Figure 26- mRNA relative expression of HL-1 pathway targets.

HL-1 cells under normoxia conditions and post- 24H4R H/R were collected for mRNA relative expression. Pathway targets for analyzed via qRT-PCR for normoxia (A) and 24H4R samples (B). Students t-tests were utilized, and data is shown as mean ± SD (n=3) where *=$p<0.05$.

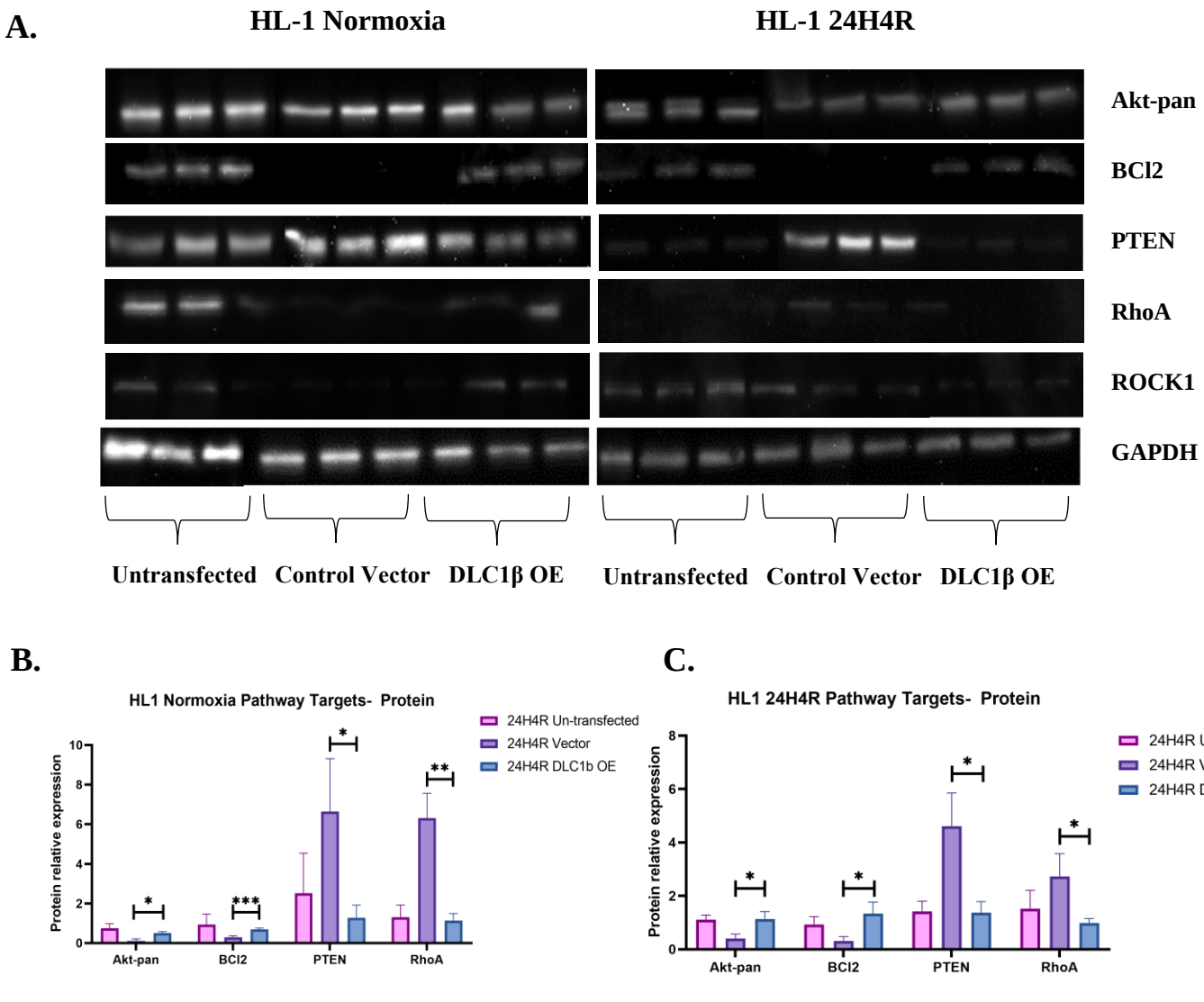

Figure 27- Protein analyses for pathway targets in HL-1 Normoxia/24H4R samples. HL-1 cells were cultured and collected under normoxia conditions/post- 24H4R for (A) Western Blotting with pathway antibodies (Akt-pan, BCl2, PTEN, RhoA, and ROCK1). 25µg of protein was added per well, where respective antibody concentrations can be found in Table 8. GAPDH was used as a normalizing control for relative expression. Relative protein expression was calculated via AlphaView densitometry for normoxia groups (B) and 24H4R groups (C) and data is shown as mean ± SD (n=3) where *=p<0.05, **=p<0.01, ***=p<0.001.

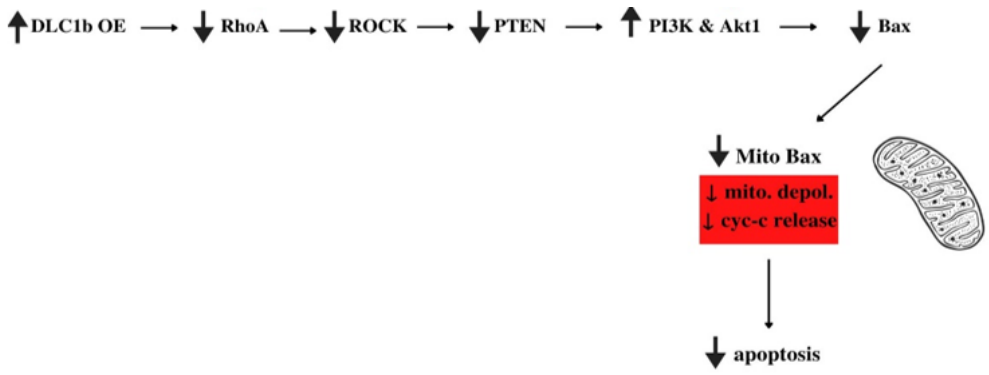

Figure 28- Proposed mechanism of DLC1β-OE protection against IRI

Chapter 4

4. Discussion

In this study, I found that in vitro, DLC1β overexpression significantly reduced H/R-induced apoptosis while maintaining similar viability to control vector cells. In vivo, POD1 grafts had significantly reduced apoptotic cell bodies (determined with TUNEL staining) compared to control vector grafts. Less neutrophilic infiltrate, and overall injury at POD1 was also statistically significant. At POD7, fibrosis was statistically reduced in DLC1β-OE grafts. Therefore, it is believed that DLC1β may participate in cardiac IRI by interacting with Akt and RhoA/ROCK targets. This preclinical work is important in the research space, in order to garner understanding of the complex pathophysiology associated with aberrant disease states that have significant mortality/morbidity.

4.1 In vitro, H/R results in cell death/apoptosis

Initially, it was thought that longer exposure to ischemic stimuli was markedly more injurious (Jernryd et al., 2020; Patel et al., 2021). However, emerging literature demonstrates that the reperfusion phase of cardiac IRI is equivocally injurious to the cardiomyocytes as well (Jernryd et al., 2020; Ibáñez et al., 2015). It was expected that cell death in H9C2/HL-1 cells would increase with increasing reperfusion times in a positive linear fashion. In parallel, cell viability was statistically reduced after 4hrs/8hrs of reperfusion (but not 2hrs) (Figure 17A). These findings are similar to published literature that greater apoptosis/cell death were noted in H/OR models simulating cardiac IRI (Foadoddini et al., 2011; Ban et al., 2020). During ischemia-reperfusion injury, an upregulation of genes conferring immune cell infiltration/inflammation have been demonstrated (Arslan et al., 2011; Feng et al., 2015; Hansson et al., 2015). Concomitantly, studies have demonstrated genes involved in mitochondrial respiration and energy production were markedly decreased (Riley & Tait, 2020; Maneechote et al., 2019; Yang et al., 2019). These findings are rational, as cardiac IRI is occurring under

hypoxia conditions, forcing the cardiomyocytes to produce energy via anaerobic respiration (Ji et al., 2022; Huang et al., 2021).

After H/R (our in vitro, “cardiac IRI” equivalent), the relative expression of Akt1 mRNA was statistically downregulated compared to normoxia un-transfected controls (Figure 17C). Bax/Caspase-3 and somatic Cytochrome c were all statistically upregulated post-H/R in HL-1 cells as well (Figure 17C). These findings indicate that the HL-1 H/R model likely was resulting in greater apoptosis, as Akt1 is widely considered to be anti-apoptotic, and Bax/Casp3 and Cyc-c are all pro-apoptotic targets. Having a greater amount of these pro-apoptotic targets after H/R is similar to what many studies have demonstrated after cardiac IRI (He et al., 2023; Liu et al., 2018; Zhu & Lu, 2019). This is namely due to cardiac IRI inciting the death modalities necrosis and apoptosis. Necrosis is typically a more acute modality that is stimulated by physical/chemical trauma during ischemia/reperfusion stages (Soares et al., 2019; Chiong et al., 2011; Vanlangenakker et al., 2012). Whereas apoptosis is another programmed form of cell death that occurs during cardiac IRI resulting in death without activating the immune system. Both of these death modalities can also incite downstream signalling pathways.

In this study, it was noted that DLC1β expression was downregulated in immortalized cardiomyocyte cell lines after 24H4R exposure (Figure 18). This was seen at the mRNA and protein levels in both H9C2/HL-1 cell lines (Figure 18). Few studies have demonstrated DLC1-specifically being downregulated after hypoxia-exposure in a cardiovascular context. However, multiple gene expression profile studies have displayed transient downregulation of the DLC1 gene in associated with adverse cardiovascular events (Sabbir et al., 2010; Kuba et al., 2007; Tse et al., 2015). Transcriptomic analyses in recent transplantation studies have also demonstrated that DLC1 mutations are likely to result in a plethora of adverse cardiovascular events (including aberrant angiogenesis) (Ding et al., 2022), suggesting that DLC1 is important for heart function. Overall, the finding that the DLC1β isoform becomes downregulated on a mRNA/protein level in immortalized cardiomyocytes post-H/R is novel. But despite the novelty, the overall trend that alludes to DLC1 as a potential protective target in the cardiovascular system is

consistent with current literature (Ding et al., 2022; Shih et al., 2017; Ward & Iskratsch, 2020; Kuba et al., 2007; Tse et al., 2015).

4.2 DLC1β can be overexpressed via plasmid transfection in vitro

To confirm the model was actually overexpressing DLC1β protein in the cell lines of interest, cells were transfected with DLC1β-OE plasmid. After 24hrs, mRNA/protein expression was analyzed to confirm an upregulation of DLC1β (Figure 19). To determine if potential effects were occurring as a result of the plasmid overexpression, plasmid specific ("recombinant") DLC1β primers were designed. Next, endogenous DLC1β primers were designed to a DLC1β-specific exon to negate that the effects were due to manipulating endogenous expression. This served as an additional control to allow for correct quantification of the fold-change/relative gene expression (Ahlemeyer et al., 2020).

Some recent studies have demonstrated that the DLC1 gene may have a regulatory role in apoptosis (Tse et al., 2015). Furthermore, it was demonstrated that hypoxia-specifically may impact DLC1 apoptotic regulation (Tse et al., 2015). However, these studies analyzing DLC1 are most often in cancer-based models. Therefore, it was of interest to manipulate DLC1β expression via plasmid transfection, to investigate if there was an impact on downstream apoptotic processes. In H9C2 models, a statistically significant reduction in H/R-induced apoptosis was noted when DLC1β was overexpressed (Figure 20/21). This was also seen in HL-1 models of H/R, that when DLC1β was overexpressed compared to control vector samples (Figure 20/21). This was confirmed via annexin v flow cytometry in both late/early stages of apoptosis displaying statistically significant decreases in DLC1β-OE groups compared to vector controls (Figure 20). And finally, it was demonstrated that in addition to a reduction of pro-apoptotic target mRNA post-24H4R compared to controls, there was a significant upregulation in anti-apoptotic Akt1/BCl2 with DLC1β-OE (Figure 21A/B). This demonstrates the ability to overexpress DLC1β plasmid in the cells, the potential protective (anti-apoptotic effects) of DLC1β-OE, all without adverse/increased cell necrosis compared to controls (Figure 21C/D/E).

4.3 DLC1β overexpression in vivo attenuates IRI severity

It appears that DLC1β-OE maybe protective against IRI severity in in vivo models of cardiac IRI. This is largely due to the significant reduction in overall injury grade noted in DLC1β-OE grafts post-MHT compared to control vector samples (Figure 22/23). At POD1, protective effects were demonstrated in DLC1β-OE grafts through reduced apoptosis, reduced neutrophilic infiltrate, and a lesser overall injury grade. These protective effects demonstrated at both POD1 are further characterized in Figure 22. At POD7, DLC1β grafts maintain a reduced overall cumulative injury grade compared to control vector samples, in addition to a statistically significant reduction in fibrosis (Figure 23).

No notable injurious effects were observed when overexpressing DLC1β in vivo. This includes no notable clotting in the graft, hypertrophy, or other complications notable during organ retrieval. This is in accordance with the few other studies that have that DLC1 overexpression was possible in vivo while remaining tolerability (Hinsenkamp et al., 2018). Therefore, it would be of interest to expand on this research in small mouse models to validate the replicability of these attenuating effects on cardiac IRI in vivo models. Understanding the complex pathophysiology associated with aberrant disease states (such as cardiac IRI) is imperative for developing informed treatments. Currently, complications due to cardiac IRI still have significant associated morbidity/mortality (Neri et al., 2017; Soares et al., 2019). Other studies have demonstrated a directly proportional relationship between cardiac IRI severity and patient survival (Silvis et al., 2020; Jernryd et al., 2020; Binder et al., 2015; Bell & Yellon, 2011; Guariento et al., 2021). Therefore, if DLC1β-OE can be further validated as a protective target in cardiac IRI via mechanism of action/co-expression studies, the potential for commercialization or clinical applications would be of interest.

4.4 DLC1β overexpression reduced apoptosis in vitro and in vivo

Preliminary data generated in the laboratory using H9C2 (rat cardiomyocytes) displayed anti-apoptotic effects with DLC1β overexpression via Annexin V Flow Cytometry.

Therefore, it was also of interest to see if DLC1β overexpression may potentially abrogate apoptotic effects associated with cardiac IRI, by using plasmid overexpression in a HL-1 cell, H/OR model. When DLC1β plasmid was OE in vitro post 24H4R, annexin v flow cytometry assays demonstrated a reduction in annexin V+ and double + cells compared to control vector samples in HL-1 cells. These findings demonstrated that DLC1β-OE had a similar number of cells in the early and late stages of apoptosis, alive and dead as the un-transfected control group. The very close similarity to the normal control was somewhat unexpected, as the uptake of an overexpression plasmid via transfection results in an altered physiological state. On an mRNA level, DLC1β overexpression also resulted in the alteration of relative expression of pro-apoptotic and anti-apoptotic targets without H/R treatment, as well as after H/R treatment (Figure 26). Therefore, in H/R models of cardiac IRI, DLC1β-OE appears to not only be tolerable (based on morphology/cell viability), but also potentially anti-apoptotic.

DAB+ percentages derived from QuPATH were used to quantitatively compare the amount of apoptotic cell bodies in the grafts at POD1. It was seen that when DLC1β was overexpressed in vivo, there was a statistically significant reduction in apoptotic cell bodies in POD1 graphs compared to control vector samples (Figure 24). It is possible that the increase in DAB+ cells in the POD1 DLC1β-OE grafts may also be associated with the statistically significant decrease in neutrophilic infiltrate compared to control vectors. This is because literature has demonstrated that with greater amounts of extravasated neutrophils, there is greater direct-cell to cell contact which is directly injurious (Zhao & Vinten-Johansen, 2002; Entman et al., 1992; Zhao et al., 2000). In addition, the PI3K/Akt signalling pathways became increasingly popular in cardiac IRI research due to their protective effects against apoptosis and cardiac fibrosis (Yu et al., 2020). As DLC1β-OE appeared to increase the relative expression of Akt1 mRNA, it is possible that the reduction in apoptotic cell bodies was a result of this anti-apoptotic upregulation as well.

4.5 DLC1β-OE exhibited anti-fibrotic effects in vivo at POD7

Cardiac fibrosis occurs post-IRI by the replacement of necrotic cardiomyocytes with a temporary fibrin clot (Talman & Ruskoaho, 2016). The clot is then phagocytosed and

replaced with a permanent collagenous scar (Talman & Ruskoaho, 2016). Unsurprisingly, the deposition of scar tissue on the heart negatively impacts hearts overall contractility and hemodynamic ability (Palatianos et al., 1988). Anti-fibrotic therapies have thereby been developed by targeting the PI3K/Akt signalling pathways that regulate the occurrence/progression and extensiveness of cardiac fibrosis (Wang et al., 2022). These pharmaceuticals have demonstrated clinical efficacy and further studies have demonstrated that increasing PIK3A (PI3K Class I p110α subunit) directly reduces cardiac fibrosis (Zhabyeyev et al., Yang et al., 2019).

When DLC1β was overexpressed in vivo, there was a significant reduction in fibrosis noted via trichrome staining (Figure 25). Therefore, if DLC1β is potentially upregulating PI3K/Akt signalling pathway targets (such as Akt1), this could potentially explain the significant reduction in fibrosis in DLC1β-OE grafts (Figure 25). Furthermore, as DLC1β has a well-characterized role as a Rho-GTPase activating protein that targets RhoA (pro-fibrotic), it is possible that the anti-fibrotic effects are directly through RhoA inactivation (Lauriol et al., 2014). As DLC1 has been empirically validated to have interactions with RhoA/ROCK and PI3K/Akt pathway targets, it was of interest to also examine any effects on fibrosis (Linnerz & Bertrand, 2021; Lin et al., 2014; Durkin et al, 2005; Liu et al., 2018).

4.6 DLC1β signalling pathways in cardiac IRI

DLC1 is also upstream of RhoA and negatively regulates RhoA expression by keeping it in its GDP-bound form (Hodge & Ridley, 2016; Salazar-Gonzalez et al., 2022; Tripathi et al., 2017; Qian et al., 2007). Many papers have demonstrated in the context of cardiac IRI, RhoA downregulation was protective against IRI severity and overall injury grade (Kilian et al., 2021; Homma et al., 2008; Eckenstaler et al., 2022; Chang et al., 2019; Tu et al., 2022; Lee et al., 2021; Lauriol et al., 2014). In HL-1 cells, DLC1β-OE was found to impact 3 targets specifically under normoxia and 24H4R conditions on a mRNA/protein level: Akt, BCl2, and RhoA. Consistently, DLC1β-OE resulted in RhoA downregulation on both a mRNA/protein level (Figure 26/Figure 27).

Other studies have demonstrated that ROCK1 and PTEN are upregulated during the reperfusion stage of cardiac IRI (Ban et al., 2020). Additionally, Ban et al. demonstrated that inhibiting PTEN alone was enough to exert cardioprotective effects (Ban et al., 2020). The demonstrated effects of PTEN inhibition were mainly an increase in PI3K/Akt signalling due to reduced PIP2 → PIP3 antagonism (Ban et al., 2020). As DLC1 is said to form a complex with PTEN (Heering et al., 2009); which could be another potential manner DLC1 may be demonstrating in vivo protective effects. DLC1β overexpression in HL-1 cells also resulted in a downregulation in the fellow tumour-suppressor PTEN on a protein level (Figure 27). These effects were not conferred on a mRNA level (although a reduction during DLC1β-OE was noted). Notably, the reduction of PTEN by miRNA targets is a current strategy in literature for reducing cardiac IRI severity (Ban et al., 2020; Bei et al., 2022). This further alludes to DLC1β as a cardioprotective target in H/R and cardiac IRI.

4.7 Summary of Findings

Overall, the findings of the project include 1) increased reperfusion times resulted in increased cell death and apoptosis. 2) DLC1β was downregulated on a mRNA/protein level in cardiomyocytes after H/R. It was also found that 3) overexpressing DLC1β did not have an injurious effect, and we were capable of doing in vitro/in vivo studies. Furthermore, 4) we demonstrated that DLC1β-OE in H92/HL-1 models reduced H/R-associated apoptosis. 5) These antiapoptotic effects were corroborated in vivo, where DLC1β-OE graphs had significantly less apoptotic cell bodies than control vectors at POD1. 6) Overexpressing DLC1β in vivo reduced in a reduction in overall injury grade and fibrosis that was statistically significant. And finally, 7) DLC1β-OE under normoxia conditions resulted in statistically significant changes in PI3K/Akt and RhoA/ROCK pathway targets. However, further models are required to validate the interplay of these signalling pathways.

4.8 Limitations

A minor but valid qualm of preclinical cardiac IRI studies is the use of small mammals/immortalized cell lines. This is largely due to differences in infarction development (not transmural), atypical infarction borders, and increased tolerance to ischemia (De Villers & Riley, 2020). Whilst large mammal, porcine models are more generalizable, small mammal models were utilized due to their quick breeding/cost effectiveness. In vitro, ideally adult myocytes would be used as they are regarded as the most generalizable to cardiac IRI (Lindsey et al., 2018). However, these cells are limited in passage and quite expensive to culture (Lindsey et al., 2018). Neonatal cardiomyocytes were also not used due to their increased ischemic tolerance (Lindsey et al., 2018). Immortalized cardiomyocyte cell lines are largely criticized due to their reduced translational capacity from cell cycle mutations to make the cells serially passible (Chen & Vunjak-Novakovic, 2018; Lindsey et al., 2018). And while HL-1 cells retain a cardiomyocyte phenotype in vitro, they also preferentially select glucose metabolism unlike primary cells (Claycomb et al., 1998; Lindsey et al., 2018).

A large limiting factor of the performed study was the use of only male mice. Literature demonstrating sex-specific differences in cardiac IRI susceptibility as well as severity (Ostadel & Ostadel, 2014). CVD/IHDs are known to demonstrate sex specific differences in susceptibility via epidemiological data (Ostadel & Ostadel, 2014; Tong et al., 2002). Incidence data has demonstrated that males display an increased risk of IHD compared to pre-menopausal/peri-menopausal women (Ostadel & Ostadel, 2014). However, post menopause, IHD increases in women compared to men (Ostadel & Ostadel, 2014). Furthermore, estrogen is cardio-protective and the severity of cardiac IRI is also decreased in females (Fels & Manfredi, 2019). However, this protective effect is lost in older female mice (Fels & Manfredi, 2019). Studies have recapitulated this in female mice that received a gonadectomy/ovariectomy (removal of the ovaries), and protective effects compared to male mice were lost (Song et al., 2003; Wang et al., 2009; Deschamps et al., 2010). As PI3K is a signalling kinase involved in the estrogen signalling pathway, it is important that these potential sex-specific differences be further

elucidated (Deschamps & Murphy, 2009; Ostadel & Ostadel, 2014; Tong et al., 2002; Ostadel et al., 2020).

Finally, a limitation in the specificity of the DLC1 antibody used for conferring protein expression was noted. The polyclonal antibody detects the DLC1 gene but predicts both DLC1α as well as DLC1β. Due to the isoforms having a large overlap, a custom antibody would have to be synthesized for a DLC1β-specific exon. Another DLC1α-specific exon would be used for an additional control to compare to the DLC1 antibody used in the performed study.

4.9 Future Directions

Despite these limitations, preclinical models of IRI are widely used in transplantation research. Some future considerations to extend off of the findings of the performed study would be to analyze sex-based differences. Incorporating sex specific differences would highlight if these differences do exist in C57/BL6 syngeneic transplantation cardiac IRI mouse models consistent with the literature (Fels & Manfredi, 2019). In addition to adding female mice to the analyses, increasing the sample size would highlight the reproducibility/validity of the study.

Another future area of this research could include incorporating co-immunoprecipitations/biomolecular interaction assays. Co-immunoprecipitation would be advantageous for the performed study to analyze if DLC1β is potentially forming a complex with the proposed pathway targets. As previous research in the field has demonstrated that DLC1 has the potential to bind PTEN and ROCK1, it would be of interest to analyze if the DLC1β isoform may physically interact with these targets. Biomolecular interaction assays (such as Label-free Bio-Layer Interferometry) would provide kinetic data directly proportional to the strength of the association between the targets of interest. This would be a high-throughput and relatively inexpensive method to validate binding affinities, protein/antibody interactions and small molecule interactions (Sartorius, 2021).

Further directions also include further validation of the DLC1β-OE effects on downstream signalling pathways/verifying anti-apoptotic effects. Firstly, to further build on the DLC1β model would be to validate the pathway interactions via a loss of function/gain of function model. By utilizing this method, one would be able to validate if the proposed pathways are being utilized. Likely PI3K/Akt inhibitors/ RhoA agonists would be used to confer effects on downstream protein/mRNA expression. Secondly, to verify the anti-apoptotic effects seen in vitro, it would be of interest to perform a microarray, to see if there are miRNA's that may be controlling DLC1β mRNA expression. If so, we could potentially substantiate the findings of DLC1β plasmid overexpression by knocking down discovered miRNAs via RNAi.

4.10 Conclusions/ Significance

In this study, it was found that DLC1β-OE reduced cell apoptosis and pro-apoptotic gene expression for Bax, Casp3, and Cycs targets. DLC1β-OE also resulted in upregulation of anti-apoptotic targets in vitro (including Akt1/BCl2). In vivo, pre-treatment of donor hearts with DLC1β-OE plasmid reduced neutrophilic infiltration and apoptosis at POD1, as well as fibrosis, and overall injury at POD7. The study demonstrated that DLC1β has protective effects in cardiac IRI during heart transplantation, likely through the regulation of RhoA signalling. This study not only increases our understanding about the mechanism of IRI, but also helps to identify a new target for potentially treating IRI in heart transplantation. The translational potential of this work could have societal impacts if this research was used as the cornerstone for novel cardiac IRI therapeutics. As cardiac IRI has a vast disease-associated global burden and mortality, expanding on research to elucidate the patho-mechanism is of great interest.

Chapter 5

5. References

Adams, C. M., Clark-Garvey, S., Porcu, P., & Eischen, C. M. (2019). Targeting the Bcl-2 family in B cell lymphoma. *Frontiers in Oncology*, *9*(JAN), 636-636. https://doi.org/10.3389/FONC.2018.00636/BIBTEX

Ahlemeyer, B., Colasante, C., & Baumgart-Vogt, E. (2020). Analysis of the Level of Plasmid-Derived mRNA in the Presence of Residual Plasmid DNA by Two-Step Quantitative RT-PCR. *Methods and Protocols*, *3*(2), 1-12. https://doi.org/10.3390/MPS3020040

Ahmed, A. (2007). DEFEAT Heart Failure: Clinical Manifestations, Diagnostic Assessment, and Etiology of Geriatric Heart Failure. *Heart Failure Clinics*, *3*(4), 389-402. https://doi.org/10.1016/J.HFC.2007.07.005

Ahmed, T., & Jain, A. (2022). Heart Transplantation. *StatPearls*.

Akande, O., Chen, Q., Toldo, S., Lesnefsky, E. J., & Quader, M. (2020). Ischemia and reperfusion injury to mitochondria and cardiac function in donation after circulatory death hearts- an experimental study. *PLoS ONE*, *15*(12). https://doi.org/10.1371/JOURNAL.PONE.0243504

Akhtar, A. (2015). The Flaws and Human Harms of Animal Experimentation. *Cambridge Quarterly of Healthcare Ethics*, *24*(4), 407-407. https://doi.org/10.1017/S0963180115000079

Alomari, M., Garg, P., Yazji, J. H., Wadiwala, I. J., Alamouti-fard, E., Hussain, M. W. A., . . . Jacob, S. (2022). Is the Organ Care System (OCS) Still the First Choice With Emerging New Strategies for Donation After Circulatory Death (DCD) in Heart Transplant? *Cureus*, *14*(6). https://doi.org/10.7759/CUREUS.26281

Anderson, R. H., & Loukas, M. (2009). The importance of attitudinally appropriate description of cardiac anatomy. *Clinical Anatomy*, *22*(1), 47-51. https://doi.org/10.1002/CA.20741

Arslan, F., De Kleijn, D. P., & Pasterkamp, G. (2011). Innate immune signaling in cardiac ischemia. *Nature Reviews Cardiology*, *8*(5), 292-300. https://doi.org/10.1038/NRCARDIO.2011.38

Arumugam, T. V., Okun, E., Tang, S. C., Thundyil, J., Taylor, S. M., & Woodruff, T. M. (2009). Toll-like receptors in ischemia-reperfusion injury. *Shock*, *32*(1), 4-16. https://doi.org/10.1097/SHK.0B013E318193E333

Auer, M., Schweigreiter, R., Hausott, B., Thongrong, S., Höltje, M., Just, I., . . . Klimaschewski, L. (2012). Rho-independent stimulation of axon outgrowth and activation of the ERK and Akt signaling pathways by C3 transferase in sensory neurons. *Frontiers in Cellular Neuroscience*, *6*(SEPTEMBER), 1-21. https://doi.org/10.3389/FNCEL.2012.00043/BIBTEX

Baldwin, W. M., Su, C. A., Shroka, T. M., & Fairchild, R. L. (2014). Experimental Models of Cardiac Transplantation - design determines relevance. *Current opinion in organ transplantation*, *19*(5), 525-525. https://doi.org/10.1097/MOT.0000000000000113

Ban, Q., Qiao, L., Xia, H., Xie, B., Liu, J., Ma, Y., . . . Qi, Z. (2020). β-catenin regulates myocardial ischemia/reperfusion injury following heterotopic heart transplantation in mice by modulating PTEN pathways. *American Journal of Translational Research*, *12*(8), 4757-4757.

Bankhead, P., Loughrey, M. B., Fernández, J. A., Dombrowski, Y., McArt, D. G., Dunne, P. D., . . . Hamilton, P. W. (2017). QuPath: Open source software for digital pathology image analysis. *Scientific Reports*, *7*(1), 16878-16878. https://doi.org/10.1038/s41598-017-17204-5

Bao, W., Hu, E., Tao, L., Boyce, R., Mirabile, R., Thudium, D. T., . . . Yue, T. L. (2004). Inhibition of Rho-kinase protects the heart against ischemia/reperfusion injury. *Cardiovascular research*, *61*(3), 548-558. https://doi.org/10.1016/J.CARDIORES.2003.12.004

Bei, Y., Lu, D., Bär, C., Chatterjee, S., Costa, A., Riedel, I., . . . Xiao, J. (2022). miR-486 attenuates cardiac ischemia/reperfusion injury and mediates the beneficial effect of exercise for myocardial protection. *Molecular Therapy*, *30*(4), 1675-1691. https://doi.org/10.1016/J.YMTHE.2022.01.031

Bell, R. M., & Yellon, D. M. (2011). There is More to Life than Revascularization: Therapeutic Targeting of Myocardial Ischemia/Reperfusion Injury. *Cardiovascular Therapeutics*, *29*(6), e67-e79. https://doi.org/10.1111/J.1755-5922.2010.00190.X

Binder, A., Ali, A., Chawla, R., Aziz, H. A., Abbate, A., & Jovin, I. S. (2015). Myocardial protection from ischemia-reperfusion injury post coronary revascularization. *http://dx.doi.org/10.1586/14779072.2015.1070669*, *13*(9), 1045-1057. https://doi.org/10.1586/14779072.2015.1070669

Bona, M., Wyss, R. K., Arnold, M., Méndez-Carmona, N., Sanz, M. N., Günsch, D., . . . Longnus, S. L. (2021). Cardiac Graft Assessment in the Era of Machine Perfusion: Current and Future Biomarkers. *Journal of the American Heart Association*, *10*(4), 1-29. https://doi.org/10.1161/JAHA.120.018966

Bozulic, L., & Hemmings, B. A. (2009). PIKKing on PKB: regulation of PKB activity by phosphorylation. *Current opinion in cell biology*, *21*(2), 256-261. https://doi.org/10.1016/J.CEB.2009.02.002

Braun, A. C., & Olayioye, M. A. (2015). Rho regulation: DLC proteins in space and time. *Cellular Signalling*, *27*(8), 1643-1651. https://doi.org/10.1016/J.CELLSIG.2015.04.003

Cesarovic, N., Lipski, M., Falk, V., & Emmert, M. Y. (2020). Animals in cardiovascular researchClinical relevance and translational limitations of animal models in cardiovascular medicine. *European Heart Journal*, *41*(2), 200-203. https://doi.org/10.1093/EURHEARTJ/EHZ933

Chang, C. C., Huang, K. H., Hsu, S. P., Lee, Y. C. G., Sue, Y. M., & Juan, S. H. (2019). Simvastatin reduces the carcinogenic effect of 3-methylcholanthrene in renal epithelial cells through histone deacetylase 1 inhibition and RhoA reactivation. *Scientific Reports 2019 9:1*, *9*(1), 1-13. https://doi.org/10.1038/s41598-019-40757-6

Chen, T., & Vunjak-Novakovic, G. (2018). In Vitro Models of Ischemia-Reperfusion Injury. *Regenerative Engineering and Translational Medicine 2018 4:3*, *4*(3), 142-153. https://doi.org/10.1007/S40883-018-0056-0

Chi, H.-j., Chen, M.-l., Yang, X.-c., Lin, X.-m., Sun, H., Zhao, W.-s., . . . Cai, J. (2017). Progress in Therapies for Myocardial Ischemia Reperfusion Injury. *Current Drug Targets*, *18*(15). https://doi.org/10.2174/1389450117666160401120308

Chih, S., McDonald, M., Dipchand, A., Kim, D., Ducharme, A., Kaan, A., . . . Senechal, M. (2020). Canadian Cardiovascular Society/Canadian Cardiac Transplant Network Position Statement on Heart Transplantation: Patient Eligibility, Selection, and Post-Transplantation Care. *Canadian Journal of Cardiology*, *36*(3), 335-356. https://doi.org/10.1016/j.cjca.2019.12.025

Chiong, M., Wang, Z. V., Pedrozo, Z., Cao, D. J., Troncoso, R., Ibacache, M., . . . Lavandero, S. (2011). Cardiomyocyte death: mechanisms and translational implications. *Cell Death & Disease 2011 2:12*, *2*(12), e244-e244. https://doi.org/10.1038/cddis.2011.130

Claycomb, W. C., Lanson, N. A., Stallworth, B. S., Egeland, D. B., Delcarpio, J. B., Bahinski, A., & Izzo, N. J. (1998). HL-1 cells: a cardiac muscle cell line that contracts and retains phenotypic characteristics of the adult cardiomyocyte. *Proceedings of the National Academy of Sciences of the United States of America*, *95*(6), 2979-2984. https://doi.org/10.1073/PNAS.95.6.2979

Concato, J. (2004). Observational Versus Experimental Studies: What's the Evidence for a Hierarchy? *NeuroRx*, *1*(3), 341-347. https://doi.org/10.1602/NEURORX.1.3.341/METRICS

Cowled, P., & Fitridge, R. (2011). Pathophysiology of Reperfusion Injury. *Mechanisms of Vascular Disease: A Reference Book for Vascular Specialists*, 331-350. https://doi.org/10.1017/UPO9781922064004.019

Daiber, A., Andreadou, I., Oelze, M., Davidson, S. M., & Hausenloy, D. J. (2021). Discovery of new therapeutic redox targets for cardioprotection against ischemia/reperfusion injury and heart failure. *Free Radical Biology and Medicine*, *163*, 325-343. https://doi.org/10.1016/J.FREERADBIOMED.2020.12.026

Dangelmaier, C., Manne, B. K., Liverani, E., Jin, J., Bray, P., & Kunapuli, S. P. (2014). PDK1 selectively phosphorylates Thr(308) on Akt and contributes to human platelet functional responses. *Thrombosis and haemostasis*, *111*(3), 508-508. https://doi.org/10.1160/TH13-06-0484

de Villiers, C., & Riley, P. R. (2020). Mouse models of myocardial infarction: Comparing permanent ligation and ischaemia-reperfusion. *DMM Disease Models and Mechanisms*, *13*(11). https://doi.org/10.1242/DMM.046565/225770

Del Re, D. P., Amgalan, D., Linkermann, A., Liu, Q., & Kitsis, R. N. (2019). Fundamental Mechanisms of Regulated Cell Death and Implications for Heart Disease. *Physiological Reviews*, *99*(4), 1765-1765. https://doi.org/10.1152/PHYSREV.00022.2018

Deschamps, A. M., & Murphy, E. (2009). Activation of a novel estrogen receptor, GPER, is cardioprotective in male and female rats. *American Journal of Physiology - Heart and Circulatory Physiology*, *297*(5), 1806-1813. https://doi.org/10.1152/AJPHEART.00283.2009/ASSET/IMAGES/LARGE/ZH40110990670006.JPEG

Deschamps, A. M., Murphy, E., & Sun, J. (2010). Estrogen Receptor Activation and Cardioprotection in Ischemia Reperfusion Injury. *Trends in Cardiovascular Medicine*, *20*(3), 73-78. https://doi.org/10.1016/J.TCM.2010.05.001

Ding, S., Wang, D., Zhou, X., Chen, L., Feng, K., Xu, X., . . . Cai, Y. (2022). Predicting Heart Cell Types by Using Transcriptome Profiles and a Machine Learning Method. *Life*, *12*(2), 228-228. https://doi.org/10.3390/LIFE12020228/S1

Durkin, M. E., Avner, M. R., Huh, C. G., Yuan, B. Z., Thorgeirsson, S. S., & Popescu, N. C. (2005). DLC-1, a Rho GTPase-activating protein with tumor suppressor function, is essential for embryonic development. *FEBS Letters*, *579*(5), 1191-1196. https://doi.org/10.1016/J.FEBSLET.2004.12.090

Dye, B., & Lincoln, J. (2020). The Endocardium and Heart Valves. *Cold Spring Harbor Perspectives in Biology*, *12*(12), 1-17. https://doi.org/10.1101/CSHPERSPECT.A036723

Eckenstaler, R., Hauke, M., & Benndorf, R. A. (2022). A current overview of RhoA, RhoB, and RhoC functions in vascular biology and pathology. *Biochemical Pharmacology*, *206*, 115321-115321. https://doi.org/10.1016/J.BCP.2022.115321

Eefting, F., Rensing, B., Wigman, J., Pannekoek, W. J., Liu, W. M., Cramer, M. J., . . . Doevendans, P. A. (2004). Role of apoptosis in reperfusion injury. *Cardiovascular Research*, *61*(3), 414-426. https://doi.org/10.1016/J.CARDIORES.2003.12.023/2/61-3-414-FIG2.GIF

Egido, J., Zaragoza, C., Gomez-Guerrero, C., Martin-Ventura, J. L., Blanco-Colio, L., Lavin, B., . . . Ortiz, A. (2011). Animal Models of Cardiovascular Diseases. *Journal of Biomedicine and Biotechnology*, *2011*, 13-13. https://doi.org/10.1155/2011/497841

Ensembl. Transcript: ENST00000276297.9 (DLC1-201) - Protein summary - Homo_sapiens - Ensembl genome browser 109. In.

Entman, M. L., Youker, K., Shoji, T., Kukielka, G., Shappell, S. B., Taylor, A. A., & Smith, C. W. (1992). Neutrophil induced oxidative injury of cardiac myocytes. A compartmented system requiring CD11b/CD18-ICAM-1 adherence. *The Journal of Clinical Investigation*, *90*(4), 1335-1345. https://doi.org/10.1172/JCI115999

Fang, J., He, L., Wang, S.-Q., Ma, M.-J., Liu, H.-Y., Zhu, X.-H., . . . Wang, C.-Y. (2013). A simplified two-stitch sleeve technique for arterial anastomosis of cervical heterotopic cardiac transplantation in mice. *American Journal of Translational Research*, *5*(5), 521-521.

Fels, J. A., & Manfredi, G. (2019). Sex differences in ischemia/reperfusion injury: the role of mitochondrial permeability transition. *Neurochemical research*, *44*(10), 2336-2336. https://doi.org/10.1007/S11064-019-02769-6

Feng, Y., Chen, H., Cai, J., Zou, L., Yan, D., Xu, G., . . . Chao, W. (2015). Cardiac RNA induces inflammatory responses in cardiomyocytes and immune cells via Toll-like receptor 7 signaling. *Journal of Biological Chemistry*, *290*(44), 26688-26698. https://doi.org/10.1074/JBC.M115.661835

Fernández, A. R., Sánchez-Tarjuelo, R., Cravedi, P., Ochando, J., & López-Hoyos, M. (2020). Review: Ischemia Reperfusion Injury—A Translational Perspective in Organ Transplantation. *International Journal of Molecular Sciences*, *21*(22), 1-21. https://doi.org/10.3390/IJMS21228549

Foadoddini, M., Esmailidehaj, M., Mehrani, H., Sadraei, S. H., Golmanesh, L., Wahhabaghai, H., . . . Khoshbaten, A. (2011). Pretreatment with hyperoxia reduces in vivo infarct size and cell death by apoptosis with an early and delayed phase of protection. *European journal of cardio-thoracic surgery : official journal of the European Association for Cardio-thoracic Surgery*, *39*(2), 233-240. https://doi.org/10.1016/J.EJCTS.2010.05.036

Frank, A., Bonney, M., Bonney, S., Weitzel, L., Koeppen, M., & Eckle, T. (2012). Myocardial ischemia reperfusion injury - from basic science to clinical bedside. *Seminars in cardiothoracic and vascular anesthesia*, *16*(3), 123-123. https://doi.org/10.1177/1089253211436350

Frey, Y., Franz-Wachtel, M., Macek, B., & Olayioye, M. A. (2022). Proteasomal turnover of the RhoGAP tumor suppressor DLC1 is regulated by HECTD1 and USP7. *Scientific Reports 2022 12:1*, *12*(1), 1-10. https://doi.org/10.1038/s41598-022-08844-3

Fyfe, B., Loh, E., Winters, G. L., Couper, G. S., Kartashov, A. I., & Schoen, F. J. (1996). Heart transplantation-associated perioperative ischemic myocardial injury: Morphological features and clinical significance. *Circulation*, *93*(6), 1133-1140. https://doi.org/10.1161/01.CIR.93.6.1133/FORMAT/EPUB

Gallegos, R. P., Rivard, A. L., & Bianco, R. W. (2005). Animal models for cardiac research. *Handbook of Cardiac Anatomy, Physiology, and Devices*, 287-301. https://doi.org/10.1007/978-1-59259-835-9_21/COVER

Garbern, J. C., & Lee, R. T. (2021). Mitochondria and metabolic transitions in cardiomyocytes: lessons from development for stem cell-derived cardiomyocytes. *Stem Cell Research & Therapy 2021 12:1*, *12*(1), 1-25. https://doi.org/10.1186/S13287-021-02252-6

Gehlbach, B. K., & Geppert, E. (2004). The Pulmonary Manifestations of Left Heart Failure. *Chest*, *125*(2), 669-682. https://doi.org/10.1378/CHEST.125.2.669

Gene Symbol. Gene symbol report | HUGO Gene Nomenclature Committee. In *n.d.*

Grant, A. O. (2009). Cardiac Ion Channels. *Circulation: Arrhythmia and Electrophysiology*, *2*(2), 185-194. https://doi.org/10.1161/CIRCEP.108.789081

Graudejus, O., Ponce Wong, R., Varghese, N., Wagner, S., & Morrison, B. (2018). Bridging the gap between in vivo and in vitro research: Reproducing in vitro the mechanical and electrical environment of cells in vivo. *Frontiers in Cellular Neuroscience*, *12*. https://doi.org/10.3389/CONF.FNCEL.2018.38.00069/EVENT_ABSTRACT

Guariento, A., Piekarski, B. L., Doulamis, I. P., Blitzer, D., Ferraro, A. M., Harrild, D. M., . . . Emani, S. M. (2021). Autologous mitochondrial transplantation for cardiogenic shock in pediatric patients following ischemia-reperfusion injury. *The Journal of thoracic and cardiovascular surgery*, *162*(3), 992-1001. https://doi.org/10.1016/J.JTCVS.2020.10.151

Guazzi, M., & Arena, R. (2010). Pulmonary hypertension with left-sided heart disease. *Nature Reviews Cardiology 2010 7:11*, *7*(11), 648-659. https://doi.org/10.1038/nrcardio.2010.144

Hansson, G. K., Libby, P., & Tabas, I. (2015). Inflammation and plaque vulnerability. *Journal of Internal Medicine*, *278*(5), 483-493. https://doi.org/10.1111/JOIM.12406

He, W., Tong, G., Fan, H., Zhen, C., Zeng, L., Xue, L., . . . He, P. (2023). Exendin-4 alleviates myocardial ischemia reperfusion injury by enhancing autophagy through promoting nuclear translocation of TFEB. *Experimental Cell Research*, *423*(2), 113469-113469. https://doi.org/10.1016/J.YEXCR.2023.113469

Hers, I., Wherlock, M., Homma, Y., Yagisawa, H., & Tavare, J. M. (2006). Identification of p122RhoGAP (deleted in liver cancer-1) Serine 322 as a substrate for protein kinase B and ribosomal S6 kinase in insulin-stimulated cells. *The Journal of biological chemistry*, *281*(8), 4762-4770. https://doi.org/10.1074/JBC.M511008200

Hidalgo, A., Glass, N., Ovchinnikov, D., Yang, S. K., Zhang, X., Mazzone, S., . . . Cooper-White, J. (2018). Modelling ischemia-reperfusion injury (IRI) in vitro using metabolically matured induced pluripotent stem cell-derived cardiomyocytes. *APL Bioengineering*, *2*(2). https://doi.org/10.1063/1.5000746

Hillman, T. C., Idnani, R., & Wilson, C. G. (2022). An Inexpensive Open-Source Chamber for Controlled Hypoxia/Hyperoxia Exposure. *Frontiers in Physiology*, *13*, 1301-1301. https://doi.org/10.3389/FPHYS.2022.891005/BIBTEX

Hinsenkamp, I. (2018). The role of DLC1 in Helicobacter-related gastric disease. In.

Hinton, R. B., & Yutzey, K. E. (2011). Heart Valve Structure and Function in Development and Disease. *Annual review of physiology*, *73*, 29-29. https://doi.org/10.1146/ANNUREV-PHYSIOL-012110-142145

Hirsch, C., & Schildknecht, S. (2019). In Vitro Research Reproducibility: Keeping Up High Standards. *Frontiers in pharmacology*, *10*. https://doi.org/10.3389/FPHAR.2019.01484

Hodge, R. G., & Ridley, A. J. (2016). Regulating Rho GTPases and their regulators. *Nature Reviews Molecular Cell Biology 2016 17:8*, *17*(8), 496-510. https://doi.org/10.1038/nrm.2016.67

Homma, N., Nagaoka, T., Karoor, V., Imamura, M., Taraseviciene-Stewart, L., Walker, L. A., . . . Oka, M. (2008). Involvement of RhoA/Rho kinase signaling in protection against monocrotaline-induced pulmonary hypertension in pneumonectomized rats by dehydroepiandrosterone. *American Journal of Physiology - Lung Cellular and Molecular Physiology*, *295*(1), 71-78. https://doi.org/10.1152/AJPLUNG.90251.2008/ASSET/IMAGES/LARGE/ZH50070852350007.JPEG

Huang, J., Li, R., & Wang, C. (2021). The Role of Mitochondrial Quality Control in Cardiac Ischemia/Reperfusion Injury. *Oxidative Medicine and Cellular Longevity*, *2021*. https://doi.org/10.1155/2021/5543452

Ibáñez, B., Heusch, G., Ovize, M., & Van De Werf, F. (2015). Evolving therapies for myocardial ischemia/reperfusion injury. *Journal of the American College of Cardiology*, *65*(14), 1454-1471. https://doi.org/10.1016/J.JACC.2015.02.032

Institute of, M. (2010). Ischemic Heart Disease.

Ishii, D., Matsuno, N., Gochi, M., Iwata, H., Shonaka, T., Nishikawa, Y., . . . Furukawa, H. (2021). Beneficial effects of end-ischemic oxygenated machine perfusion preservation for split-liver transplantation in recovering graft function and reducing ischemia–reperfusion injury. *Scientific Reports*, *11*(1), 22608-22608. https://doi.org/10.1038/S41598-021-01467-0

Jackson, J. G., St. Clair, P., Sliwkowski, M. X., & Brattain, M. G. (2004). Blockade of epidermal growth factor- or heregulin-dependent ErbB2 activation with the anti-ErbB2 monoclonal antibody 2C4 has divergent downstream signaling and growth effects. *Cancer research*, *64*(7), 2601-2609. https://doi.org/10.1158/0008-5472.CAN-03-3106

Jacob, S., Garg, P., Wadiwala, I., Yazji, J. H., Alomari, M., Alamouti-Fard, E., . . . Pham, S. M. (2022). Strategies for Expanding Donors Pool in Heart Transplantation. *Reviews in Cardiovascular Medicine*, *23*(8), 285-285. https://doi.org/10.31083/J.RCM2308285/2153-8174-23-8-285/FIG4.JPG

Javed, Z., Haisum Maqsood, M., Yahya, T., Amin, Z., Acquah, I., Valero-Elizondo, J., . . . Nasir, K. (2022). Race, Racism, and Cardiovascular Health: Applying a Social Determinants of Health Framework to Racial/Ethnic Disparities in Cardiovascular Disease. *Circulation. Cardiovascular quality and outcomes*, *15*(1), e007917-e007917. https://doi.org/10.1161/CIRCOUTCOMES.121.007917

Jedrzejczak-Silicka, M. (2017). History of Cell Culture. *New Insights into Cell Culture Technology*. https://doi.org/10.5772/66905

Jernryd, V., Metzsch, C., Andersson, B., & Nilsson, J. (2020). The influence of ischemia and reperfusion time on outcome in heart transplantation. *Clinical transplantation*, *34*(5). https://doi.org/10.1111/CTR.13840

Jernryd, V., Metzsch, C., Andersson, B., & Nilsson, J. (2020). The influence of ischemia and reperfusion time on outcome in heart transplantation. *Clinical transplantation*, *34*(5). https://doi.org/10.1111/CTR.13840

Ji, H., Wang, J., Muid, D., Song, W., Jiang, Y., & Zhou, H. (2022). FUNDC1 activates the mitochondrial unfolded protein response to preserve mitochondrial quality control in cardiac ischemia/reperfusion injury. *Cellular Signalling*.

Jia, T., Wang, C., Han, Z., Wang, X., Ding, M., & Wang, Q. (2020). Experimental Rodent Models of Cardiovascular Diseases. *Frontiers in Cardiovascular Medicine*, *7*, 310-310. https://doi.org/10.3389/FCVM.2020.588075/BIBTEX

Jiang, X., & Wang, X. (2004). Cytochrome C-Mediated Apoptosis. *https://doi.org/10.1146/annurev.biochem.73.011303.073706*, *73*, 87-106. https://doi.org/10.1146/ANNUREV.BIOCHEM.73.011303.073706

Joshi, R., Qin, L., Cao, X., Zhong, S., Voss, C., Min, W., & Li, S. S. C. (2020). DLC1 SAM domain-binding peptides inhibit cancer cell growth and migration by inactivating RhoA. *Journal of Biological Chemistry*, *295*(2), 645-656. https://doi.org/10.1074/JBC.RA119.011929/ATTACHMENT/87912C36-792C-4093-A516-13F326ADCD96/MMC1.PDF

Kalogeris, T., Baines, C. P., Krenz, M., & Korthuis, R. J. (2012). Cell Biology of Ischemia/Reperfusion Injury. *International review of cell and molecular biology*, *298*, 229-229. https://doi.org/10.1016/B978-0-12-394309-5.00006-7

Kang, Z., Xu, F., Zhang, Q. A., Lin, J., Wu, Z., Zhang, X., . . . Guan, M. (2012). Correlation of DLC1 gene methylation with oncogenic PIK3CA mutations in extramammary Paget's disease. *Modern pathology : an official journal of the United States and Canadian Academy of Pathology, Inc*, *25*(8), 1160-1168. https://doi.org/10.1038/MODPATHOL.2012.65

Kawai, K., Iwamae, Y., Yamaga, M., Kiyota, M., Ishii, H., Hirata, H., . . . Yagisawa, H. (2009). Focal adhesion-localization of START-GAP1/DLC1 is essential for cell motility and morphology. *Genes to cells : devoted to molecular & cellular mechanisms*, *14*(2), 227-241. https://doi.org/10.1111/J.1365-2443.2008.01265.X

Kilian, L. S., Frank, D., & Rangrez, A. Y. (2021). RhoA Signaling in Immune Cell Response and Cardiac Disease. *Cells 2021, Vol. 10, Page 1681*, *10*(7), 1681-1681. https://doi.org/10.3390/CELLS10071681

Kim, S. C., Stice, J. P., Chen, L., Jung, J. S., Gupta, S., Wang, Y., . . . Knowlton, A. A. (2009). Extracellular heat shock protein 60, cardiac myocytes, and apoptosis. *Circulation Research*, *105*(12), 1186-1195. https://doi.org/10.1161/CIRCRESAHA.109.209643

Ko, F. C. F., Chan, L. K., Tung, E. K. K., Lowe, S. W., Ng, I. O. L., & Yam, J. W. P. (2010). Akt phosphorylation of deleted in liver cancer 1 abrogates its suppression of liver cancer tumorigenesis and metastasis. *Gastroenterology*, *139*(4). https://doi.org/10.1053/J.GASTRO.2010.06.051

Koeppen, M., Lee, J. W., Seo, S. W., Brodsky, K. S., Kreth, S., Yang, I. V., . . . Eltzschig, H. K. (2018). Hypoxia-inducible factor 2-alpha-dependent induction of amphiregulin dampens myocardial ischemia-reperfusion injury. *Nature Communications 2018 9:1*, *9*(1), 1-13. https://doi.org/10.1038/s41467-018-03105-2

Krugmann, S., Anderson, K. E., Ridley, S. H., Risso, N., McGregor, A., Coadwell, J., . . . Hawkins, P. T. (2002). Identification of ARAP3, a novel PI3K effector regulating both Arf and Rho GTPases, by selective capture on phosphoinositide affinity matrices. *Molecular cell*, *9*(1), 95-108. https://doi.org/10.1016/S1097-2765(02)00434-3

Kuba, K., Zhang, L., Imai, Y., Arab, S., Chen, M., Maekawa, Y., . . . Penninger, J. M. (2007). Impaired Heart Contractility in Apelin Gene–Deficient Mice Associated With Aging and Pressure Overload. *Circulation Research*, *101*(4). https://doi.org/10.1161/CIRCRESAHA.107.158659

Lauriol, J., Keith, K., Jaffré, F., Couvillon, A., Saci, A., Goonasekera, S. A., . . . Kontaridis, M. I. (2014). RhoA signaling in cardiomyocytes protects against stress-induced heart failure but facilitates cardiac fibrosis. *Science signaling*, *7*(348), ra100-ra100. https://doi.org/10.1126/SCISIGNAL.2005262

Le Bras, A. (2021). Distinct microenvironments in primary and transplant tumor models determine response to therapy. *Lab Animal 2021 50:2*, *50*(2), 47-47. https://doi.org/10.1038/s41684-021-00712-3

Leong, X. F., Ng, C. Y., & Jaarin, K. (2015). Animal Models in Cardiovascular Research: Hypertension and Atherosclerosis. *BioMed Research International*, *2015*. https://doi.org/10.1155/2015/528757

Lin, B., Wang, Y., Wang, Z., Tan, H., Kong, X., Shu, Y., . . . Hu, L. (2014). Uncovering the Rare Variants of DLC1 Isoform 1 and Their Functional Effects in a Chinese Sporadic Congenital Heart Disease Cohort. *PLoS ONE*, *9*(2). https://doi.org/10.1371/JOURNAL.PONE.0090215

Lindsey, M. L., Bolli, R., Canty, J. M., Du, X. J., Frangogiannis, N. G., Frantz, S., . . . Heusch, G. (2018). Guidelines for experimental models of myocardial ischemia and infarction. *American Journal of Physiology - Heart and Circulatory Physiology*, *314*(4), H812-H838. https://doi.org/10.1152/AJPHEART.00335.2017/ASSET/IMAGES/LARGE/ZH40031824550001.JPEG

Linnerz, T., & Bertrand, J. Y. (2021). Dlc1 controls cardio-vascular development downstream of Vegfa/Kdrl/Nrp1 signaling in the zebrafish embryo. *bioRxiv*, 2021.2002.2011.430763-432021.430702.430711.430763. https://doi.org/10.1101/2021.02.11.430763

Liu, F., & Kang, S. M. (2007). Heterotopic Heart Transplantation in Mice. *Journal of Visualized Experiments : JoVE*, *6*(6). https://doi.org/10.3791/238

Liu, G., Zhang, H., Hao, F., Hao, J., Pan, L., Zhao, Q., & Wo, J. (2018). Clusterin Reduces Cold Ischemia-Reperfusion Injury in Heart Transplantation Through Regulation of NF-kB Signaling and Bax/Bcl-xL Expression. *Cellular Physiology and Biochemistry*, *45*(3), 1003-1012. https://doi.org/10.1159/000487295

Liu, K., Chen, H., You, Q. S., Ye, Q., Wang, F., Wang, S., . . . Lu, Q. (2017). Curcumin attenuates myocardial ischemia–reperfusion injury. *Oncotarget*, *8*(67), 112051-112051. https://doi.org/10.18632/ONCOTARGET.23002

Lopez, E. O., Ballard, B. D., & Jan, A. (2022). Cardiovascular Disease.

Ma, L., Shi, H., Li, Y., Gao, W., Guo, J., Zhu, J., . . . Ge, J. (2021). Hypertrophic preconditioning attenuates myocardial ischemia/reperfusion injury through the deacetylation of isocitrate dehydrogenase 2. *Science Bulletin*, *66*(20), 2099-2114. https://doi.org/10.1016/J.SCIB.2021.04.008

Maneechote, C., Palee, S., …, S. K. C., & undefined. mitochondrial dynamics via increasing mitochondrial fusion attenuates infarct size and left ventricular dysfunction in rats with cardiac ischemia/reperfusion injury. *portlandpress.com*.

Mangini, S., Alves, B. R., Silvestre, O. M., Pires, P. V. i., Pires, L. J. o. T., Curiati, M. N. o. C., & Bacal, F. (2015). Heart transplantation: review. *Einstein (Sao Paulo, Brazil)*, *13*(2), 310-318. https://doi.org/10.1590/S1679-45082015RW3154

Marin, W., Marin, D., Ao, X., & Liu, Y. (2021). Mitochondria as a therapeutic target for cardiac ischemia-reperfusion injury (Review). *International Journal of Molecular Medicine*, *47*(2), 485-499. https://doi.org/10.3892/IJMM.2020.4823

Martin, M. L., & Blaxall, B. C. (2012). Cardiac Intercellular Communication: Are myocytes and fibroblasts fair-weather friends? *Journal of cardiovascular translational research*, *5*(6), 768-768. https://doi.org/10.1007/S12265-012-9404-5

Mauerhofer, C., Grumet, L., Schemmer, P., Leber, B., & Stiegler, P. (2021). Combating Ischemia-Reperfusion Injury with Micronutrients and Natural Compounds during Solid Organ Transplantation: Data of Clinical Trials and Lessons of Preclinical Findings. *International Journal of Molecular Sciences 2021, Vol. 22, Page 10675*, *22*(19), 10675-10675. https://doi.org/10.3390/IJMS221910675

McCance, K. L., & Huether, S. E. (2018). *Pathophysiology: the biologic basis for disease in adults and children* (Eighth edition ed.).

McKeown, S. R. (2014). Defining normoxia, physoxia and hypoxia in tumours—implications for treatment response. *The British Journal of Radiology*, *87*(1035). https://doi.org/10.1259/BJR.20130676

Menéndez-Menéndez, Y., Otero-Hernández, J., Vega, J. A., Pérez-Basterrechea, M., Pérez-López, S., Álvarez-Viejo, M., & Ferrero-Gutiérrez, A. (2017). The role of bone marrow mononuclear cell-conditioned medium in the proliferation and migration of human dermal fibroblasts. *Cellular and Molecular Biology Letters*, *22*(1), 1-12. https://doi.org/10.1186/S11658-017-0055-Z/FIGURES/6

Mertins, P., Mani, D. R., Ruggles, K. V., Gillette, M. A., Clauser, K. R., Wang, P., . . . Carr, S. A. (2016). Proteogenomics connects somatic mutations to signalling in breast cancer. *Nature*, *534*(7605), 55-62. https://doi.org/10.1038/NATURE18003

Ming, C. L. C., Sesperez, K., Ben-Sefer, E., Arpon, D., McGrath, K., McClements, L., & Gentile, C. (2021). Considerations to Model Heart Disease in Women with Preeclampsia and Cardiovascular Disease. *Cells 2021, Vol. 10, Page 899*, *10*(4), 899-899. https://doi.org/10.3390/CELLS10040899

Mitra, S., Sammani, S., Wang, T., Boone, D. L., Meyer, N. J., Dudek, S. M., . . . Jacobson, J. R. (2011). Role of growth arrest and DNA damage-inducible α in Akt phosphorylation and ubiquitination after mechanical stress-induced vascular injury. *American journal of respiratory and critical care medicine*, *184*(9), 1030-1040. https://doi.org/10.1164/RCCM.201103-0447OC

Mori, D. N., Kreisel, D., Fullerton, J. N., Gilroy, D. W., & Goldstein, D. R. (2014). Inflammatory triggers of acute rejection of organ allografts. *Immunological Reviews*, *258*(1), 132-144. https://doi.org/10.1111/IMR.12146

Murga, C., Fukuhara, S., & Gutkind, J. S. (2000). A novel role for phosphatidylinositol 3-kinase beta in signaling from G protein-coupled receptors to Akt. *The Journal of biological chemistry*, *275*(16), 12069-12073. https://doi.org/10.1074/JBC.275.16.12069

Nagoshi, T., Matsui, T., Aoyama, T., Leri, A., Anversa, P., Li, L., . . . Rosenzweig, A. (2005). PI3K rescues the detrimental effects of chronic Akt activation in the heart during ischemia/reperfusion injury. *The Journal of Clinical Investigation*, *115*(8), 2128-2138. https://doi.org/10.1172/JCI23073

Naito, H., Nojima, T., Fujisaki, N., Tsukahara, K., Yamamoto, H., Yamada, T., . . . Nakao, A. (2020). Therapeutic strategies for ischemia reperfusion injury in emergency medicine. *Acute Medicine & Surgery*, *7*(1), e501-e501. https://doi.org/10.1002/AMS2.501

Navas-Blanco, J., & Modak, R. (2021). Perioperative Care of Heart Transplant Recipients Undergoing Non-Cardiac Surgery. *Annals of Cardiac Anaesthesia*, *24*(2), 140-140. https://doi.org/10.4103/ACA.ACA_130_19

NCBI. DLC1 DLC1 Rho GTPase activating protein [Homo sapiens (human)] - Gene-NCBI. In.

Nci. Definition of vena cava - NCI Dictionary of Cancer Terms - NCI. In *n.d.*

Neri, M., Riezzo, I., Pascale, N., Pomara, C., & Turillazzi, E. (2017). Ischemia/Reperfusion Injury following Acute Myocardial Infarction: A Critical Issue for Clinicians and Forensic Pathologists. *Mediators of Inflammation*, *2017*. https://doi.org/10.1155/2017/7018393

Nieuwenhuijs-Moeke, G. J., Pischke, S. E., Berger, S. P., Sanders, J. S. F., Pol, R. A., Struys, M. M. R. F., . . . Leuvenink, H. G. D. (2020). Ischemia and reperfusion injury in kidney transplantation: Relevant mechanisms in injury and repair. In *Journal of Clinical Medicine* (Vol. 9): MDPI.

Niimi, M. (2001). The technique for heterotopic cardiac transplantation in mice: experience of 3000 operations by one surgeon. *The Journal of Heart and Lung Transplantation*, *20*(10), 1123-1128. https://doi.org/10.1016/S1053-2498(01)00309-6

O'Donnell, A., & Yutz, K. E. (2020). Mechanisms of heart valve development and disease. *Development (Cambridge, England)*, *147*(13). https://doi.org/10.1242/DEV.183020

Ogobuiro, I., Wehrle, C. J., & Tuma, F. (2022). Anatomy, Thorax, Heart Coronary Arteries. *StatPearls*.

O'Neill, B. T., & Abel, E. D. (2005). Akt1 in the cardiovascular system: friend or foe? *Journal of Clinical Investigation*, *115*(8), 2059-2059. https://doi.org/10.1172/JCI25900

Ostadal, B., & Ostadal, P. (2014). Sex-based differences in cardiac ischaemic injury and protection: therapeutic implications. *British Journal of Pharmacology*, *171*(3), 541-541. https://doi.org/10.1111/BPH.12270

Palatianos, G. M., Craythorne, C. B., Schor, J. S., & Bolooki, H. (1988). Hemodynamic effects of radical left ventricular scar resection in patients with and without congestive heart failure. *The Journal of surgical research*, *44*(6), 690-695. https://doi.org/10.1016/0022-4804(88)90102-3

Park, C. O., Xiao, X. H., & Allen, D. G. (1999). Changes in intracellular Na+ and pH in rat heart during ischemia: Role of Na+/H+ exchanger. *American Journal of Physiology - Heart and Circulatory Physiology*, *276*(5 45-5). https://doi.org/10.1152/AJPHEART.1999.276.5.H1581/ASSET/IMAGES/LARGE/AHEA40536008X.JPEG

Park, D. S., & Fishman, G. I. (2017). Development and Function of the Cardiac Conduction System in Health and Disease. *Journal of Cardiovascular Development and Disease*, *4*(2). https://doi.org/10.3390/JCDD4020007

Patel, P. M., Connolly, M. R., Coe, T. M., Calhoun, A., Pollok, F., Markmann, J. F., . . . Pierson, R. N. (2021). Minimizing Ischemia Reperfusion Injury in Xenotransplantation. *Frontiers in Immunology*, *12*, 3506-3506. https://doi.org/10.3389/FIMMU.2021.681504/BIBTEX

Perez-de-Puig, I., Miró-Mur, F., Ferrer-Ferrer, M., Gelpi, E., Pedragosa, J., Justicia, C., . . . Planas, A. M. (2015). Neutrophil recruitment to the brain in mouse and human ischemic stroke. *Acta neuropathologica*, *129*(2), 239-257. https://doi.org/10.1007/S00401-014-1381-0

Pignatelli, P., Menichelli, D., Pastori, D., & Violi, F. (2018). Oxidative stress and cardiovascular disease: New insights. *Kardiologia Polska*, *76*(4), 713-722. https://doi.org/10.5603/KP.a2018.0071

Portal, L., Martin, V., Assaly, R., D'Anglemont De Tassigny, A., Michineau, S., Berdeaux, A., . . . Pons, S. (2013). A model of hypoxia-reoxygenation on isolated adult mouse cardiomyocytes: Characterization, comparison with ischemia-reperfusion, and application to the cardioprotective effect of regular treadmill exercise. *Journal of Cardiovascular Pharmacology and Therapeutics*, *18*(4), 367-375. https://doi.org/10.1177/1074248412475158/ASSET/IMAGES/LARGE/10.1177_1074248412475158-FIG7.JPEG

Powell-Wiley, T. M., Baumer, Y., Baah, F. O., Baez, A. S., Farmer, N., Mahlobo, C. T., . . . Wallen, G. R. (2022). Social Determinants of Cardiovascular Disease. *Circulation Research*, *130*(5), 782-799. https://doi.org/10.1161/CIRCRESAHA.121.319811

Prakash, S. K., Paylor, R., Jenna, S., Lamarche-Vane, N., Armstrong, D. L., Xu, B., . . . Zoghbi, H. Y. (2000). Functional analysis of ARHGAP6, a novel GTPase-activating protein for RhoA. *Human molecular genetics*, *9*(4), 477-488. https://doi.org/10.1093/HMG/9.4.477

Putcha, G. V., Le, S., Frank, S., Besirli, C. G., Clark, K., Chu, B., . . . Johnson, E. M. (2003). JNK-mediated BIM phosphorylation potentiates BAX-dependent apoptosis. *Neuron*, *38*(6), 899-914. https://doi.org/10.1016/S0896-6273(03)00355-6

Qian, X., Li, G., Asmussen, H. K., Asnaghi, L., Vass, W. C., Braverman, R., . . . Lowy, D. R. (2007). Oncogenic inhibition by a deleted in liver cancer gene requires cooperation between tensin binding and Rho-specific GTPase-activating protein activities. *Proceedings of the National Academy of Sciences of the United States of America*, *104*(21), 9012-9017. https://doi.org/10.1073/PNAS.0703033104/SUPPL_FILE/03033FIG12.PDF

Quijada, P., Trembley, M. A., & Small, E. M. (2020). The Role of the Epicardium During Heart Development and Repair. *Circulation Research*, *126*, 377-394. https://doi.org/10.1161/CIRCRESAHA.119.315857

Rabinovitch, R. C., Samborska, B., Faubert, B., Ma, E. H., Gravel, S. P., Andrzejewski, S., . . . Jones, R. G. (2017). AMPK Maintains Cellular Metabolic Homeostasis through Regulation of Mitochondrial Reactive Oxygen Species. *Cell Reports*, *21*(1), 1-9. https://doi.org/10.1016/J.CELREP.2017.09.026

Rahman, A., Li, Y., Chan, T.-K., Zhao, H., Xiang, Y., Chang, X., . . . Ong, S.-B. (2023). Large animal models of cardiac ischemia-reperfusion injury: Where are we now? *Zoological Research, 2023, Vol. 44, Issue 3, Pages: 591-603*, *44*(3), 591-603. https://doi.org/10.24272/J.ISSN.2095-8137.2022.487

Rands, S. A. (2011). Inclusion of Policies on Ethical Standards in Animal Experiments in Biomedical Science Journals. *Journal of the American Association for Laboratory Animal Science : JAALAS*, *50*(6), 901-901.

Reaven, P. D., & Sacks, J. (2005). Coronary artery and abdominal aortic calcification are associated with cardiovascular disease in type 2 diabetes. *Diabetologia*, *48*(2), 379-385. https://doi.org/10.1007/S00125-004-1640-Z/TABLES/3

Ren, G., & Li, G. (2021). Tumor suppressor gene DLC1: Its modifications, interactive molecules, and potential prospects for clinical cancer application. *International Journal of Biological Macromolecules*, *182*, 264-275. https://doi.org/10.1016/J.IJBIOMAC.2021.04.022

Richardson, W. J., Clarke, S. A., Alexander Quinn, T., & Holmes, J. W. (2015). Physiological Implications of Myocardial Scar Structure. *Comprehensive Physiology*, *5*(4), 1877-1877. https://doi.org/10.1002/CPHY.C140067

Riedl, S. J., & Shi, Y. (2004). Molecular mechanisms of caspase regulation during apoptosis. *Nature Reviews Molecular Cell Biology 2004 5:11*, *5*(11), 897-907. https://doi.org/10.1038/nrm1496

Riley, J. S., & Tait, S. W. G. (2020). Mitochondrial DNA in inflammation and immunity. *EMBO reports*, *21*(4). https://doi.org/10.15252/EMBR.201949799

Ripa, R., George, T., & Sattar, Y. (2022). Physiology, Cardiac Muscle. *StatPearls*.

Rodrigues, G. A., Falasca, M., Zhang, Z., Ong, S. H., & Schlessinger, J. (2000). A novel positive feedback loop mediated by the docking protein Gab1 and phosphatidylinositol 3-kinase in epidermal growth factor receptor signaling. *Molecular and cellular biology*, *20*(4), 1448-1459. https://doi.org/10.1128/MCB.20.4.1448-1459.2000

Sabbir, M. G., Wigle, N., Loewen, S., Gu, Y., Buse, C., Hicks, G. G., & Mowat, M. R. A. (2010). Identification and characterization of Dlc1 isoforms in the mouse and study of the biological function of a single gene trapped isoform. *BMC Biology*, *8*(1), 1-21. https://doi.org/10.1186/1741-7007-8-17/TABLES/1

Saeidnia, S., Manayi, A., & Abdollahi, M. (2015). From in vitro Experiments to in vivo and Clinical Studies; Pros and Cons. *Current drug discovery technologies*, *12*(4), 218-224. https://doi.org/10.2174/1570163813666160114093140

Salazar-Gonzalez, H., Gutierrez-Mercado, Y. K., Munguia-Galaviz, F. J., & Echavarria, R. (2022). Signaling Pathways Involved in Myocardial Ischemia–Reperfusion Injury and Cardioprotection: A Systematic Review of Transcriptomic Studies in Sus scrofa. *Journal of Cardiovascular Development and Disease*, *9*(5). https://doi.org/10.3390/JCDD9050132/S1

Salmena, L., Carracedo, A., & Pandolfi, P. P. (2008). Tenets of PTEN tumor suppression. *Cell*, *133*(3), 403-414. https://doi.org/10.1016/J.CELL.2008.04.013

Sánchez-Hernández, C. D., Torres-Alarcón, L. A., González-Cortés, A., Peón, A. N., & Rungatscher, A. (2020). Ischemia/Reperfusion Injury: Pathophysiology, Current Clinical Management, and Potential Preventive Approaches. *Mediators of Inflammation*, *2020*. https://doi.org/10.1155/2020/8405370

Sanchez-Solana, B., Wang, D., Qian, X., Velayoudame, P., Simanshu, D. K., Acharya, J. K., & Lowy, D. R. (2021). The tumor suppressor activity of DLC1 requires the interaction of its START domain with Phosphatidylserine, PLCD1, and Caveolin-1. *Molecular Cancer*, *20*(1), 1-18. https://doi.org/10.1186/S12943-021-01439-Y/FIGURES/8

Santy, L. C., & Casanova, J. E. (2002). GTPase signaling: bridging the GAP between ARF and Rho. *Current biology : CB*, *12*(10), R360-R362. https://doi.org/10.1016/S0960-9822(02)00860-6

Sárközy, M., Márványkövi, F. M., Szűcs, G., Kovács, Z. Z. A., Szabó, M. R., Gáspár, R., . . . Csont, T. (2021). Ischemic preconditioning protects the heart against ischemia-reperfusion injury in chronic kidney disease in both males and females. *Biology of Sex Differences*, *12*(1), 1-20. https://doi.org/10.1186/S13293-021-00392-1/FIGURES/6

Sartorius. Octet® BLI Systems | Protein Analysis. In.

Savarese, G., Becher, P. M., Lund, L. H., Seferovic, P., Rosano, G. M. C., & Coats, A. J. S. (2023). Global burden of heart failure: a comprehensive and updated review of epidemiology. *Cardiovascular Research*, *118*(17), 3272-3287. https://doi.org/10.1093/CVR/CVAC013

Scheiermann, P., Beiras-Fernandez, A., Mutlak, H., & Weis, F. (2011). The protective effects of levosimendan on ischemia/reperfusion injury and apoptosis. *Recent Patents on Cardiovascular Drug Discovery*, *6*(1), 20-26. https://doi.org/10.2174/157489011794578482

Schuppli, C. A., & Fraser, D. (2005). The Interpretation and Application of the Three Rs by Animal Ethics Committee Members. *https://doi.org/10.1177/026119290503300511*, *33*(5), 487-500. https://doi.org/10.1177/026119290503300511

See Hoe, L. E., Wells, M. A., Bartnikowski, N., Obonyo, N. G., Millar, J. E., Khoo, A., . . . Fraser, J. F. (2020). Heart transplantation from brain dead donors: A systematic review of animal models. *Transplantation*, 2272-2289. https://doi.org/10.1097/TP.0000000000003217

Shang, X., Marchioni, F., Sipes, N., Evelyn, C. R., Jerabek-Willemsen, M., Duhr, S., . . . Zheng, Y. (2012). Rational Design of Small Molecule Inhibitors Targeting RhoA Subfamily Rho GTPases. *Chemistry & Biology*, *19*(6), 699-710. https://doi.org/10.1016/J.CHEMBIOL.2012.05.009

Shattock, M. J., Ottolia, M., Bers, D. M., Blaustein, M. P., Boguslavskyi, A., Bossuyt, J., . . . Xie, Z. J. (2015). Na+/Ca2+ exchange and Na+/K+-ATPase in the heart. *The*

Journal of physiology, *593*(6), 1361-1382. https://doi.org/10.1113/JPHYSIOL.2014.282319

Shih, Y.-P., Yuan, S. Y., & Lo, S. H. (2017). Down-regulation of DLC1 in endothelial cells compromises the angiogenesis process. *Cancer Letters*, *398*, 46-51. https://doi.org/10.1016/j.canlet.2017.04.004

Silvis, M. J. M., Kaffka genaamd Dengler, S. E., Odille, C. A., Mishra, M., van der Kaaij, N. P., Doevendans, P. A., . . . van Hout, G. P. J. (2020). Damage-Associated Molecular Patterns in Myocardial Infarction and Heart Transplantation: The Road to Translational Success. *Frontiers in Immunology*, *11*, 1-1. https://doi.org/10.3389/FIMMU.2020.599511

Soares, R. O. S., Losada, D. M., Jordani, M. C., Évora, P., & Castro-E-Silva, O. (2019). Ischemia/Reperfusion Injury Revisited: An Overview of the Latest Pharmacological Strategies. *International Journal of Molecular Sciences*, *20*(20). https://doi.org/10.3390/IJMS20205034

Song, X., Li, G., Vaage, J., & Valen, G. (2003). Effects of sex, gonadectomy, and oestrogen substitution on ischaemic preconditioning and ischaemia–reperfusion injury in mice. *Acta Physiologica Scandinavica*, *177*(4), 459-466. https://doi.org/10.1046/J.1365-201X.2003.01068.X

Sotillos, S., Aguilar-Aragon, M., & Hombría, J. C. G. (2018). Functional analysis of the Drosophila RhoGAP Cv-c protein and its equivalence to the human DLC3 and DLC1 proteins. *Scientific Reports 2018 8:1*, *8*(1), 1-11. https://doi.org/10.1038/s41598-018-22794-9

Spiess, C., Beil, A., & Ehrmann, M. (1999). A Temperature-Dependent Switch from Chaperone to Protease in a Widely Conserved Heat Shock Protein. *Cell*, *97*(3), 339-347. https://doi.org/10.1016/S0092-8674(00)80743-6

Steichen, C., Hervé, C., Hauet, T., & Bourmeyster, N. (2022). Rho GTPases in kidney physiology and diseases. *Small GTPases*, *13*(1), 141-141. https://doi.org/10.1080/21541248.2021.1932402

Strassheim, D., Gerasimovskaya, E., Irwin, D., Dempsey, E. C., Stenmark, K., & Karoor, V. (2019). RhoGTPase in Vascular Disease. *Cells 2019, Vol. 8, Page 551*, *8*(6), 551-551. https://doi.org/10.3390/CELLS8060551

Streef, T. J., & Smits, A. M. (2021). Epicardial Contribution to the Developing and Injured Heart: Exploring the Cellular Composition of the Epicardium. *Frontiers in Cardiovascular Medicine*, *8*, 1177-1177. https://doi.org/10.3389/FCVM.2021.750243

Sun, Y., Lee, S. M., Ku, B. J., & Moon, M. J. (2020). Fine structure of the intercalated disc and cardiac junctions in the black widow spider Latrodectus mactans. *Applied Microscopy*, *50*(1). https://doi.org/10.1186/S42649-020-00040-9

Talman, V., & Ruskoaho, H. (2016). Cardiac fibrosis in myocardial infarction—from repair and remodeling to regeneration. *Cell and Tissue Research*, *365*(3), 563-563. https://doi.org/10.1007/S00441-016-2431-9

Timmis, A., Group, o. b. o. t. A. W., Vardas, P., Townsend, N., Torbica, A., Katus, H., . . . Sebastiao, D. (2022). European Society of Cardiology: cardiovascular disease statistics 2021. *European Heart Journal*, *43*(8), 716-799. https://doi.org/10.1093/EURHEARTJ/EHAB892

Tong, H., Imahashi, K., Steenbergen, C., & Murphy, E. (2002). Phosphorylation of Glycogen Synthase Kinase-3β During Preconditioning Through a Phosphatidylinositol-3-Kinase–Dependent Pathway Is Cardioprotective. *Circulation Research*, *90*(4), 377-379. https://doi.org/10.1161/01.RES.0000012567.95445.55

Tran, D. B., Weber, C., & Lopez, R. A. (2022). Anatomy, Thorax, Heart Muscles. *StatPearls*.

Trillium Gift of Life, N. (2018). *Ontario's Referral and Listing Criteria for Adult Heart Transplantation Trillium Gift of Life Network*.

Tripathi, B. K., Grant, T., Qian, X., Zhou, M., Mertins, P., Wang, D., . . . Lowy, D. R. (2017). Receptor tyrosine kinase activation of RhoA is mediated by AKT phosphorylation of DLC1. *The Journal of Cell Biology*, *216*(12), 4255-4255. https://doi.org/10.1083/JCB.201703105

Tse, A. C. K., Li, J. W., Chan, T. F., Wu, R. S. S., & Lai, K. P. (2015). Hypoxia induces miR-210, leading to anti-apoptosis in ovarian follicular cells of marine medaka Oryzias melastigma. *Aquatic Toxicology*, *165*, 189-196. https://doi.org/10.1016/J.AQUATOX.2015.06.002

Tu, M., Tan, V. P., Yu, J. D., Tripathi, R., Bigham, Z., Barlow, M., . . . Miyamoto, S. (2022). RhoA signaling increases mitophagy and protects cardiomyocytes against ischemia by stabilizing PINK1 protein and recruiting Parkin to mitochondria. *Cell Death & Differentiation 2022 29:12*, *29*(12), 2472-2486. https://doi.org/10.1038/s41418-022-01032-w

Tuuminen, R., Syrjälä, S., Krebs, R., Keränen, M. A. I., Koli, K., Abo-Ramadan, U., . . . Lemström, K. B. (2011). Donor simvastatin treatment abolishes rat cardiac allograft ischemia/reperfusion injury and chronic rejection through microvascular

protection. *Circulation*, *124*(10), 1138-1150. https://doi.org/10.1161/CIRCULATIONAHA.110.005249

Van Buul, J. D., Geerts, D., & Huveneers, S. (2014). Rho GAPs and GEFs. *https://doi.org/10.4161/cam.27599*, *8*(2), 108-124. https://doi.org/10.4161/CAM.27599

Vanhaesebroeck, B., Guillermet-Guibert, J., Graupera, M., & Bilanges, B. (2010). The emerging mechanisms of isoform-specific PI3K signalling. *Nature reviews. Molecular cell biology*, *11*(5), 329-341. https://doi.org/10.1038/NRM2882

Vanlangenakker, N., Vanden Berghe, T., & Vandenabeele, P. (2012). Many stimuli pull the necrotic trigger, an overview. *Cell death and differentiation*, *19*(1), 75-86. https://doi.org/10.1038/CDD.2011.164

Vassalli, G., Milano, G., & Moccetti, T. (2012). Role of Mitogen-Activated Protein Kinases in Myocardial Ischemia-Reperfusion Injury during Heart Transplantation. *Journal of Transplantation*, *2012*, 1-16. https://doi.org/10.1155/2012/928954

Vela, M. M., Sáez, D. G., & Simon, A. R. (2018). Current approaches in retrieval and heart preservation. *Annals of Cardiothoracic Surgery*, *7*(1), 67-67. https://doi.org/10.21037/ACS.2018.01.06

Verma, S., Fedak, P. W. M., Weisel, R. D., Butany, J., Rao, V., Maitland, A., . . . Yau, T. M. (2002). Fundamentals of Reperfusion Injury for the Clinical Cardiologist. *Circulation*, *105*(20), 2332-2336. https://doi.org/10.1161/01.CIR.0000016602.96363.36

Virani, S. S., Alonso, A., Aparicio, H. J., Benjamin, E. J., Bittencourt, M. S., Callaway, C. W., . . . Tsao, C. W. (2021). Heart Disease and Stroke Statistics-2021 Update: A Report From the American Heart Association. *Circulation*, *143*(8), E254-E743. https://doi.org/10.1161/CIR.0000000000000950

Voigt, P., Dorner, M. B., & Schaefer, M. (2006). Characterization of p87PIKAP, a novel regulatory subunit of phosphoinositide 3-kinase gamma that is highly expressed in heart and interacts with PDE3B. *The Journal of biological chemistry*, *281*(15), 9977-9986. https://doi.org/10.1074/JBC.M512502200

von Samson-Himmelstjerna, F. A., Kolbrink, B., Riebeling, T., Kunzendorf, U., & Krautwald, S. (2022). Progress and Setbacks in Translating a Decade of Ferroptosis Research into Clinical Practice. *Cells 2022, Vol. 11, Page 2134*, *11*(14), 2134-2134. https://doi.org/10.3390/CELLS11142134

Walkowski, B., Kleibert, M., Majka, M., & Wojciechowska, M. (2022). Insight into the Role of the PI3K/Akt Pathway in Ischemic Injury and Post-Infarct Left

Ventricular Remodeling in Normal and Diabetic Heart. *Cells 2022, Vol. 11, Page 1553*, *11*(9), 1553-1553. https://doi.org/10.3390/CELLS11091553

Wang, D., Qian, X., Rajaram, M., Durkin, M. E., & Lowy, D. R. (2016). DLC1 is the principal biologically-relevant down-regulated DLC family member in several cancers. *Oncotarget*, *7*(29), 45144-45157. https://doi.org/10.18632/ONCOTARGET.9266

Wang, J., Hu, K., Cai, X., Yang, B., He, Q., Wang, J., & Weng, Q. (2022). Targeting PI3K/AKT signaling for treatment of idiopathic pulmonary fibrosis. *Acta Pharmaceutica Sinica. B*, *12*(1), 18-18. https://doi.org/10.1016/J.APSB.2021.07.023

Wang, M., Wang, Y., Weil, B., Abarbanell, A., Herrmann, J., Tan, J., . . . Meldrum, D. R. (2009). Estrogen receptor β mediates increased activation of PI3K/Akt signaling and improved myocardial function in female hearts following acute ischemia. *American Journal of Physiology - Regulatory Integrative and Comparative Physiology*, *296*(4), 972-978. https://doi.org/10.1152/AJPREGU.00045.2009/ASSET/IMAGES/LARGE/ZH60040967510006.JPEG

Ward, M., & Iskratsch, T. (2020). Mix and (mis-)match - The mechanosensing machinery in the changing environment of the developing, healthy adult and diseased heart. *Biochimica et biophysica acta. Molecular cell research*, *1867*(3). https://doi.org/10.1016/J.BBAMCR.2019.01.017

Weitzenblum, E. (2003). CHRONIC COR PULMONALE. *Heart*, *89*(2), 225-230. https://doi.org/10.1136/HEART.89.2.225

Wenzel, N., Blasczyk, R., & Figueiredo, C. (2021). Animal Models in Allogenic Solid Organ Transplantation. *Transplantology 2021, Vol. 2, Pages 412-424*, *2*(4), 412-424. https://doi.org/10.3390/TRANSPLANTOLOGY2040039

Westhofen, S., Jelinek, M., Dreher, L., Biermann, D., Martin, J., Vitzhum, H., . . . Schwoerer, A. P. (2019). The heterotopic heart transplantation in mice as a small animal model to study mechanical unloading – Establishment of the procedure, perioperative management and postoperative scoring. *PLOS ONE*, *14*(4), e0214513-e0214513. https://doi.org/10.1371/JOURNAL.PONE.0214513

Westreich, D., Pence, B. W., & Turner, A. N. (2010). In populo. *Epidemiology (Cambridge, Mass.)*, *21*(1), 152-152. https://doi.org/10.1097/EDE.0B013E3181C1E92A

Wong, C. C. L., Wong, C. M., Ko, F. C. F., Chan, L. K., Ching, Y. P., Yam, J. W. P., & Ng, I. O. I. (2008). Deleted in Liver Cancer 1 (DLC1) Negatively Regulates

Rho/ROCK/MLC Pathway in Hepatocellular Carcinoma. *PLoS ONE*, *3*(7), 2779-2779. https://doi.org/10.1371/JOURNAL.PONE.0002779

Wong, K., Ren, X. R., Huang, Y. Z., Xie, Y., Liu, G., Saito, H., . . . Rao, Y. (2001). Signal transduction in neuronal migration: roles of GTPase activating proteins and the small GTPase Cdc42 in the Slit-Robo pathway. *Cell*, *107*(2), 209-221. https://doi.org/10.1016/S0092-8674(01)00530-X

Xia, Z., Li, H., & Irwin, M. G. (2016). Myocardial ischaemia reperfusion injury: the challenge of translating ischaemic and anaesthetic protection from animal models to humans. *British journal of anaesthesia*, *117 Suppl 2*, ii44-ii62. https://doi.org/10.1093/BJA/AEW267

Xu, P., Jacobs, A. R., & Taylor, S. I. (1999). Interaction of insulin receptor substrate 3 with insulin receptor, insulin receptor-related receptor, insulin-like growth factor-1 receptor, and downstream signaling proteins. *The Journal of biological chemistry*, *274*(21), 15262-15270. https://doi.org/10.1074/JBC.274.21.15262

Yang, M., Linn, B. S., Zhang, Y., & Ren, J. (2019). Mitophagy and mitochondrial integrity in cardiac ischemia-reperfusion injury. *Biochimica et Biophysica Acta (BBA) - Molecular Basis of Disease*, *1865*(9).

Yu, B., Sladojevic, N., Blair, J. E., & Liao, J. K. (2020). Targeting Rho-associated coiled-coil forming protein kinase (ROCK) in cardiovascular fibrosis and stiffening. *https://doi.org/10.1080/14728222.2020.1712593*, *24*(1), 47-62. https://doi.org/10.1080/14728222.2020.1712593

Yu, D., Xiong, J., Gao, Y., Li, J., Zhu, D., Shen, X., . . . Wang, X. (2021). Resveratrol activates PI3K/AKT to reduce myocardial cell apoptosis and mitochondrial oxidative damage caused by myocardial ischemia/reperfusion injury. *Acta Histochemica*, *123*(5), 151739-151739. https://doi.org/10.1016/J.ACTHIS.2021.151739

Zhabyeyev, P., Gandhi, M., Mori, J., Basu, R., Kassiri, Z., Clanachan, A., . . . Oudit, G. Y. (2013). Pressure-overload-induced heart failure induces a selective reduction in glucose oxidation at physiological afterload. *Cardiovascular Research*, *97*(4), 676-685. https://doi.org/10.1093/CVR/CVS424

Zhao, Z. Q., & Vinten-Johansen, J. (2002). Myocardial apoptosis and ischemic preconditioning. *Cardiovascular Research*, *55*(3), 438-455. https://doi.org/10.1016/S0008-6363(02)00442-X/2/55-3-438-FIG8.GIF

Zhao, Z. Q., Nakamura, M., Wang, N. P., Wilcox, J. N., Shearer, S., Ronson, R. S., . . . Vinten-Johansen, J. (2000). Reperfusion induces myocardial apoptotic cell death. *Cardiovascular Research*, *45*(3), 651-660. https://doi.org/10.1016/S0008-6363(99)00354-5/2/45-3-651-FIG6.GIF

Zheng, D., Cao, T., Zhang, L. l., Fan, G. c., Qiu, J., & Peng, T. q. (2021). Targeted inhibition of calpain in mitochondria alleviates oxidative stress-induced myocardial injury. *Acta Pharmacologica Sinica*, *42*(6), 909-920. https://doi.org/10.1038/s41401-020-00526-y

Zhou, T., Prather, E. R., Garrison, D. E., & Zuo, L. (2018). Interplay between ROS and Antioxidants during Ischemia-Reperfusion Injuries in Cardiac and Skeletal Muscle. *International Journal of Molecular Sciences*, *19*(2). https://doi.org/10.3390/IJMS19020417

Zhu, P., Hu, S., Jin, Q., Li, D., Tian, F., Toan, S., . . . Zhou, H. (2018). Ripk3 promotes ER stress-induced necroptosis in cardiac IR injury: a mechanism involving calcium overload/XO/ROS/mPTP pathway. *Elsevier*.

Zhu, X., & Lu, X. (2019). MiR-423-5p inhibition alleviates cardiomyocyte apoptosis and mitochondrial dysfunction caused by hypoxia/reoxygenation through activation of the wnt/β-catenin signaling pathway via targeting MYBL2. *Journal of Cellular Physiology*, *234*(12), 22034-22043. https://doi.org/10.1002/JCP.28766

Zimmerman, A. N. E. (2000). The Calcium Paradox. *Cardiovascular Research*, *45*(1), 121-121. https://doi.org/10.1016/S0008-6363(99)00323-5

Appendices

Appendix A- Human DLC1β insert sequence information:

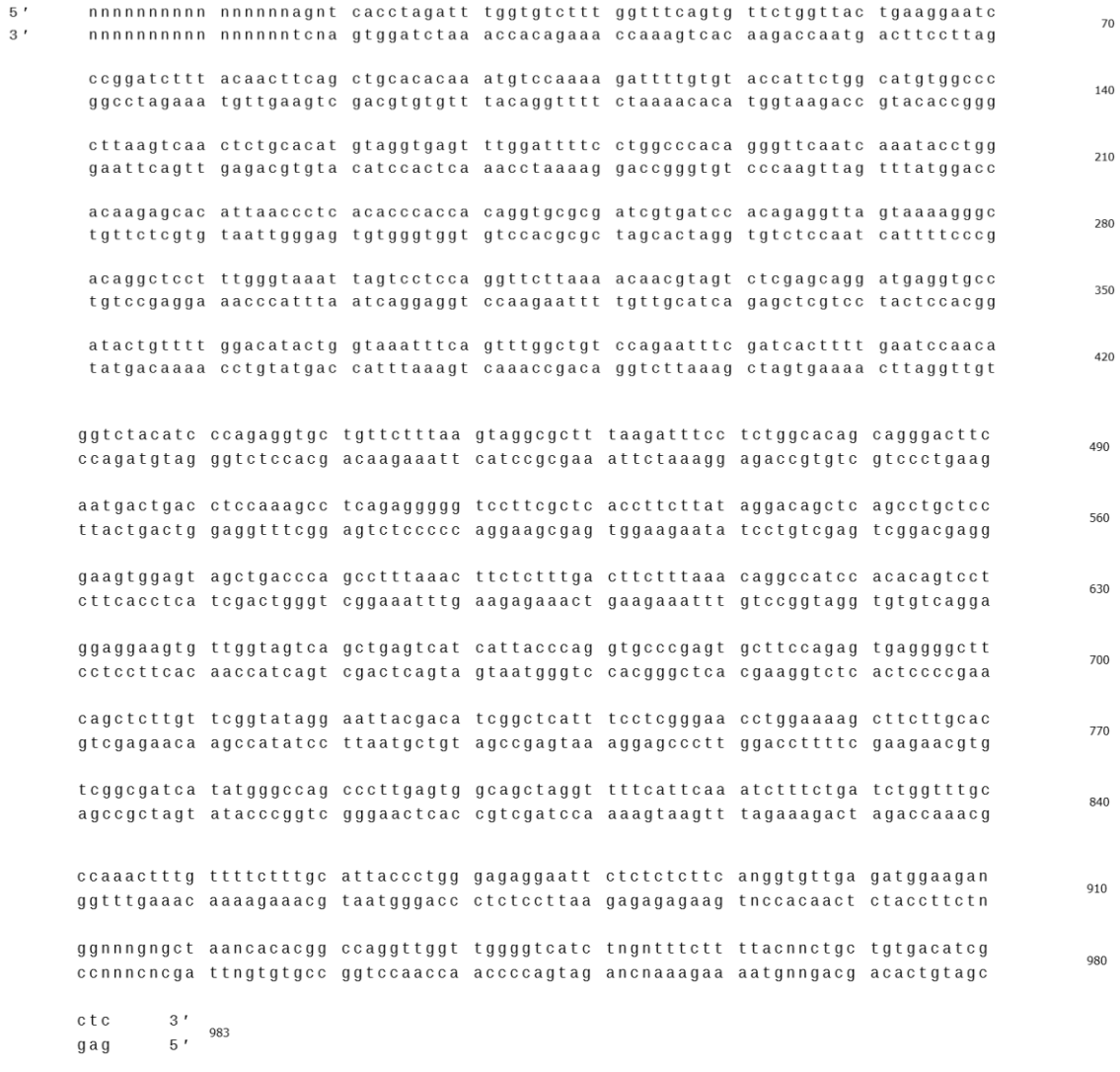

Figure 29- Human DLC1β Insert Sequence cloned into pcDNA3.1 backbone

Appendix B- Scoring Sheets used for Semi-quantitative Scoring of MHT's:

Animal ID	Fibrosis (TRI)	PMNs	Lymphocytes	Infarction (acute)	Injury Grade (%)

Figure 30- Blank Semi-quantitative Scoring Sheet for MHT's

Given to the single-blinded histopathologist to be filled out upon assessment of the MHT tissues with H&E and TRI stains. TUNEL staining was simply scored by the pathologist on TUNEL+ percentage (% DAB+ cells). Another section for any other notes/ pertinent information was also given at the time of scoring.

Animal ID	Sample	Fibrosis	PMNs	Lymphocytes	Infarction	Injury Grade (%)
1845	C24hr	1	0	1	1	0
1846	D24hr	0	0	1	0	0
1847	DD7	1	0	2	0	0
1848	D24hr	1	0	1	1	0
1849	DD7	1	0	1	0	0
1851	CD7	1	0	1	0	1
1852	CD7	1	0	2	1	2
1853	CD7	2	1	2	0	1
1854	DD7	0	0	1	0	1
1855	C24hr	1	1	0	0	0
1856	C24hr	1	1	0	0	0
1857	C24hr	1	0	1	0	0
1859	CD7	1	2	1	0	1
1863	Normal	0	0	0	0	0
1921	DD7	1	0	1	0	1
1922	D24hr	0	0	0	0	0
1923	DD7	2	1	2	1	2
1925	CD7	3	3	3	0	3
1926	CD7	1	0	1	0	1
1927	C24hr	0	1	1	2	2
1928	C24hr	0	1	1	1	1
1929	C24hr	0	0	1	1	1
1939	D24hr	0	0	1	1	1
1940	CD7	2	1	1	0	2
1941	DD7	1	0	1	0	1
1942	DD7	1	0	0	0	1
1943	D24hr	0	1	1	1	1
1944	C24hr	0	1	0	2	1
1945	D24hr	0	1	1	2	1
1946	C24hr	0	1	1	2	1
1947	CD7	0	0	1	0	1
1948	CD7	1	1	1	0	1
N-A	Normal	0	0	0	0	0
N-B	Normal	0	0	0	0	0

Figure 31- Semiquantitative Scoring for H&E/TRI MHT's

Where the scale was from 0-4 (0= 0%, 1= <25%, 2= 25-50%, 3= 50-75%, 4= 75+%). These scores are only for H&E/TRI staining, as TUNEL+ sections were scored on DAB+%.

Animal ID	Sample ID	% Positive
1848	D24hr	<1%
1922	D24hr	0
1927	C24hr	15%
1928	C24hr	5%
1929	C24hr	10%
1939	D24hr	0
1943	D24hr	<1%
1944	C24hr	~10%
1946	C24hr	~10%

Figure 32- Semiquantitative scoring for TUNEL+ MHT's

The TUNEL+ tissues were scored based on the % of DAB+ cells present in a TUNEL stained section.

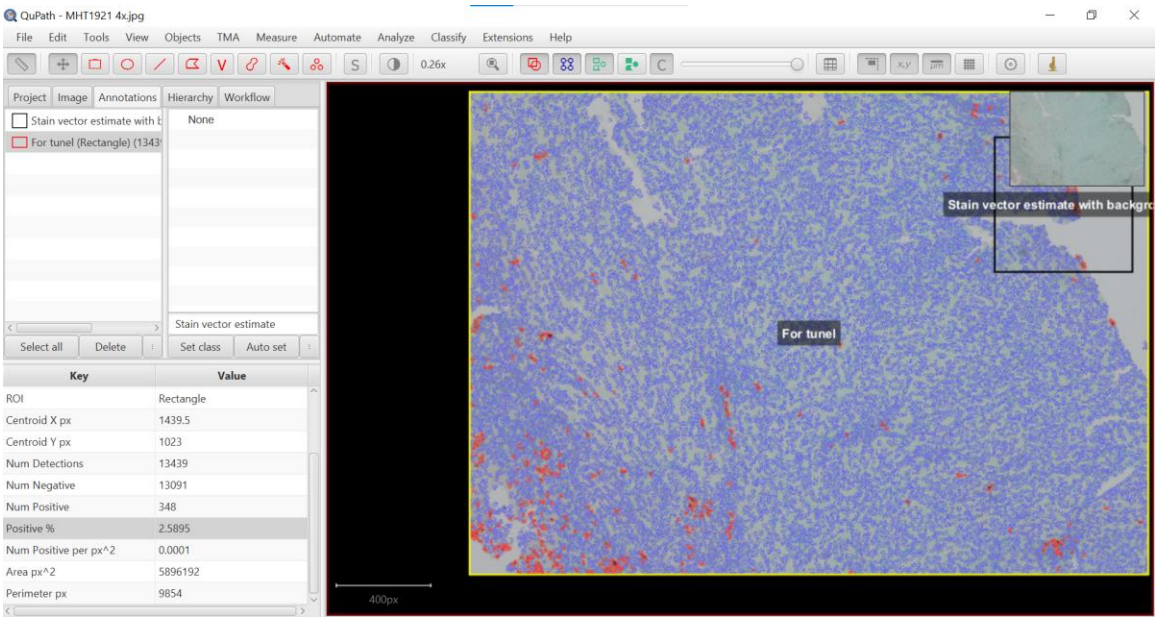

Figure 33- QuPATH TUNEL positive percentage output

The photo displays a screenshot of the output from a MHT graft TUNEL+ quantification. After the ROI was used to determine nuclear positivity (DAB + or -), the positive cell count automation was run. Then, the number of detections, number of negative and positive cells were used to determine the positive % (seen above). The software highlights DAB negative cells as blue, and DAB positive cells as red within the yellow field of view.

Curriculum Vitae

Name:	Samantha Collings
Post-secondary Education and Degrees:	Trent University Peterborough, Ontario, Canada 2016-2021 BSc. The University of Western Ontario London, Ontario, Canada 2021-2023 MSc. (current)
Honours and Awards:	Deans Honour Role Trent University 2020/2021 Western Graduate Research Scholarship Western University 2021-2023 Dutkevich Award Western University 2023
Related Work Experience	Graduate Student Researcher Western University 2021-2023 Notetaker Trent University 2019-2021

Knowledge Translation Events:

1. GSEL Meeting Presentations (2022/2023) Oral presentation(s)
2. Peter Zhong Seminar Series (2021-2023 attendance)
3. Laboratory Training (1 MSc student, 1 undergraduate student)
4. London Health Science Day (2022/2023 attendance)
5. Translational Immuno-oncology Retreat (TIORG) (2022 attendance)

Abstracts & Presentations:

1. **Collings S**, Liu, Q, Diao, H, Won, S, Zheng, X, and Min, W. The role of DLC1β in attenuating cardiac ischemia-reperfusion injury during heart transplantation. [Poster] Pathology Research Day 2022, London, Ontario.

2. **Collings S**, Liu, Q, Diao, H, Taray-Matheson, D, Li, S, Joshi, R, Won, S, Zheng, X, and Min, W. The role of DLC1 beta in attenuating cardiac ischemia-reperfusion injury during heterotopic heart transplantation. [Oral presentation] International Transplantation Society 2023, Niagara-on-the-lake, Ontario

3. **Collings S**, Liu, Q, Diao, H, Taray-Matheson, D, Li, S, Joshi, R, Won, S, Zheng, X, and Min, W. The role of DLC1β in attenuating cardiac ischemia-reperfusion injury during heart transplantation. [Poster] Pathology Research Day 2023, London, Ontario.

4. **Collings S**, Liu, Q, Diao, H, Taray-Matheson, D, Li, S, Joshi, R, Won, S, Zheng, X, and Min, W. The role of DLC1β in attenuating cardiac ischemia-reperfusion injury during heterotopic heart transplantation. [Poster] Surgery Research Day 2023, London, Ontario

Publications:

1. **Collings S,** Liu Q, Diao H, Taray-Matheson D, Li S, Joshi R, Won S, Zheng X, and Min W. DLC1β overexpression impacts transplantation-associated cardiac ischemia-reperfusion injury outcome in mice. J Pathol, In preparation for publication.

2. **Collings S,** Taray-Matheson D, Greasley A, Zheng X, and Min W. J. Cardiol. Translational capacity in preclinical models of transplantation-associated cardiac ischemia-reperfusion injury [Review paper]. In preparation for publication.